Determinants of transport probability and voltage dependence of endosomal Cl^-/H^+ exchangers

Der Naturwissenschaftlichen Fakultät
der Gottfried Wilhelm Leibniz Universität Hannover
zur Erlangung des Grades

Doktor der Naturwissenschaften

-Dr. rer. nat.-

genehmigte Dissertation
von

Dipl.-Biol., Matthias Grieschat
geboren am 20.07.1981 in Hildesheim

2013

Referentin/Referent: Prof. Dr. med. Christoph Fahlke

Korreferentin/Korreferent: Prof. Dr. Theresia Kraft

Drittprüfer/Prüfungsvorsitzender: Prof. Dr. Anaclet Ngezahayo

Tag der Promotion: 19.04.2013

Für meine Eltern

Contents

List of Figures

List of Tables

Abbreviations

Amino acids

A (Ala)	alanine		**M (Met)**	methionine
C (Cys)	cysteine		**N (Asn)**	asparagine
D (Asp)	aspartic acid		**P (Pro)**	proline
E (Glu)	glutamic acid		**Q (Gln)**	glutamine
F (Phe)	phenylalanine		**R (Arg)**	arginine
G (Gly)	glycine		**S (Ser)**	serine
H (His)	histidine		**T (Thr)**	threonine
I (Ile)	isoleucine		**V (Val)**	valine
K (Lys)	lysine		**W (Try)**	tryptophan
L (Leu)	leucine		**Y (Tyr)**	tyrosine

General abbreviations

A	ampere		**HEK**	Human embryonic kidney
Å	Ångstrom = 10^{-10} m		**HEK-MSR**	HEK cells expressing human macrophage scavenger receptor
AMPSO	N-(1,1-Dimethyl-2-hydroxyethyl)-3-amino-2-hydroxypropanesulfonic acid		**HEPES**	4-(2-hydroxyethyl)-1-piperazineethanesulfonic acid
AtClCa	*Arabidopsis thaliana* chloride channel a		**HPLC**	High-performance liquid chromatography
ATP	adenosine-5'-triphosphate		**M**	mol l^{-1}
ATPase	adenosine-5'-triphosphatase		**MEM**	Minimum Essential Medium
BafA1	Bafilomycin A1		**MES**	2-(N-morpholino)ethanesulfonic acid
BCECF	2',7'-Bis-(2-Carboxyethyl)-5-(and-6)-Carboxyfluorescein		**min**	minute
bp	base pairs		**MTSES**	2-sulfonatoethyl methanethiosulfonate
CBS	cystathione β-synthase		**MTSET**	2-(trimethylammonium)ethyl methanethiosulfonate
CFP	cyan fluorescent protein		**NADPH**	nicotinamide adenine dinucleotide phosphate
ClC	chloride channel		**PBS**	phosphate buffered saline
Clcn	the gene encoding for a ClC in mice		**PFA**	paraformaldehyde
CLCN	the gene encoding for a ClC in humans		**PT**	proximal tubule
CmClC	*Cyanidioschyzon merolae* chloride channel		**R**	universal gas constant; 8.3144621 J K^{-1} mol^{-1}
CMV	Cytomegalovirus		**ROI**	region of interest
DMEM	Dulbecco's Modified Eagle's Medium		**SERCA**	sarcoplasmic/endoplasmic reticulum calcium ATPase

DNA	deoxyribonucleic acid	**SV40**	Simian Virus 40
DTT	Dithiothreitol	**SyClC**	*Synechocystis* sp. PCC6803 chloride channel
E.coli	*Escherichia coli*	**T**	absolute temperature
EAAT	excitatory amino acid transporter	**TAE**	Tris-acetate-EDTA
EcClC	*Escherichia coli* chloride channel	**Tfn**	transferrin
EDTA	ethylenediaminetetraacetic acid	**T-tubuli**	transverse tubuli
EGTA	ethylene glycol tetraacetic acid	**UV**	ultra violet
F	Faraday constant; 96485.3365 C mol^{-1}	**V**	volt
FBA	feedback amplifier	**VAMP**	vesicle-associated membrane protein
FBS	fetal bovine serum	**w/v**	weight per volume
FITC	fluorescein isothiocyanate	**w/w**	volume per volume
GFP	green fluorescent protein	**WT**	wildtype
h	hour	**WT**	wildtype
		YFP	yellow fluorescent protein

1 Abstract

ClC-5 belongs to the ClC membrane protein family. This family is sub-divided in classical ion channels, mediating passive ion flux and intracellular transporters, stoichiometrically exchanging Cl^- for H^+. ClC-5 is an endosomally-localized transporter and involved in endocytosis. Mutations in the *CLCN5* gene cause the renal disorder Dent's disease. ClC-5 transport is voltage-dependent and displays strong rectification. Moreover, its voltage-dependent activation is additionally hallmarked by the presence of pronounced capacitive currents that are also characterized as gating currents. ClC proteins have been shown to have three anion binding sites in a row: S_{int}, S_{cen}, S_{ext}. A conserved negatively charged residue at the external side, the so called *gating glutamate* 211, can occupy two of these sites – either S_{cen}, S_{ext} or swings out upon protonation. Substrate translocation probably involves protonation of the external gating glutamate at S_{cen}, mediated by another conserved glutamate residue at the internal side, the so called *proton glutamate* 268. This entails also a concerted movement of Cl^- ions in the opposite direction (coupled "transporter mode"). Additionally, ClC exchangers can operate in a different transport mode. Large polyatomic anions, like SCN^- and NO_3^- can be transported by ClC-5 at higher magnitudes than Cl^-, and only partially be coupled to proton antiport (uncoupled "channel mode").

One part of the thesis investigates the regulation of transport probability of both coupled and uncoupled transport modes by various external anions, by internal protons and the properties of the side chain at position 268. This regulation has been only insufficiently described previously and seems to be important for a variety of physiological processes, including endocytosis, exocytosis, protein trafficking and apoptosis. The experiments showed that lower internal pH led to a much stronger current increase upon exchanging extracellular Cl^- for SCN^- than a neutral pH. Using patch-clamp combined with simultaneous fluorometric pH measurements, relative uncoupling could be quantified and was shown to be unchanged by internal protons. Non-stationary noise analysis reported also unchanged unitary current amplitudes, suggesting that apparent substrate affinities are not altered by internal protons. Likewise, the voltage-dependence of the depolarization-activated gating process was unchanged, studied by measuring nonlinear capacitances, which result from the ClC-5 gating machinery. However, the magnitude of the nonlinear capacitances was larger at higher internal pH and also when the proton glutamate 268 was substituted by less protonatable residues. This indicates that the capacitance results from incomplete transport cycles and depends on the availability of internal protons and on the ability of the residue at position 268

to accept protons and donate them to the gating glutamate at S_{cen}. As a consequence, high capacitances at high internal pH reflect that ClC-5 exhibits low transport probability.

The structural determinants of voltage-dependent gating were probed by analyzing the effects of mutations of lysine 210, next to the gating glutamate. By substituting this residue by other residues of different size and charge, cysteine and arginine, large changes of voltage dependence were evoked. Site-directed Cd^{2+} or covalent MTSET modification of the cysteine mutant K210C produced further changes of time and voltage dependence of gating. The voltage dependence of MTSET modification suggests voltage-dependent changes in the accessibility of this residue from the external medium during transport activation. This and other results indicate that lysine 210 plays an important role in regulating the transport machinery of ClC-5 by taking part in voltage-dependent gating by conformational changes and interaction with other more exterior parts of the protein.

2 Zusammenfassung

ClC-5 gehört zur Familie der ClC Membranproteine. Diese Familie ist unterteilt in klassische Ionenkanäle, die passiven Cl^- Fluss vermitteln, und intrazelluläre Transporter, welche Cl^- stöchiometrisch gegen H^+ austauschen. ClC-5 ist ein endosomal lokalisierter Transporter und an der Endozytose beteiligt. Mutationen des *CLCN5*-Gens verursachen die Dent-Krankheit, eine Nierenstörung. ClC-5 Transport ist spannungsabhängig und zeigt eine starke Gleichrichtung. Zudem ist seine spannungsabhängige Aktivierung zusätzlich durch die Anwesenheit ausgeprägter kapazitativer Ströme gekennzeichnet, die auch *Gating*ströme genannt werden. Es wurde gezeigt, dass ClC Proteine drei in einer Reihe angeordnete Bindestellen aufweisen: S_{int}, S_{cen}, S_{ext}. Ein konservierter, negativ geladener Rest an der Außenseite, das sogenannte *gating*-Glutamat 211, kann zwei dieser Stellen besetzen, entweder S_{cen} oder S_{ext} oder schwingt nach Protonierung heraus. Die Substrattranslokation beinhaltet wahrscheinlich die Protonierung des externen *gating*-Glutamats an S_{cen}, bewirkt durch einen anderen konservieren Glutamatrest an der Innenseite, das sogenannte Protonen-Glutamat 268. Dies beinhaltet außerdem eine abgestimmte Bewegung von Cl^--Ionen in die Gegenrichtung (gekoppelter „Transporter-Modus"). Zusätzlich können ClC-Transporter in einem anderen Modus arbeiten. Große mehratomige Moleküle wie NO_3^- und SCN^- können von ClC-5 in größerem Maße transportiert werden als Cl^-, und nur teilweise an Protonen-Antiport gekoppelt sein (entkoppelter „Kanal-Modus").

Ein Teil dieser Doktorarbeit befasst sich mit der Erforschung der Regulation der Transportwahrscheinlichkeit – sowohl in gekoppelten als auch entkoppelten Transportmodi – durch unterschiedliche externe Anionen, interne Protonen und die Eigenschaften der Seitenkette an Position 268. Diese Regulation wurde bisher nur ungenügend beschrieben und scheint für eine Vielzahl physiologischer Prozesse von Bedeutung zu sein, wie etwa Endozytose, Exozytose, intrazellulärem Proteintransport und Apoptose. Die Experimente haben gezeigt, dass ein niedriger intrazellulärer pH einen viel stärkeren Stromanstieg beim Wechsel von extrazellulärem Cl^- zu SCN^- verursacht als bei neutralem pH. Die Durchführung von *patch-clamp*-Messungen, kombiniert mit gleichzeitigen pH Messungen zur Quantifizierung relativer Entkopplung ergab, dass diese relative Entkopplung durch interne Protonen unverändert blieb. Nichtstationäre Rauschanalyse ergab ebenfalls unveränderte Einzelkanalamplituden, was auf eine vom internen pH unabhängige apparente Substrataffinität hindeutet. Ebenfalls blieb die Spannungsabhängigkeit des durch Depolarisation aktivierten Schaltprozesses unverändert. Dies wurde durch die Messung

nichtlinearer Kapazitäten gezeigt, welche beim ClC-5 Schaltvorgang entstehen. Jedoch waren diese nichtlinearen Kapazitäten größer, sowohl bei höherem internem pH als auch, wenn das Protonen-Glutamat durch schlechter protonierbare Reste substituiert wurde. Dies deutet darauf hin, dass eine höhere Kapazität aus unvollständigen Transportzyklen resultiert und sowohl von der Verfügbarkeit von internen Protonen als auch der Fähigkeit des Aminosäurerestes an Position 268, diese aufzunehmen und an das *gating*-Glutamat an S_{cent} weiterzugeben, abhängt. Es folgt daraus, dass hohe Kapazitäten bei hohen internen pH eine geringe ClC-5 Transportwahrscheinlichkeit widerspiegeln.

Die strukturellen Gegebenheiten spannungsgesteuerten Schaltens wurden sondiert indem der Aminosäurerest neben dem *gating*-Glutamat – Lysin 210 – durch Mutation verändert wurde. Das Ersetzen dieses Restes durch Reste anderer Größe und Ladung, Arginin und Cystein, bewirkte eine starke Verschiebung der Spannungsabhängigkeit. Gerichtete Cd^{2+} und kovalente MTSET-Modifikation der Cysteinmutante deuten auf eine spannungsabhängige Veränderung der Zugänglichkeit von außen während der Aktivierung des Transportes hin. Dieses und andere Ergebnisse zeigen, dass Lysin 210 eine wichtige Rolle bei der Regulation der Transportmaschinerie von ClC-5 spielt, indem es am spannungsabhängigen Schalten durch Konformationsänderung und Interaktion mit weiter außen befindlichen Teilen des Proteins teilnimmt.

3 Introduction

3.1 Membrane transport

Ion transport across plasma or intracellular biological membranes requires the presence of dedicated membrane proteins, membrane channels and transporters that facilitate the movements of charged particles through nonpolar lipid bilayers. For example, the transport of Na^+ and K^+ that underlies action potentials in excitable cells (i.e. neurons and muscle cells) relies on *channel proteins* that mediate the passive flow of these ions along their electrochemical gradients. Channel proteins exhibit high specifity for the transported ions and a have so called *gates* controlling the flow of ions [1] (Figure 3.1 A). These gates close and open upon specific stimuli. For example, many neuronal and muscular Na^+ and K^+ channels respond to changes in the transmembrane voltage [2]. Other channels are gated mechanically [3] or chemically by ligand binding [4]. The energy required for directed ion movements through the channel pore is provided by the electrochemical gradient for the corresponding ion.
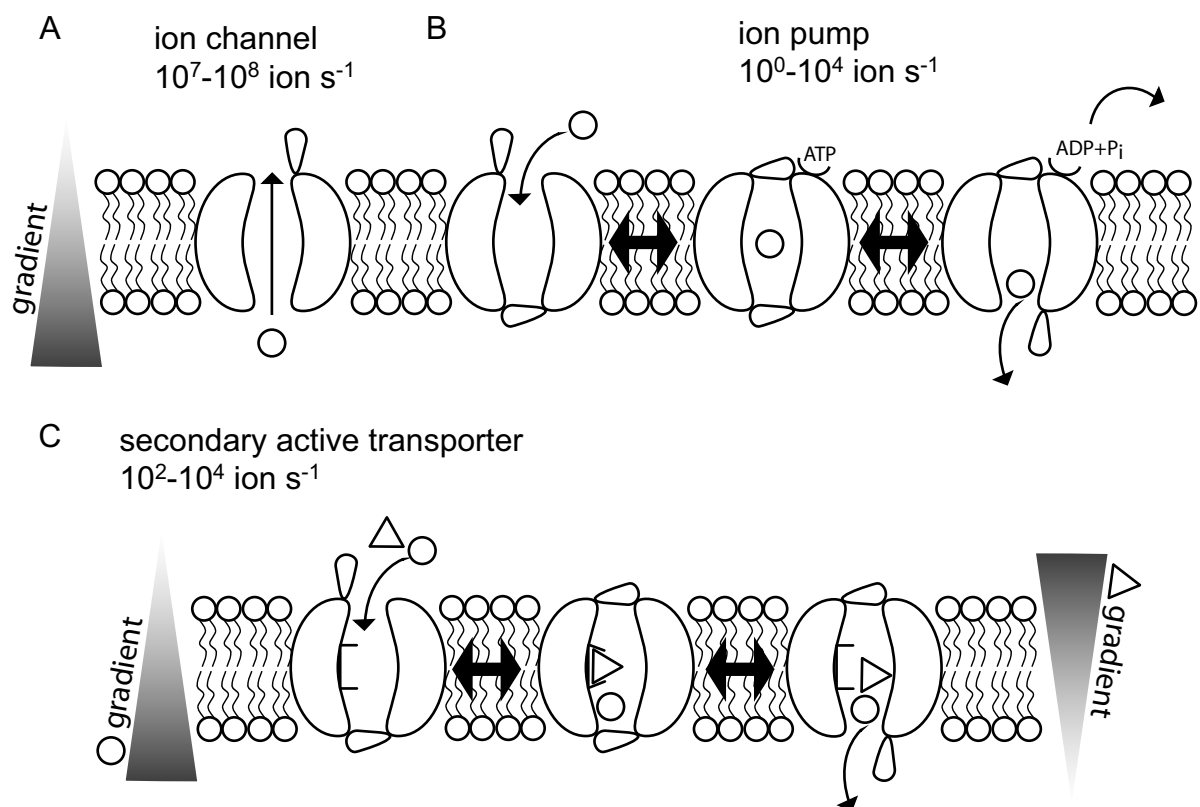
Figure 3.1: Simplified scheme of membrane transport. A. Membrane embedded ion channel with open gate to mediate facilitated diffusion of an ion along its electrochemical gradient. **B.** Primary active transporters that pumps ions against their electrochemical gradients with the required energy provided by ATP. A transporter possesses at least two gates that are never open simultaneously. **C.** Secondary active transporters (here: co-transporter) that uses the energy stored in the electrochemical gradient of one substrate, to transport another substrate against its electrochemical gradient. Some intermediate states and the cyclic behaviour in B and C have been omitted (modified from [5]).

For example, the Cl⁻ flux involved in maintaining the skeletal muscle resting potential is of such passive nature. Electrochemical gradients, which are necessary for the passive transport of ions, first have to be built up on the expense of energy, because here, ions have to move against their electrochemical gradient. This is the major difference between channels and transporters. Channels directly use the electrochemical gradient of an ion species to transport them downhill along this gradient. In contrast, transporters transport them uphill against their electrochemical gradients, thereby increasing those gradients further on the expense of energy. In this way, they are able to concentrate substrates and build up electrochemical gradients by utilizing other sources of energy. Active transporters have at least two gates which may never be opened at the same time [6] (Figure 3.1 B), because otherwise it would be a channel, unable to move ions against their gradients. Since first, one gate has to close before the other one opens, and often larger conformational changes occur, transporters are much slower than channels.

For example, the aforementioned Na^+ and K^+ gradients are built up by the Na^+/K^+-pumps and the energy for this process is provided by ATP hydrolysis. One can distinguish between primary (pumps) and secondary active transport (co-transporters or exchangers). The first group of proteins utilize energy, e.g. the chemical energy of ATP molecules. The latter couples the transport of one type of ions to the electrochemical gradient of one or more different substrates (Figure 3.1 C). Glutamate transporters for example (EAATs, excitatory amino acid transporters) use the electrochemical gradient of sodium to remove neurotransmitter molecules from the synaptic cleft which terminates excitatory signalling and prevents neurotoxicity [7].

Intracellular organelles also have membrane channels and transporters which are involved in maintaining their ionic homeostasis. Calcium channels control the passive release of the important second messenger Ca^{2+} out of the sarcoplasmic reticulum during muscle contraction. In the same compartment, the active SERCA pumps (sarcoplasmic/endoplasmic reticulum calcium ATPase) transport Ca^{2+} back into the sarcoplasmic reticulum and restore and maintain Ca^{2+} homeostasis after muscle contraction. Likewise, the acidification of endosomes during endocytosis is accomplished by active pumping of H^+ into the endosomal lumen, performed by the vesicular-type ATPase.

Cell membranes also contain channels that couple cells with one another – the connexins, which are rather unspecific, can be gated electrically or chemically and passively conduct even large molecules to maintain exchange of metabolites or provide electrical connection between cells [8].

3.2 Chloride channel (ClC) isoforms and their tasks

Chloride channels and transporters are involved in a variety of physiological processes. They are present in animals, plants, fungi and prokaryotes [9], [10]. Mammals possess nine ClC isoforms: ClC-1 to 7 and ClC-Ka and ClC-Kb. Initially, all ClCs were regarded as ion channels. However, this view had to be revised, after Accardi and Miller were able to demonstrate a coupled Cl^-/H^+ antiport for the prokaryotic isoform EcClC of *Escherichia coli* by measurements of reversal potentials of purified protein in an artificial lipid bilayer system with solutions of different Cl^- content or pH on both sides of the membrane [11]. These measurements revealed a 2:1 coupling stoichiometry for Cl^- and H^+, meaning that transport of two chloride ions is coupled to the antiport of one proton. Later on, coupled transport has been demonstrated also for several mammalian ClC isoforms, including ClC-4, ClC-5, ClC-6 and ClC-7 [12]–[15].

Thus, the ClC family is divided in two sub-branches – channels, mediating passive Cl^- flux and secondary active exchangers that use the energy of a H^+ gradient to pump Cl^- against its gradient or *vice versa*. ClC channels are often localized in the plasma membrane, whereas ClC transporters are mainly found in the membranes of endocytotic or lysosomal vesicles and intracellular compartments [16].

3.2.1 ClC channel isoforms

The first cloned ClC channel was ClC-0 from the electric organ of the marbled electric ray (*Torpedo marmorata*) [17]. The first mammalian ClC channel could be identified based on its high homology to ClC-0. This was ClC-1, which is expressed in skeletal muscle. ClC-1 is open already at membrane resting potential, it activates further upon depolarization [18], [19] and provides the major contribution to the stabilization of the resting potential of the muscle cell [20]. The resting potential of cells is normally mostly maintained by K^+, likewise is the repolarization after an action potential an efflux of K^+. When this occurs in the T-tubuli (transverse tubuli, which protrude into the muscle cell) of muscle cells, after repetitive excitation, the elevated K^+ concentration in the small volume of the T-tubuli would result in persisting depolarization of this membrane. A Cl^- conductance – most probably mediated by ClC-1 – reduces the T-tubular length constant. This way, the after-depolarization cannot propagate to the surface membrane electrotonically and cause action potentials without stimulation. However controversies concerning the absence or presence of ClC-1 in T-tubuli [21]. Nevertheless, hereditary mutations that change the functional properties of ClC-1 cause myotonia congenita [22], [23], a disease characterized by prolonged muscle action potential generation after initial excitation, resulting in subsequent muscle stiffness [24].

ClC-2 is a broadly expressed channel [25] and has been demonstrated to play a role in the pathophysiology of generalized idiopathic epilepsy [26]. It activates slowly upon hyperpolarization and its voltage dependence is modulated by internal Cl^- concentration and external pH [27], [28]. Based on the pathological consequences upon knock-out of *Clcn2* in mice (the gene encoding for ClC-2 in mice), including testicular and retinal degeneration [29] and demyelination of central neurons (leukodystrophy) [30], it has been postulated that ClC-2 is involved in transepithelial ion transport [29] to maintain ion composition of the extracellular space around neurons. Yet, in patients with leukodystrophy no *CLCN2* (the gene encoding for ClC-2 in humans) mutations were found [28], [31].

The two closely related channels ClC-Ka and ClC-Kb were identified in humans in 1994 [32] and in rodents in 1992, where they were dubbed ClC-K1 and -K2 [33]. They are expressed in kidney and inner ear and require the accessory β-subunit barttin [34] for proper trafficking and function in transfected mammalian cells [35][36]. Both proteins take part in trans-epithelial transport. Defects of ClC-Kb are associated with Bartter's syndrome type III, a form of kidney insufficiency characterized by a strong salt loss [37], [38]. Bartter's syndrome type IV is additionally accompanied by congenital deafness, because neither ClC-Kb nor ClC-Ka are functional due to a mutation of barttin [34], [39]. Initially, the rodent variant ClC-K1 was characterized electrophysiologically, exhibiting ionic currents with nearly linear appearance in a broad voltage range [33]. After the discovery of barttin, the human isoforms ClC-Ka and -Kb could be expressed and characterized in *Xenopus laevis* oocyte membranes. Estévez *et al.* showed that currents are inhibited by extracellular protons and activated by extracellular Ca^{2+} [34].
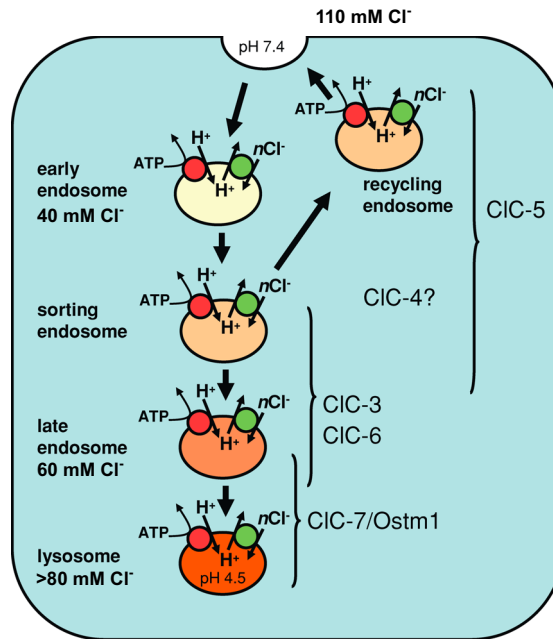
Figure 3.2. Subcellular localization of ClC transporter isoforms in the endosomal/lysosomal pathway. Endosomes are formed by invagination of the cell membrane. During their travel to cell interior they progressively acidify due to the action on the V-type ATPase. The increase of positive charge inside the endosome inhibits further proton pumping and the ClC transporters are proposed to provide an electrical shunt mechanism by stoichiometrically transporting Cl$^-$ into the endosomal lumen in exchange for protons (modified from: [40]).

3.2.2 ClC transporter isoforms of the endosomes

The endosomal pathway begins with the off-pinching of a vesicle from the cell membrane and is called endocytosis (Figure 3.2). This can be a specific receptor/ligand-dependent process to endocytose a specific compound or alternatively a rather unspecific uptake of larger amounts of extracellular fluid and all its contents (fluid-phase endocytosis, "pinocytosis")[41]. In both cases, endosomes are acidified by ATP-dependent proton pumps, which is important for the dissociation of receptor/ligand complexes or the activation of luminal enzymes. Endosomes can be classified by their pH and Cl$^-$ content. Although the extracellular fluid is characterized by a high Cl$^-$-concentration, [Cl$^-$] values in early endosomes are low immediately after their formation, probably due to the negative Donnan potential at the inner surface of budding endosomes, repelling negatively charged Cl$^-$ ions [42]. After formation, early endosomes acidify and accumulate Cl$^-$. They wander further into the cell interior and become sorting endosomes. Some of them travel back to the cell membrane (recycling endosome) to promote for example receptor recycling and another fraction further acidifies, to become late endosomes and finally lysosomes, which are characterized by a high Cl$^-$ content and a pH less than 5.

ClC-3 is mainly expressed in brain and kidney, but also in other tissues [43], [44]. It has been postulated to play an important role in the acidification of endosomes and is presumed to pump Cl^- into the endosomal lumen, which would otherwise be too positive for further acidification, due to the action of the V-type ATPase [45]. The electrophysiological characterization of this endosomally localized protein proved very difficult in the past due to the low surface expression, even when heterologously overexpressed. So far, several controversial and contradicting reports were published, ascribing volume activated currents in one case [46], H^+ activated currents [47], [48] or kinase-regulated currents in other cases [46], [49]–[51] to the presence of ClC-3. Another role was proposed for ClC-3, requiring it to operate in the opposite direction – not a as a shunt for the V-Type ATPase by transporting Cl^- into the endosome but by pumping protons into a signalling endosome of smooth vascular muscle cells. The colocalizing NADPH oxidase would otherwise cause the endosomal lumen to be too negative as a consequence of the production of the second messenger H_2O_2 [52]. Until now, no human disease was linked to a defect of ClC-3, although the ClC-3 deficient knock-out mouse model displays a degradation of the central nervous system [53], [54].

ClC-4 was first identified and cloned in 1994 [55], and its physiological role is rather obscure, the more so as there is no known disorder associated to a defect in ClC-4. It is broadly expressed, but in humans mainly in muscle and brain [55] and in rats in brain, intestine and kidney [56], [57]. Although it is an intracellular membrane transporter, overexpression in *Xenopus laevis* oocytes or mammalian cells results in substantial amounts of proteins in the plasma membrane, enabling electrophysiological studies. ClC-4 currents are strongly outward rectifying [58] and it was shown to be a Cl^-/H^+ antiporter [12], [13]. When external Cl^- is substituted by NO_3^- or SCN^-, currents increase, but proton transport is strongly diminished or abolished [59], [60]. The strong rectification impairs precise measurements of equilibrium potentials, so an inference on the coupling stoichiometry like Accardi and Miller did for the nonrectifying EcClC [11] is hindered. It is presumed that this transporter supports acidification of early endosomes and plays a role in endocytosis. In transfected HEK293 (human embryonic kidney) cells, ClC-4 was shown to partially colocalize with ClC-3 and ClC-5 [61]. Endocytosis assays with fibroblasts of ClC-4 knock-out mice reported a decrease of receptor-mediated transferrin uptake, a reduced transferrin receptor recycling and impaired acidification of early and sorting endosomes [62].

ClC-6 is a not well characterized isoform, first cloned in 1995 [63], which localizes to late endosomes [64] and is almost only expressed in neurons [64]. It is also a transporter [65] and mediates outwardly rectifying current [65]. Knock-out mice develop a mild form of

neuronal ceroid lipofuscinosis, a manifestation of lysosomal storage disorder, characterized by deposition of degradation products of certain proteins in lysosomes of proximal axons [64].

Graves and colleagues [15] showed that the endosomal ClC-7 [63] is a Cl^-/H^+ antiporter by performing fluorometric measurements on enriched endosomes. Before this, ClC-7 was already shown to be a membrane protein of lysosomes, late endosomes and of the osteoclast membrane [66], [67]. In this report it is supposed to promote acidification by a V-type ATPase, which causes bone resorption. *CLCN7* mutations are linked to osteopetrosis, a disease with impaired balance of bone generation and degradation is disturbed [66]. Being an intracellular localized transporter, the electrophysiological approach was difficult until recently sufficient plasma membrane insertion could be achieved by mutating an endosomal sorting motif [68], permitting measurements in heterologous expression systems [69]. ClC-7 currents are outwardly rectifying upon depolarization, but activation and deactivation are very slow, enabling analysis even in the negative voltage range after the transporter has been activated. This makes ClC-7 the only mammalian ClC transporter, at which reversal potential measurements [11] could reliably be carried out to assess the stoichiometry of transported substrates Cl^- and H^+, which resulted to be 2:1 [69]. Besides ClC-Ka and -Kb ClC-7 is the second member of the ClC family to require a β-subunit, in this case Ostm1, for stability [67] and transport activity [69].

The question why ClC transporter isoforms shunt the positive charge accumulation in the vesicle by Cl^-/H^+ exchange and not by simple chloride conduction (as a channel would provide) has recently been addressed by the group of T. Jentsch group using knock-in mice, expressing ClC-5 and ClC-7 proteins, respectively, that only mediate passive nonrectifying Cl^- flux instead of coupled transport. These mice displayed the same pathological phenotype as the corresponding knock-out mice lacking those proteins, but demonstrated normal acidification of endosomes and lysosomes [70], [71].

3.3 ClC-5 is an endosomal transporter and involved in Dent's disease

ClC-5 is the best-studied transporter of the ClC family and was cloned in 1995 [72] and shown to be mostly expressed in epithelial cells of the kidney. ClC-5 is localized in the membrane of early endosomes in cells of the proximal tubule [73]. Mutations in the *CLCN5* gene cause Dent's disease, which is hallmarked by excessive excretion of small proteins, phosphate and calcium into the urine and often by kidney stones [74]. This indicates the possible role of ClC-5, which it shares with the other intracellular ClCs – providing and electrical shunt for a vesicular ATPase, thereby facilitating the acidification of endosomal compartments. *In vivo* experiments with ClC-5 knock-out mice showed decreased abundance of the endocytosis receptor megalin in proximal tubule cells, resulting in both decreased receptor mediated and fluid-phase endocytosis and elevated endosomal pH [75]. This was also reported in cell-culture experiments, along with elevated endosomal Cl^- concentration [76]. Piwon *et al.* hypothesized that the increased phosphate content of the urine results due to an increased removal of the phosphate transporter NaPi-2a from the proximal tubule plasma membrane, mediated by excessive levels of parathyroid hormone, which is not endocytosed sufficiently in ClC-5 deficiency [75]. Abnormal high levels of this hormone are also thought to account for increased transcription of the mitochondrial enzyme 1α-25(OH)-VitD$_3$-hydroxylase [77], which converts its substrate to the active hormone 1,25-(OH)$_2$-VitD$_3$. This hormone was demonstrated to be slightly increased in the serum of Dent's disease patients [78] and is presumably responsible for the intestinal resorption of Ca^{2+}, eventually filtered into the urine resulting in higher levels. The precursor form of 1,25-(OH)$_2$-VitD$_3$, however, has to be apically endocytosed via the megalin-dependent pathway, which is hindered upon ClC-5 defects. Thus, in ClC-5 deficient patients the 1α-25(OH)-VitD$_3$-hydrolase is indeed upregulated, but the pathway to provide it with substrate is reduced and because of this not all patients display hypercalciuria and kidney stones.

When ClC-5 is overexpressed in *Xenopus* oocytes and studied electrophysiologically, currents closely resemble those of ClC-4 in terms of rectification and anion selectivity [58], [72]. Picollo *et al.* and Scheel *et al.* also demonstrated in *Xenopus laevis* oocytes or mammalian cells that ClC-5 is a Cl^-/H^+ antiporter [12], [13] and transport becomes uncoupled by external NO_3^- or SCN^- [59]. For ClC-5, several estimates have been published for the stoichiometry [12], [13] and the most recent article reports a 2:1 ratio [79].

Additionally ClC-5 was the first ClC for which the gating currents recently were reported [80]. Gating currents were predicted by Hodgkin and Huxley [81] and first recorded and published by Armstrong and Bezanilla for the sodium channel [82] as intrinsic properties

of the gating machinery of some voltage-gated channels or transporters. They were proposed to rise as a response to an activating voltage, because charged amino acids of a voltage sensor domain move, resembling ion flow. For the sodium channel gating currents were recorded as a transient current preceding the actual ionic current. Since gating currents arise from voltage-dependent processes, they are nonlinear and can be separated from linear capacitances by so called leak-subtraction ([83], see Sections 4.3.7.1 and 5.5).

3.4 ClC structure and function

Electrophysiological characterizations of ClC-0 by Miller and White [84] implied first assumptions on ClC structure: They function as a homodimer, with each monomer forming an ion conduction pathway of its own. Every protopore can open and close independently on a millisecond time scale ("fast gate"). Additionally both pores can be closed simultaneously by a slower gating process ("common gate"). But this behaviour of two strictly separated gating processes is not always observed in all ClC isoforms and the molecular mechanism of common gating is still unclear.
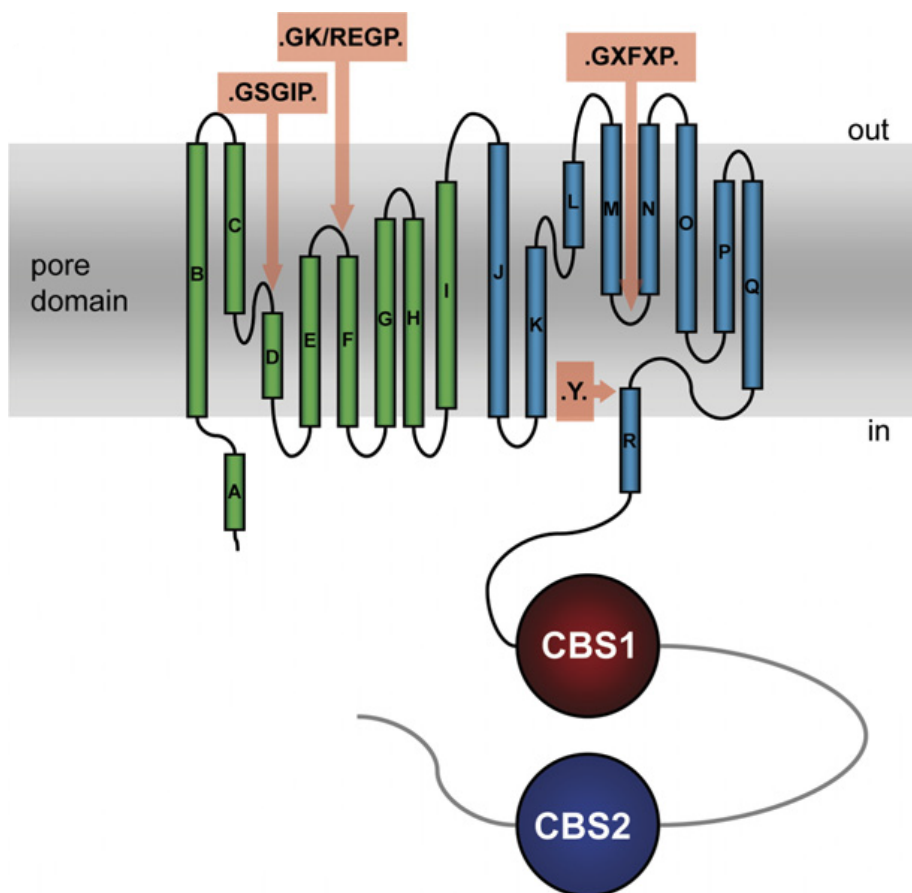
Figure 3.3 ClC membrane topology of a monomer. In green and blue depicted are the pseudo-symmetrical repeats of the helical patterns and in red and purple the two CBS domains, present in all eukaryotic ClCs, but not in the prokaryotic EcClC. Arrows indicate regions that contribute to the selectivity filter with conserved sequences given in the boxes (from: [85]).

In 2002, before the exchanger function was known, EcClC was the first ClC, for which the structure could be obtained crystallographically by Dutzler *et al.* [86]. The dimeric ClC structure proposed by Miller and White structure was verified and can be regarded as representative for other ClCs, although this prokaryotic isoform is lacking two cytoplasmic CBS (cystathione β-synthase) domains, present in all eukaryotic ClCs [87], [88]. Instead of 10

or 12 trans-membrane segments, as predicted from biochemical experiments [89], a ClC monomer consists of 18 α-helices, with only some of which spanning the entire cell membrane (Figure 3.3). Monomers display anti-parallel symmetry, formed by helices B to I being inversely repeated by helices J to Q. Nearly all of the helices are heavily tilted with respect to the membrane, visible in the crystal structure (Figure 3.4)[90]. In the wildtype crystal (Figure 3.4 and Figure 3.5, left) Cl$^-$ ions could be detected in two positions.
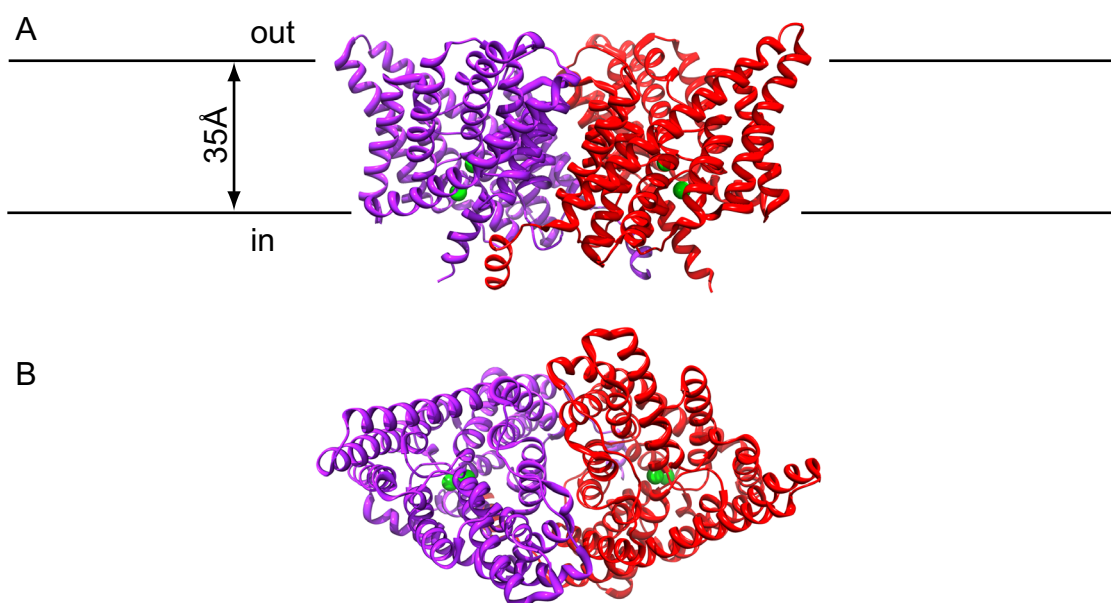
Figure 3.4. Crystal structure of EcClC of *Escherichia coli* (PDB ID 1OTS). A. Side view of the "double-barreled" dimer, with each monomer shown in purple or red, respectively. Two bound Cl$^-$ ions per monomer are shown in green. Orientation and thickness of the membrane are indicated. **B.** View from above.

As a selectivity filter, a row of three binding sites was proposed. Binding to those sites is stabilized by interaction of the anion with the protein backbone and certain side chains of amino acids. Three binding sites can result from those interactions: an external (S_{ext}), a central (S_{cen}) and an internal (S_{int}) binding site [90]. The external binding site in wildtype ClCs (Figure 3.5, left) is occupied by a negatively charged glutamate side chain E148, which represents the closed conformation of the transporter. In this case, no third anion is visible. The external binding site is only accessible to an anion, if the glutamate side chain is protonated and swings out, which can be mimicked artificially by mutating the glutamate to the uncharged residues alanine or glutamine (E148Q; Figure 3.5, right). Here, the external binding site is free to interact with an anion, which becomes visible in the structure [90], and this conformation represents the open state. This glutamate residue is the so-called gating glutamate because by blocking the access for external Cl$^-$ to the pore, it acts like a gate. It is present in all ClC isoforms, except ClC-Ka and Kb, which have a valine at the corresponding position (Figure 3.6) and are constantly in a conducting state [36]. The neutralizing mutation

to glutamine in other ClCs also keeps them constantly open [91] and, additionally, in the transporter isoforms no proton translocation takes place [11], [13] and rectification is switched to a rather ohmic behaviour [51], [58], [65], [69]. Conversely, an introduction of a glutamate in place of the valine in the ClC-K isoforms is able to produce gated, rectifying behaviour [92].

Figure 3.5: The selectivity filter of EcClC. Sections from X-ray crystallographic structures of EcClC, showing external, central and internal anion binding sites S_{ext}, S_{cen}, S_{int} with bound anions shown as red spheres. Left structure represents the wildtype protein, right structure is the gating glutamate mutant E148Q, featuring a third anion bound to the external binding site (taken from:**[85]**)

It was proposed that the central binding site is a water-free environment and that both the positively charged N-termini of helices N and F and a conserved tyrosine at position 445 (in EcClC) have a stabilizing effect on an anion bound there [90]. A conserved serine 107 is supposed to isolate the Cl⁻ ion against the intracellular solution [93] (Figure 3.5, left). The internal anion binding site is thought to be created by interactions of the anion with an amide group of the protein backbone [90]. Of all three binding sites, a recent calorimetric study estimates smallest binding forces to Cl⁻ at this position [94].

```
  EcClC  146 GREGPTVQIG GNIGRMVLDI FRLKG..... .......DEA RHTLLATGAA AGLAAAFNAP LAGILFIIEE MRP  206
  CmClC  208 GWEGPNVHIA CIIAHQFYRL GVFKELC... .....TDRAL RLQTLAAACA VGLASSFGAP LGGVLYSIET IAS  272
 AtClCa  201 GKEGPLVHIG SCIASLLGQG GPDNHRIKWR WLRYFNNDRD RRDLITCGSA SGVCAAFRSP VGGVLFALEE VAT  273
   ClC-0  164 GKEGPFVHIA SICATLLNQL LCFISGRRE. .....EPYYL RADILTVGCA LGISCCFGTP LAGVLFSIEV TCS  230
   ClC-1  230 GKEGPFVHIA SICAAVLSKF MSVFCGVY.. .....EQPYY YSDILTVGCA VGVGCCFGTP LGGVLFSIEV TST  295
   ClC-2  203 GKEGPFVHIA SMCAALLSKF LSLFGGIY.. .....ENESR NTEMLAAACA VGVGCCFAAP IGGVLFSIEV TST  268
  ClC-Ka  164 GKVGPFVHLS VMIAAYLGRV RTTTIGEP.. .....ENKSK QNEMLVAAAA VGVATVFAAP FSGVLFSIEV MSS  229
  ClC-Kb  164 GKVGPFVHLS VMMAAYLGRV RTTTIGEP.. .....ENKSK QNEMLVAAAA VGVATVFAAP FSGVLFSIEV MSS  229
   ClC-3  222 GKEGPLVHVA CCCGNIFSYL FPKYS..... .....TNEAK KREVLSASAS AGVSVAFGAP IGGVLFSLEE VSY  284
   ClC-4  222 GKEGPLVHVA CCCGNFFSSL FSKYS..... .....KNEGK RREVLSAAAA AGVSVAFGAP IGGVLFSLEE VSY  284
   ClC-5  209 GKEGPLVHVA CCCGNILCHC FNKYR..... .....KNEAK RREVLSAAAA AGVSVAFGAP IGGVLFSLEE VSY  271
   ClC-6  198 GKEGPMIHSG SVVGAGLPQF QSISLRKIQF NFPYFRSDRD KRDFVSAGAA AGVAAAFGAP IGGTLFSLEE GSS  270
   ClC-7  245 GKEGPMIHSG SVIAAGISQG RSTSLKRDFK IFEYFRRDTE KRDFVSAGAA AGVSAAFGAP VGGVLFSLEE GAS  317

helices        ┌──────────F──────────┐        ┌──────────G──────────┐  ┌───H───┐
```

Figure 3.6: Sequence alignment of several members of the ClC family. Conserved gating and proton glutamates are marked. The sequences come from *Escherichia coli* (EcClC), *Cyanidioschyzon merolae* (CmClC), *Arabidopsis thaliana* (AtClCa), *Torpedo marmorata* (ClC-0) or humans. And were aligned using the AlignX module of VectorNTI. Lowest row designates position on helices as seen in the EcClC crystal [86].

Another critical glutamate residue only occurs in transporter isoforms of ClC (Figure 3.6) and mutations of this glutamate 203 in EcClC to other amino acids determined this residue to be crucial for proton transport [93]. An exchange for glutamine at this position mediated Cl$^-$ flux without coupled proton transport. This so called proton glutamate is located at the intracellular interface, but is not in close vicinity to the Cl$^-$ binding pathway and Accardi and colleagues have suggested therefore separate conduction routes for Cl$^-$ and H$^+$ that converge near the gating glutamate. In contrast to the prokaryotic EcClC, a neutralizing mutation of this proton glutamate halts not only the proton transport, but also the Cl$^-$ transport in eukaryotic isoforms ClC-4 to ClC-7. [59], [65], [69]

How protons travel from the internal proton acceptor through the protein to reach the rather distant gating glutamate in the ClC transporter forms still remains obscure. Miller and Nguitragool suggested that the proton is shuttled from the proton glutamate to the central binding site, where it forms a transient HCl molecule before it protonates the external glutamate and they also proposed a simple model to explain the occurrence of the 2:1 Cl$^-$/H$^+$ stoichiometry [95]. Recent crystallographic work by Feng *et al.* [96] presents a structure of a eukaryotic ClC from the unicellular red algae *Cyanidioschyzon merolae*, which may serve as a complementation of the EcClC crystal: In CmClC, an anion was visible at the external binding site and the gating glutamate was bound to the central binding site. This conformation could possibly also occur in EcClC. This way, the gating glutamate would already be at the central binding site without the necessity of a hypothetical and quite unstable formation of HCl to bridge the distance between proton and gating glutamate. Based on the three possible conformations of the gating glutamate, they developed a kinetic model which also might explain the 2:1 coupling.

ClC transporters isoforms can conduct several types of anions better than Cl$^-$, namely large polyatomic anions like NO$_3^-$ or SCN$^-$ [58], [59], [97]–[99], but those substrates fail in maintaining the 2:1 transport stoichiometry and partly or fully uncouple anionic current from proton transport [59], [60], [97]. The mechanism of uncoupling is still not well understood. EcClC crystals grown in presence of SeCN$^-$, an anion similar to SCN$^-$ show the anion only bound at the internal binding site [97] while electrophysiological and calorimetric results imply a reduced binding affinity of NO$_3^-$ or SCN$^-$ [60], [94], [97], [99]. In EcClC Accardi *et al.* [100] mutated the tyrosine 445 stabilizing the Br$^-$ ion (a crystallization equivalent to Cl$^-$) in the central binding site to other amino acids and determined ion occupancy at this site in the crystal as well as Cl$^-$/H$^+$ transport coupling of those mutants. They report that the degree of

coupling is diminished when shorter amino acids take the place of the tyrosine. With reduced coupling, reduced anion occupancy at the central binding site goes along.

The prementioned CBS domains are present in all eukaryotic ClC isoforms and much conserved among them [101]. In ClC-0 of *Torpedo marmorata* the CBS domains influence common gating [102]. In ClC-1 they were shown to mediate ATP induced inhibition [103], [104] and crystallized CBS domains from ClC-5 in presence of ATP, ADP or AMP show those nucleotides bound at the interface between the two CBS subdomains [105]. Contrary to the inhibiting effect of ATP in ClC-1, intracellular ATP is needed to prevent a dramatic rundown of ClC-4 currents in heterologously expressing mammalian cells [98] and acts as an activator of ClC-5 [106]. Also in ClC-2 the CBS domains are able to bind ATP [107], but the effects are unclear [108].

3.5 Voltage dependence of ClC gating

The voltage dependence of gating is present in most ClC isoforms. ClCs are lacking a dedicated domain in which positively charged amino acids of a helix fulfill the task of voltage sensing and mediate structural changes [86], [109], as for example the S4 domain in cation selective channels [2], [110]. Moreover, the voltage dependence is also influenced by the concentration and transmembrane gradient of the transported ion itself [111]. For the fast gating process in ClC-0 it was proposed that the external Cl^- ion itself opens the channel by voltage-dependent binding to a site located in the pore [112]. Shortly after that, Chen and Miller [113] presented a minimal model, which argues against this idea, based on their kinetic data and the fact that at different external Cl^- concentrations the minimal open probability approached the same value, which was never zero (Scheme 1).

$$
\begin{array}{ccc}
C & \underset{\beta_1}{\overset{\alpha_1}{\rightleftharpoons}} & O \\
\Big\updownarrow{K_C} & & \Big\updownarrow{K_O} \\
C{:}Cl & \underset{\beta_2}{\overset{\alpha_2}{\rightleftharpoons}} & O{:}Cl
\end{array}
$$
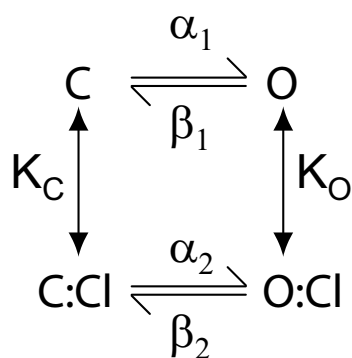
Scheme 1

In this scheme, the channel opening rate α depends on both Cl^- concentration and voltage and is composed of α_1 and α_2 according to the probabilities of the occupation and non-occupation of the binding site. In the closed conformation, only internal Cl^- can bind with an apparent dissociation constant K_C, whereas in the open conformation, the binding site is accessible from both sides, resulting in K_O.

3.6 *Aim of this thesis*

ClC-5 is an endosomal Cl^-/H^+ exchanger and defects are associated with Dent's disease. One object of this thesis was to study the impacts of ClC-5 mutations on the acidification of endosomes. To this end, fluorescence microscopic analysis of endosomally-localized pH sensors should be performed. The pH sensors were either genetically encoded (synapto-pHluorin) or inserted into the endosomal pathway by receptor-mediated endocytosis (FITC-transferrin). As a prerequisite for the validity of the analysis, a quantitative assessment of sufficient colocalization of the pH-sensitive dyes to ClC-5, based on 3D confocal datasets was sought.

ClC-5 transport activity is regulated by voltage and by the transported substrates Cl^- and H^+. Furthermore, large polyatomic anions are transported with less coupling to proton transport. By measuring total anion transport and proton transport simultaneously using the patch-clamp fluorometry technique, it was pursued to gain insights into the determinants of uncoupling. Additionally, those results, combined with non-stationary noise measurements, measurements of nonlinear capacitance and conventional patch clamp should contribute to the evaluation of the role of internal protons on the transport probability of ClC-5.

Voltage-dependent gating of ClC-5 crucially depends on the external gating glutamate 211, but is also modulated by other parameters. By characterizing the voltage-dependence of activation of different mutants of lysine 210, the contribution of this residue to the gating of ClC-5 was a subject of research in conjunction with the role of internal and external Cl^-. Furthermore, to investigate how structural determinants in the region near the gating glutamate modify gating, the voltage-dependent accessibility of K210C for cysteine-reactive compounds was sought to be investigated.

4 Material and methods

4.1 Molecular biology

4.1.1 Generation of expression constructs

The plasmid pTLN hClC-5 was a gift from Dr. Thomas J. Jentsch. Due to the fact that this is a vector designed for expression in *Xenopus laevis* oocytes, a new construct suitable for expression in mammalian cells was created using several constructs available. Strategies were done with the bioinformatics computer program Vector NTI Advance 10 (Invitrogen):

source construct	fragment	techniques used
pRcCMV hClC-4	vector	restriction with XbaI & HindIII
pTLN hClC-5	215 bp fragment of ClC-5 and part of vector	restriction with HindIII & DraIII
pTLN hClC-5	2.2 kbp ClC-5 fragment with linker	standard PCR (polymerase chain reaction), restriction with DraIII & BamHI
pCINeo SOD1 WT link mCherry	mCherry	restriction with BamHI & XbaI

Table 1: Summarized strategy for the generation of a plasmid for heterologous expression of fluorescently labelled ClC-5 in mammalian cells.

The desired construct pRcCMV ClC-5 link mCherry (Figure 4.1) possesses a CMV (Cytomegalovirus) promoter for expression in mammalian cells [114], an SV40 (Simian Virus 40) promoter for enhanced replication and expression in mammalian cells expressing the large T antigen, an ampicillin resistance as a selectable marker for transformed *E.coli* cells and a neomycin resistance as a selectable marker for transfected HEK293 cells [115]. Furthermore, the C-terminal tag with the red fluorescence protein mCherry [116] makes it possible to identify transfected cells, study the localization under a fluorescence microscope or identify bands in a fluorescent protein gel.
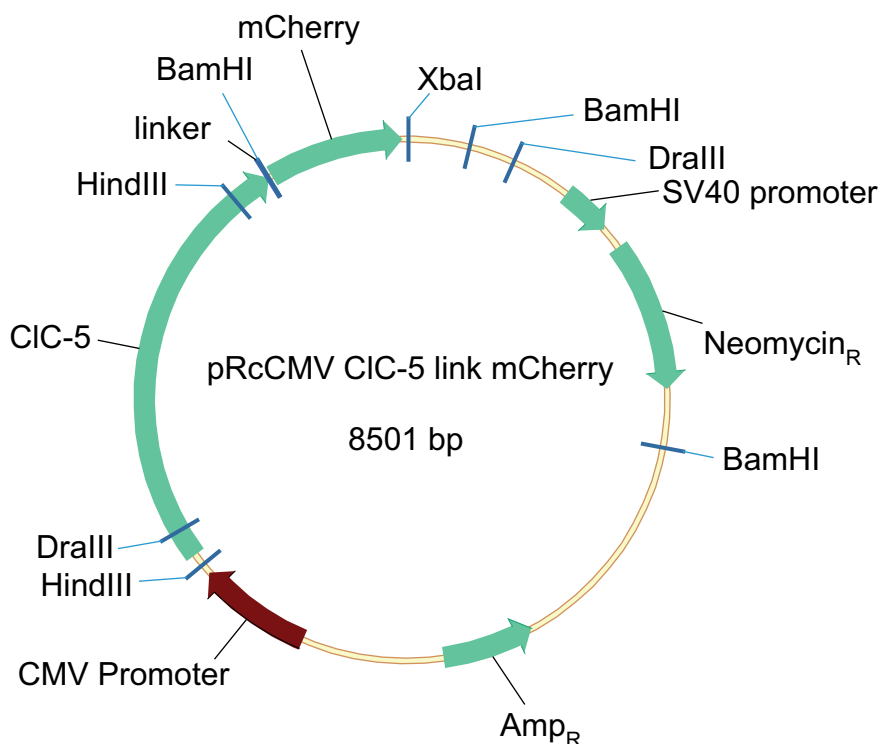
Figure 4.1: Plasmid pRcCMV ClC-5 link mCherry or mutated forms of it were used for most experiments throughout this work. Depicted are the CMV (Cytomegalovirus) promoter for expression in mammalian cells, the coding sequence for ClC-5, a linker and the red fluorescent protein mCherry. The SV40 (Simian virus 40) promoter enhances the replication and expression in HEK293T cells and the neomycin resistance (Neomycin$_R$) confers G418 antibiotic resistance to HEK293 cells and allows selection and generation of stable cell line. Ampicillin resistance (Amp$_R$) allows selection of successfully transformed *E.coli* clones for applications in molecular biology.

4.1.2 Standard polymerase chain reaction

Standard polymerase chain reaction (PCR) was carried out in a thermocycler (MJ Research).

The reaction mixture contained:

template DNA	100 ng
10 x PCR buffer (Roche)	5 µl
10 mM dNTP mixture (QIAGEN)	1 µl
Pfu/HiFi polymerase (Roche)	0.5 µl
HPLC water (Fluka)	40.5 µl
sense and antisense primers (25 ng/µl)	1 µl each

Primers used to amplify the 2.2 kbp fragment of ClC-5 in pTLN hClC-5, had the sequences:

sense	5'-AATTGATTGGGTGAGAGAGA-3'
antisense	5'-TAAATACCGGTGGATCCGTGTTGAAGAGAATGGAATCAG-3'

The antisense primer was designed to remove the stop codon after ClC-5, introduce restriction sites for BamHI and AgeI and code for a linker with the amino acid sequence TDPPVAT.

The PCR program contained a first denaturation step at 94°C for 10 min, before conducting 35 cycles:

94°C	1 min
54°C	1 min
72°C	2.5 min

A final synthesis step at 72°C was carried out for 10 min and the resulting DNA fragment was purified via agarose gel electrophoresis and subsequent gel extraction.

4.1.3 Restriction digest

The following preparation applies to a standard single or double digest:

Plasmid DNA	1-2 µg
10 x Fast Digest Buffer (Fermentas)	2 µl
Enzyme (Fermentas Fast Digest Enzymes)	1 µl/enzyme
HPLC water (Fluka)	*ad* 20 µl

Incubation took place at 37°C for 1 h. Preparative digests with up to 5 µg DNA were performed with an up-scaled preparation at 50 µl final volume.

4.1.4 Agarose gel electrophoresis

Gels consisted of 1% (w/v) agarose (Invitrogen), dissolved in TAE running buffer (50x contains 2 M Tris, 5.96 % (v/v) acetic acid, 10 % (v/v) 0.5 M EDTA pH 8.0), supplemented with 0.005% (v/v) ethidium bromide (Fluka). Samples were mixed with 6x loading buffer (0.25 % (w/v) bromphenol blue, 0.25 % (w/v) xylene cyanol, 30-40 % (v/v) glycerol) and electrophoresis was carried out at 110 V (*EC 105* power supply, E-C Apparatus Corporation) in gel chambers (Kodak BioMax MP1015) filled with TAE buffer. UV-induced ethidium bromide fluorescence of DNA bands was analyzed with a Gel-Doc 2000 (Bio-RAD) and, if necessary, quantified with the computer program Quantify One (Bio-RAD).

4.1.5 Gel extraction

DNA bands of the correct length were excised with a scalpel and transferred to 1.5 ml reaction tubes (G. Kisker). Extraction was done with the QIAquick Gel Extraction Kit (QIAGEN) according to the manufacturer's manual.

4.1.6 Ligation

Prior to ligation, a concentration gel with 4 µl of gel extracted DNA was run to determine the concentration of the samples. The amount of insert fragments used for ligation was 3 times the amount of vector fragments and 20 units T4-DNA ligase (New England Biolabs) and 2 µl ligase buffer (50 mM Tris-HCl pH 7.5; 10 mM $MgCl_2$; 1 mM ATP; 10 mM DTT, New England Biolabs) were used in a reaction, filled up to 20 µl with HPLC water (Fluka) in a 1.5 ml reaction tube. As a control, ligation was also carried out with the vector fragment alone and the incubation took place overnight at 18°C.

4.1.7 Transformation

For transformation, the competent *E.coli* strain DH5α was used. In a chilled 1.5 ml reaction tube, 5 µl of a ligation mix was incubated on ice with 40 µl of bacteria suspension (freshly thawed) for 20 min. As a positive control, 50 ng of the plasmid pcDNA 3.1 (+) and as a negative control 1 µl water were used. After a heat shock at 42°C for 2 min in a Dry Block Heating Thermostat (G. Kisker), samples were put back on ice and after 2 min 300 µl SOC-medium without antibiotics (100 ml contain 2 g Bacto-tryptone (BD Biosciences), 0.5 g Bacto-yeast extract (BD Biosciences), 10 mM NaCl, 2.5 mM KCl, 10 mM $MgCl_2$, 10 mM $MgSO_4$, 20 mM glucose, pH 7, last three compounds were sterile filtered and added after autoclaving of the medium) was added and carefully mixed. After a shaking incubation at 150 rpm and 37°C for 45 min (Multicon eco, Infors AG), bacteria were centrifuged at 6000 rpm in a microcentrifuge (Centrifuge 5415D; rotor F45-24-11, Eppendorf) and 280 µl of supernatant were discarded. The bacteria pellet was resuspended in the remaining supernatant and plated on LB-agar plates (25 g DB Difco LB-Boullion, Miller (Luria-Bertani) and 20 g BD Bacto Agar per liter, autoclaved) with a selection antibiotic (100 µg/ml), which were incubated overnight at 37°C. To produce pre-cultures, colonies were picked and transferred into 5 ml LB-medium (25 g BD Difco LB-Boullion, Miller (Luria-Bertani) per liter, autoclaved) with antibiotics (100 µg/ml) in 14 ml round-bottom tubes (BD Biosciences) and incubated shaking at 150 rpm and 37°C for 14 hours.

4.1.8 DNA preparation

The QIAprep 8 Miniprep Kit (QIAGEN) was used to recover the plasmid from *E.coli* pre-cultures using the vacuum method (KNF Laboport) following the manufacturer's instructions. Larger amounts of DNA were obtained using the Plasmid Maxi Kit (QIAGEN) according to the manufacturer's manual.

4.1.9 Determination of DNA concentration

DNA concentrations were measured in an Ultrospec 2100 pro (Amersham Biosciences) spectrophotometer at a 1:100 water dilution in a quartz cuvette. The extinction was measured at a wavelength of 260 nm and the concentration was calculated automatically.

4.1.10   Sequencing

Sequencing was done by the company GATC, Konstanz. The obtained sequences were checked for correctness using *Vector NTI Advance 10* (Invitrogen).

4.1.11   Site-directed Mutagenesis

Mutagenesis was done using the QuikChange Site-Directed Mutagenesis Kit (Agilent Technologies) a PCR-based technique, where a whole plasmid is replicated using complementary primers, differing from the template in several base pairs. As only the template plasmid – and not the newly synthesized mutated plasmid – contains methylated DNA, in a subsequent DpnI digestion, the non-mutated template DNA is destroyed and only mutated plasmids are present. Primers were designed with a combination of VectorNTI together with one of the two www-based programs PrimerX [117] or Agilent's own QuikChange Primer Design program. Primers were ordered from Sigma-Aldrich. Sequences for primers are given in Table 2. QuikChange was performed following the manufacturer's instructions. To reduce the probability of random mutations additional to the desired one, the DNA section containing the mutation was subcloned back into the original plasmid, using appropriate enzymes (see 4.1.3) and the entire subcloned insert was verified by sequencing (see 4.1.10).

Mutant	Sequence 5'-3'
D76C sense	TTTATCAGGTTCGTTAGCTGGTTTGATATGCATCTCTGCTCATTGG
antisense	CCAATGAGCAGAGATGCATATCAAACCAGCTAACGAACCTGATAAA
H80C sense	CGTTAGCTGGTTTGATAGACATCTCTGCATGCTGGATGACAGACTTAAAAGAAGG TATAT
antisense	ATATACCTTCTTTTAAGTCTGTCATCCAGCATGCAGAGATGTCTATCAAACCAGC TAACG
H80D sense	GCTGGTTTGATAGACATCTCTGCAGACTGGATGACAGACTTAAAAGAAGG
antisense	CCTTCTTTTAAGTCTGTCATCCAGTCTGCAGAGATGTCTATCAAACCAGC
S168P sense	CTTATGCCTGTGGCCCTGGAATCCCTGAG
antisense	CTCAGGGATTCCAGGGCCACAGGCATAAG
K210C sense	GCTTGAGCCTGGGCTGCGAGGGCCCTCTAGTG
antisense	CACTAGAGGGCCCTCGCAGCCCAGGCTCAAGC
K210R sense	GTCGTCTGGCTTGAGCCTCGGGAGAGAGGGCCCT
antisense	AGGGCCCTCTCTCCCGAGGCTCAAGCCAGACGAC
E211C sense	CTTGAGCCTGGGCAAATGCGGCCCTCTAGTGCAC
antisense	GTGCACTAGAGGGCCGCATTTGCCCAGGCTCAAG
E268C sense	GGAGTATTATTCAGCCTTGAATGCGTCAGCTACTATTTTCCCCTC
antisense	GAGGGGAAAATAGTAGCTGACGCATTCAAGGCTGAATAATACTCC
E268H sense	GGAGTATTATTCAGCCTTGAACACGTCAGCTACTATTTTCCCCTC
antisense	GAGGGGAAAATAGTAGCTGACGTGTTCAAGGCTGAATAATACTCC
E268Q sense	GAGTATTATTCAGCCTTGAACAGGTCAGCTACTATTTTCC
antisense	GGAAAATAGTAGCTGACCTGTTCAAGGCTGAATAATACTC
PCR pHluorin sense	TAAGGATCCACCGGTATGAGTAAAGGAGAAGAACTTTTCACTG
antisense	ACCGTCATCACCGAAACGCG

Table 2: Sequences of primers used for QuikChange site-directed mutagenesis of ClC-5 and PCR of ratiometric pHluorin (see 4.2.3.1).

4.2 Cell culture

4.2.1 Transfection and splitting of HEK293T cells

HEK293T cells, which are human embryonic kidney cells (HEK293), stably transfected with the SV40 large T antigen [118] were grown in 10 cm dishes (Sarstedt) in 15 ml DMEM (Dulbecco's Modified Eagle Medium; Gibco), supplemented with 10% FBS (fetal bovine serum, Biochrom AG), 2 mM L-glutamine and 50 units/ml penicillin/streptomycin (Invitrogen) in a cell incubator (Sanyo MCO-18AIC(UV)) in humid atmosphere at 37°C and 5% CO_2. At a confluence of approximately 50%, cells were transfected using the calcium phosphate precipitation method [119]. To this end, 10 µg of plasmid DNA was mixed in a sterile 1.5 ml reaction tube with 10 µl Salmon Sperm DNA (Invitrogen), diluted 1:10 in TE-buffer (QIAGEN) and 500 µl of 250 mM $CaCl_2$. This mixture was added dropwise into a second tube with 500 µl of 2 x HEBS solution (in mM: 274 NaCl, 40 HEPES, 12 D-glucose, 10 KCl, 1.4 Na_2HPO_4, pH 7.05) and mixed thoroughly. After 20-30 min of incubation this mixture was added to the dish containing the cells in fresh medium and gently swayed. Splitting was done 24 hours later by removing the medium and washing the cells with PBS (phosphate buffered saline; Lonza) and applying 3 mL of trypsin-EDTA (Gibco). After incubation of 1 min at 37°C cells were manually individualized by rigorous pipetting with a transfer pipette (Sarstedt 86.1175.001). Several drops of this trypsin/cell mixture were transferred into a new dish with fresh medium to achieve the desired density. Electrophysiological measurements were carried out 12-24 hours after splitting.

4.2.2 Generation of stable HEK293 cells

HEK293 cells were used to generate stable cell lines. They were grown in 10 cm dishes in MEM medium (Minimum Essential Medium, Gibco) supplemented wit 10% FBS. Transfection was carried out as in 4.2.1, but cell density was chosen much lower. As the pRcCMV vector contains the gene for neomycin resistance [115], successfully transfected mammalian cells not only express the desired protein, but can be selected using antibiotics. 24 hours after transfection, the medium was exchanged and the new medium was supplemented with 900 µg/ml of the selection antibiotic G418 (Geneticin, Invitrogen). In order to remove dead cells and renew the antibiotic, every three days the cells were endowed new medium. After several weeks, the surviving cells were splitted with low density into several new dishes to achieve single cells, which can form monoclonal round colonies. Those with mCherry fluorescence were selectively detached from the dish bottom and transferred into a new 6 cm dish per colony. After a growing period clones were subsequently checked for expression levels by patch clamping them.

4.2.3 Labelling of ClC-5 endosomes with pH-sensitive dyes

4.2.3.1 Synapto-pHluorin

Synapto-pHluorin [120] is a GFP (green fluorescent protein) variant, whose pH dependence is increased by several mutations. Originally, two variants were created; superecliptic pHluorin and ratiometric pHluorin, the latter of which used here. It differs from WT by the mutations E132D, S147E, N149L, N164I, K166Q, I167V, R168H, S202H and L220F. The ratiometric and the superecliptic constructs were a gift from Dr. Gero Miesenböck (University of Oxford), but the ratiometric form was only given in a prokaryotic expression vector pGEX-2T, whereas only the superecliptic variant was in the desired vector pCIneo VAMPII. By standard PCR (for primers see Table 2) with overhangs and restriction by AgeI, the coding sequence was inserted into pCIneo VAMPII after the coding sequence for VAMPII (vesicle associated membrane protein II), which is a part of the vesicular fusion machinery [121], [122] and targets and anchors the pHluorin protein to the inner face of the vesicular membrane.

For labelling endosomes and comparing the localizations of synapto-pHluorin with ClC-5, HEK293 cells, stably expressing WT ClC-5 linked to mCherry and grown in 6-well plates (Sarstedt) were cotransfected with 0.75 µg pCIneo synapto-pHluorin ratiometric. As a positive control for the assessment of colocalization native HEK293 cells were cotransfected with 1 µg pRcCMV YFP ClC-Kb and 2 µg pcDNA3.1 G47R barttin CFP (cyan fluorescent protein), which have been published to colocalize and to show a similar intracellular staining pattern like ClC-5 mCherry transfected cells [35]. To verify that there was no cross-talk of dyes into the acquisition channel of the other dye during fluorescence microscopy, single transfections were carried out and recorded under the same conditions. 24 hours after transfection, cells were splitted on coated glass coverslips (see Section 4.2.4) at the desired density.

4.2.3.2 FITC-transferrin

Transferrin is a glycoprotein that binds Fe^{3+} and is endocytosed via receptor-mediated uptake and thereby carries iron into the cell [123]. By using similar approaches as Mohammad-Panah *et al.*[57], it is possible to use the ratiometric pH-sensitive dye FITC (fluorescein isothiocyanate) conjugated to transferrin to stain endocytotic vesicles and measure the intravesicular pH.

FITC-transferrin (Sigma-Aldrich) was dissolved to a 5 mg/ml (w/v) stock solution in H_2O, containing 2 mM N_3Na. For labelling, HEK293T cells, grown on coated glass coverslips (see Section 4.2.4), were washed with PBS, pH 5 to deplete transferrin receptors from ligands and

incubated light protected for 30 min in DMEM containing 300 μg/ml FITC-transferrin. Before fixation, an additional washing step with PBS, pH 5 to remove surface bound FITC-transferrin was performed.

4.2.4 Coating of glass coverslips

In cases of cell fixation (see Section 4.2.5) or patch clamp fluorometry (see Section 4.3.7.4) glass coverslips (Assistent 24x24 mm, Karl Hecht AG) were coated with poly-L-lysine (Sigma Aldrich, 0.01% w/v) for 20 minutes at a 1:20 to 1:30 dilution in autoclaved water. After that, coverslips were rinsed three times with autoclaved water.

4.2.5 Cell fixation

Cells were grown on coated glass coverslips, and washed twice for 3 min with PBS before fixation with 4% (w/v) PFA (paraformaldehyde; Merck) in PBS, pH 7.4 for 20 min. After two washing steps for 3 min with PBS cells were mounted with the ProLong Antifade Kit (Invitrogen) according to the manufacturer's instructions. FITC-transferrin labelled cells were fixed with minimal exposure to light.

4.2.6 Image Acquisition

Confocal image stacks were acquired in the Confocal Laser Microscopy facility of the MHH at an Olympus FW1000 equipped with a UPLSAPO 60X O NA:1.35 60x oil immersion objective. Pinhole diameter was 105 μm and stacks with sizes of (0.2 - 0.44 μm) μm were acquired. Both FITC and pHluorin were excited at 488 nm and emission was detected after bandpass filtering at 498-538 nm and 500-545 nm, respectively. CFP, YFP and mCherry were excited at 440, 488 and 559 nm, respectively and emission was detected after bandpass filtering at 475-515, 530-630 and 570-670 nm, respectively. In cases of double staining, each line was scanned sequentially for 2-3 times at each wavelength and averaged (Kalman filtering).

4.2.7 Image Analysis

Quantification of colocalization was done using the JACoP plugin (Just Another Colocalization Plugin, [124]) in ImageJ. Prior to analysis, images were prepared as follows. To reduce noise, images were smoothed, which means, that every pixel was replaced by a pixel with the average intensity of its 3x3 neighbouring pixels. To compensate differences in illumination, emission or detection in two channel images, a linear histogram stretching was applied, which interpolates the histogram to span the whole intensity range, without distorting the intensity distribution. This was done based on the histogram of the whole stack.

In frequent cases, images not only contained cells that were double stained, for example because not all HEK293T cells in a cluster were transfected with ClC-5 mCherry, but all of them endocytosed FITC-transferrin. Since this would interfere with the analysis of colocalization and JACoP does not allow defining of ROIs (regions of interest) all the area not containing double stained cells was assigned zero intensity.

In JACoP, threshold values for both channels were set to the same value and a scatter plot of the gray intensities of every pixel in both channels was created (cytofluorogram). The plugin fitted a straight line to the data and the slope reports on the correlation of the fluorescence in both channels with a slope of 1 being the best correlation. The calculated Pearson's coefficient (PC) evaluates the spread of the data respective to the line and thereby the quality of the fit. For example, a broad distribution around a line with the slope of 1 gives a low or even negative PC and renders the statement of perfect colocalization invalid.

4.3 Electrophysiology

4.3.1 Theory of the voltage clamp

The voltage clamp technique was developed in the 1940s and 50s, initially to study electrical processes at the squid giant-axon [125], [126]. With this method, it was possible to impose a certain voltage across a cell membrane, set by the experimentator. To this end, one electrode impaling the cell measures the intracellular voltage (E', Figure 4.2) and feeds this signal into a feedback amplifier (FBA). A second electrode injects an ionic current I' to charge the membrane to the specified value. This current corresponds to the reciprocal current I (e.g. currents through ion channels). One or more bath electrodes define the extracellular medium as the zero-potential and serve as a reference for the voltage measurement. By convention, positive voltages mean a positively charged cell interior. A positive current means influx of anions into or an efflux of cations out of the cell.

While early setups for giant axons consisted of wire electrodes, the use of microelectrodes was established to measure smaller cells, like *Xenopus laevis* oocytes [127]. Here, the electrode is a chlorided silver/silver chloride wire, which is inserted into a sharp glass pipette, filled with 3 M KCl. This microelectrode is then used to impale a cell.
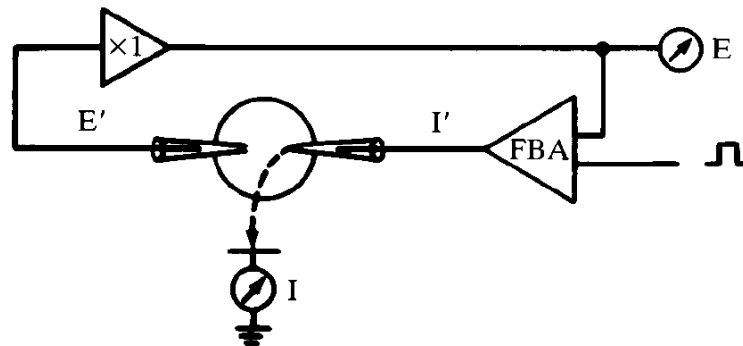
Figure 4.2: Schematic representation of the voltage clamp circuit. From: [1]

4.3.2 Conventional patch clamp

Patch clamping was developed in 1976 by Erwin Neher and Bert Sakmann [128]. In principle, patch clamp is a variant of voltage clamp with the major difference, that voltage measurement and injection of current are fulfilled by a single electrode and that the initial application of this technique was to measure currents in the pA range in a small membrane portion ("patch"), often mediated by a single ion channel protein. To this end, the glass microelectrode is not impaling the cell, but the tip is touching the membrane. Membrane and rim of the microelectrode can form a very tight connection, resulting in a very high resistance between

pipette interior and bath, the so-called "gigaseal" [129], [130]. This "cell-attached" configuration allows to measure currents of one or more ion channels which are contained in the patch while preserving the intracellular environment. From this configuration, several other configurations can be achieved:

"Whole-cell" configuration: Suction or a strong electrical impulse is imposed to disrupt the membrane area within the rim of the pipette to form a connection between the pipette and the intracellular space. Here, a very strong advantage comes into action: the control of the intracellular environment by choosing the desired pipette solution.

"Inside-out" configuration: Instead of disrupting the membrane patch to create the inside-out configuration, the pipette is lifted up rapidly, so the membrane patch is pulled out of the cell membrane while still forming the gigaseal with the pipette. Thus, the extracellular membrane area is inside the pipette and the inner pacing part of the membrane is exposed to the bath solution, which can be exchanged several times to study effects of several "intracellular" conditions.

"Outside-out" configuration: After establishing whole-cell configuration, the pipette is lifted up and remaining parts of the membrane outside the pipette rim can reform a closed compartment, similar to a very small cell with less ion channels than in whole-cell configuration.

4.3.3 Description of the setup

The patch clamp setup consisted of an inverted Olympus IX71 microscope, mounted on an air shock dampened table (TMC) surrounded by a Faraday cage to shield against external electric fields. A headstage acted as a preamplifier and as a mounting for the pipette holder. In order to move the pipette in all three directions, the headstage was mounted on a LM-1 micromanipulator (Luigs & Neumann). The amplifier was an EPC-10 (HEKA) which was connected via an integrated LIH 8+8 AD/DA interface to a Windows computer. The data acquisition program, which also controlled the amplifier parameters, was HEKA PatchMaster. To identify transfected cells by fluorescence or conduct fluorescence measurements, a Polychrome V monochromator (Till Photonics) was connected to the rear port of the microscope via a light conductor. For fluorescence measurements the side port of the microscope additionally contained a PMT-equipped ViewFinder III (Till Photonics), connected to a video monitor and a breakout box for communication with the computer.

4.3.4 Pulling of microelectrodes

Microelectrodes were pulled from borosilicate capillaries (Harvard Apparatus GC120TF-10) with a Sutter P-97 horizontal puller and fire polished with a Narishige MF-830 microforge to achieve resistances of 1-2 MΩ. For measurements of non-stationary noise or capacitances, prior to polishing, pipette tips were coated in a hot wax bath (Thomas Oertel Dental x-hard) to reduce background noise and pipette capacitance.

4.3.5 Cell perfusion

Perfusion of cells was done in two different ways: In cases of anion selectivity and uncoupling experiments, the whole bath solution was exchanged by a combination of gravity driven solution flow from reservoirs of different solutions and simultaneous extraction by suction via a membrane pump connected to a waste bottle. To keep the exchange time and volume small, cells were grown on round coverslips and put into a small measuring vessel consisting of Teflon rings of 18mm inner diameter, glued with Sylgard (Dow Corning) on square coverslips (Assistent 24x24 mm, Karl Hecht AG) and fixed in a custom sample holder. In cases where a perishable reagent (like MTS reagents) was used and therefore a reservoir could not be utilized, a small volume of the solution was filled into a glass capillary which was previously pulled and broken to a narrow tip of 80 μm diameters. The walls of the capillary were made hydrophobic by silanization with Sigmacote (Sigma-Aldrich), so that gravitiy causes the fluid to run out as soon as the pipette tip is inserted into the bath solution. For perfusion, the cell was manipulated into the stream of solution.

In both cases, the progress of perfusion was monitored by regularly applying a voltage pulse and perfusion was considered finished when the current response reached a steady value.

4.3.6 Solutions and reagents

All reagents used were at least purity p.a. and purchased from Fluka, Sigma-Aldrich, Roth, Serva and Merck.

internal	composition (mM)
1	105 NaCl, 20 HEPES, 2 MgCl$_2$, 5 EGTA, pH 7.4
2	105 NaCl, 20 MES, 2 MgCl$_2$, 5 EGTA, pH 6.0
3	105 NaCl, 20 AMPSO, 2 MgCl$_2$, 5 EGTA, pH 8.8
4	120 NaCl, 0.25 HEPES, 2 MgCl$_2$, 5 EGTA, 33μM BCECF, 100 nM BafA1, pH 7.4
5	120 NaCl, 0.25 MES, 2 MgCl$_2$, 5 EGTA, 33μM BCECF, 100 nM BafA1, pH 6.4
6	120 NaI, 20 HEPES, 2 MgGluconate,1 NaCl, 5 EGTA pH 7.4
7	120 NaI, 20 MES, 2 MgGluconate,1 NaCl, 5 EGTA pH 6.0
8	320 NaCl, 20 HEPES 2 MgCl2, 5 EGTA, pH 7.4
9	320 NaCl, 20 MES 2 MgCl2, 5 EGTA, pH 6.0
10	30 NaCl, 135 TrisSO4, 20 HEPES, 2 MgSO4, 5 EGTA, pH 7.4
11	1 NaCl, 160 TrisSO4, 20 HEPES, 2 MgSO4, 5 EGTA, pH 7.4
12	105 NaCl, 15 HEPES, 5 EGTA, 5 MgCl$_2$, pH 7.4
external	
I	145 NaCl, 15 HEPES, 4 KCl, 2 CaCl$_2$, 1 MgCl$_2$, pH 7.4
II	145 NaNO$_3$, 15 HEPES, 4 KGluconate, 2 CaGluconate$_2$, 1 MgGluconate, pH 7.4
III	145 NaSCN, 15 HEPES, 4 KGluconate, 2 CaGluconate$_2$, 1 MgGluconate, pH 7.4
IV	145 NaGluconate, 15 HEPES, 4 KGluconate, 2 CaGluconate$_2$, 1 MgGluconate, 0.1 NaCl, pH 7.4
V	145 NaCl, 5 HEPES, 4 KCl, 2 CaCl$_2$, 1 MgCl$_2$, pH 7.4
VI	145 NaNO$_3$, 15 HEPES, 4 KGluconate, 2 CaGluconate$_2$, 1 MgGluconate, pH 7.4
VII	145 NaSCN, 5 HEPES, 4 KGluconate, 2 CaGluconate$_2$, 1 MgGluconate, pH 7.4
VIII	400 NaCl, 15 HEPES, 4 KGluconate, 2 CaGluconate, 1 MgGluconate, pH 7.4
IX	200 NaCl, 15 HEPES, 4 KGluconate, 2 CaGluconate, 1 MgGluconate, 200 NaGluconate, pH 7.4
X	100 NaCl, 15 HEPES, 4 KGluconate, 2 CaGluconate, 1 MgGluconate, 300 NaGluconate, pH 7.4
XI	40 NaCl, 15 HEPES, 4 KGluconate, 2 CaGluconate, 1 MgGluconate, 360 NaGluconate, pH 7.4
XII	4 NaCl, 15 HEPES, 4 KGluconate, 2 CaGluconate, 1 MgGluconate, 396 NaGluconate, pH 7.4
XIII	400 NaSCN, 15 HEPES, 4 KGluconate, 2 CaGluconate, 1 MgGluconate, pH 7.4
XIV	200 NaSCN, 15 HEPES, 4 KGluconate, 2 CaGluconate, 1 MgGluconate, 200 NaGluconate, pH 7.4
XV	100 NaSCN, 15 HEPES, 4 KGluconate, 2 CaGluconate, 1 MgGluconate, 300 NaGluconate, pH 7.4
XVI	40 NaSCN, 15 HEPES, 4 KGluconate, 2 CaGluconate, 1 MgGluconate, 360 NaGluconate, pH 7.4
XVII	4 NaSCN, 15 HEPES, 4 KGluconate, 2 CaGluconate, 1 MgGluconate, 396 NaGluconate, pH 7.4
XVIII	160 NaCl, 15 HEPES, 4KGluconate, CaCl$_2$, 1 MgCl$_2$

Table 3: Composition of internal and external solutions, used for electrophysiological experiments. Numbers are given in figure legends throughout this work.

4.3.6.1 MTS reagents

MTS reagents [131], [132] (Figure 4.3) were obtained from Biotium and were used for site-directed covalent modification of cysteine residues in ClC-5. Stock solutions of MTSES (2-sulfonatoethyl methanethiosulfonate) and MTSET (2-(trimethylammonium)ethyl methanethiosulfonate) were prepared as stock solutions at 1 M and 0.1 M, respectively in H_2O and stored at -20°C.
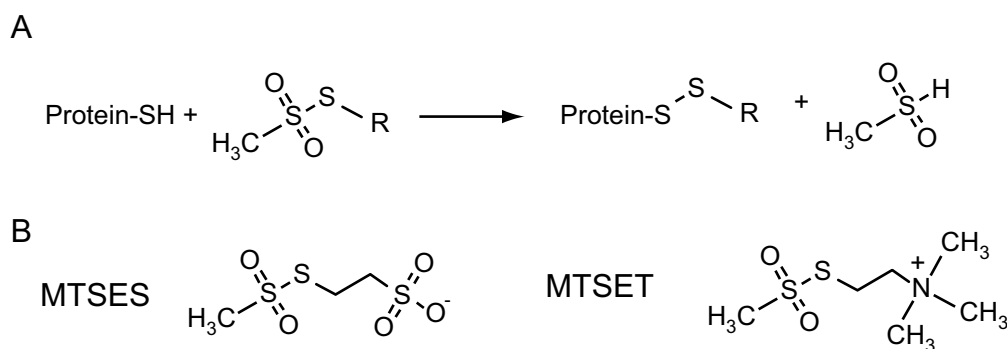
Figure 4.3: MTS reagents can be used for covalent modification of cysteine residues. A. Reaction scheme of oxidation of a protein thiol group to firm s disulfide bond to the functional residue of the MTS reagents. **B.** Structural formulas for MTSES and MTSET (Source: Interchim Uptima (modified))

4.3.7 Acquisition of measurements

4.3.7.1 Standard measurements

Cells were seeded 12 hours prior measurements. Cells were bathed in external solution and mounted on the microscope and the bath electrode, a silver wire, previously chlorided in NaOCl (DanKlorix), was introduced into the extracellular medium. In chloride substitution experiments the external electrode was connected to the bath via an agar bridge, made of poly-ethylene tubing filled with 3 M KCl in 1% agar. A measuring pipette was backfilled with pipette solution and mounted in the pipette holder, which also contained a silver/silver chloride wire. A mouthpiece or a syringe is connected to the pipette holder via a tube, making it possible to apply pressure or suction to the pipette in order to facilitate the formation of the gigaohm seal.

In "idle mode", the amplifier sends a repetitive 5-mV, 5-ms square pulse. After inserting the tip of the pipette into the bath, and thereby closing the electrical circuit, a current response to the voltage of the square pulse, is seen in the oscilloscope window of the acquisition program. From this current, the amplifier calculates the resistance of the pipette. The voltage offset is adjusted to 0 mV and the cell is touched by the pipette on which a slight pressure is applied. When the pressure is released, the cell membrane is slightly sucked into

the pipette. When additional suction is applied, the connection between pipette wall and cell membrane is enforced, so that the measured resistance between internal electrode and bath reference is increased. When the resistance is >20 MΩ, a -80-mV hyperpolarization is applied, which facilitates seal formation. Releasing the suction causes in most cases the formation of the gigaseal. In most cases the cell is detached from the substrate by carefully moving the pipette sideways before lifting it up.

Next, the pipette capacitance (C_{fast}) is compensated by an automatic algorithm of the amplifier and the cell is opened by applying a suction impulse to the pipette. The cell capacitance (C_{slow}) is compensated and the cell is left for 4-5 min to equilibrate its interior with the pipette. The ionic solution, the size of the opening of the pipette and possible membrane elements, jamming the pipette contribute to the so-called series resistance R_s which is a parameter of the algorithm to compensate C_{slow}. This series resistance causes a voltage drop between the pipette wire and the intracellular space, so that the clamped membrane potential is lower than the predetermined voltage. This is called voltage error and can be compensated at the amplifier to a certain extent, by applying a calculated voltage, corrected for this error. In practice, compensation was applied, so that the remaining voltage error was below 5 mV.

In cases, where nonlinear capacitances were to be analyzed, a -P/n leak subtraction [83] was applied. Briefly, to cancel out the linear portions of capacitative peaks, always appearing when voltage jumps are applied, preceding voltage pulses of a fraction of the actual voltage protocols are applied in the opposite direction, the evoked currents are summarized and then added to the current responses to the actual voltage protocol. This should be done at voltage ranges, where nonlinear capacitances are not expected and is an implemented function of the HEKA electrophysiology setup.

Strongly different ionic compositions of internal and external solutions can give rise to so called junction potentials [133], because ions with different charge and mobility in two adjacent volumes can impose an electrochemical gradient. This artificial potential would lead to an erroneous offset correction and thereby to wrong clamping voltages. The junction potential calculation module of the electrophysiology software Clampex 10.2 (Molecular Devices) was used to calculate this artificial offset and correction was done *a priori*, if necessary, before opening the cell.

4.3.7.2 Non-stationary noise analysis

Non-stationary noise analysis can be utilized to calculate single-channel amplitudes and absolute open probabilities at a given voltage, when a channel shows time-dependent kinetics of activation. Detailed information is given elsewhere [134], therefore only a short summary of the method is given here. The noise (i.e. the time-dependent current variance) of a membrane is dependent on the time-dependent open probability of the channels embedded in the membrane. Theoretically, when all the channels are either closed or all the channels are open, the variance is predicted to be zero. At other states, channels change stochastically between an open and closed state, thereby increasing the noise. The corresponding plot of variance versus current describes a section of an inverted parabola (Equation 1) with the initial slope providing the single channel amplitude. The setup and other endogenous membrane channels can contribute to the measured noise, so measurements of background noise at a voltage which is not sufficient to activate the channel of interest, should be done and subtracted to improve the accuracy of the method.

For whole-cell measurements of non-stationary noise, it is useful to choose ionic conditions which give rise to currents with pronounced and slow time dependence of activation [60], [99], which is true for I^- and SCN^- as internal and external anion, respectively. Pipette solutions 6 and 7 (see Table 3) and bath solution III were used. For inside-out measurements bath and pipette solutions were switched. Internal and external agar bridges, made of silicon tubing filled with 1 M KCl in 1% Agar, were used. Noise of at least 180 test pulses at +135 mV and background pulses at -40 mV were measured and filtered with 10 kHz before digitization at 100 kHz. Data analysis was performed with PulseTools (HEKA), by subtracting two subsequent measurements and calculating the variances, which were binned and subtracted by the background noise. This background corrected variance was plotted against the voltage fitted with Equation 1, which is an inverted parabola with zero variance at the maximum and minimum current and maximum variance at half-maximal current (i.e. open probability).

$$\sigma^2 = i \cdot I - \frac{I^2}{N} \qquad \text{Equation 1}$$

Here, σ^2 represents the variance, i the single channel amplitude, I the macroscopic current and N the number of channels.

4.3.7.3 Nonlinear capacitances

Nonlinear capacitances can be measured with the software lock-in extension of the EPC-10 amplifier. The sine + DC method [135] was used, which utilizes the real and imaginary part of a sine wave in combination with the DC admittance (which consists of membrane and series conduction). When the whole-cell patch clamp configuration was achieved, a voltage protocol was applied, consisting of a pulse with incrementing DC-voltage, superimposed by a sinus oscillation with a peak-to-peak amplitude of 10 mV at a frequency of 800 Hz. Currents were filtered with two Bessel filters of 10 and 2.873 kHz and digitized at 40 kHz. The capacitance plotted versus the value of the DC-voltage was fit with the first derivative of a standard Boltzmann function (Equation 2, [136]).

$$C(V) = \frac{\beta C_{max} \, e^{-\beta(V_0 - V_{0.5})}}{(1 + e^{-\beta(V_0 - V_{0.5})})^2} \qquad \text{Equation 2}$$

with

$$\beta = z \left(\frac{e_0 \delta}{k_B T} \right) \qquad \text{Equation 3}$$

C_{max} is the capacitance at the voltage of half-maximal activation $V_{0.5}$, z is the number of elementary charges e_0 displaced over a fraction δ of the membrane and k_B and T are the Boltzmann constant and the absolute temperature, respectively.

4.3.7.4 Fluorescent measurements of intracellular pH

The pipette medium was supplemented with the fluorescent pH-sensitive dye BCECF (2',7'-bis-(2-carboxyethyl)-5-(and-6)-carboxy-fluorescein, Invitrogen) [137]. Because the spectral properties of the dye (Figure 4.4 A) allow a ratiometric measurement, this method is largely independent of the concentration of the dye and more sensitive than measurements with only one fluorescence value.

A

B
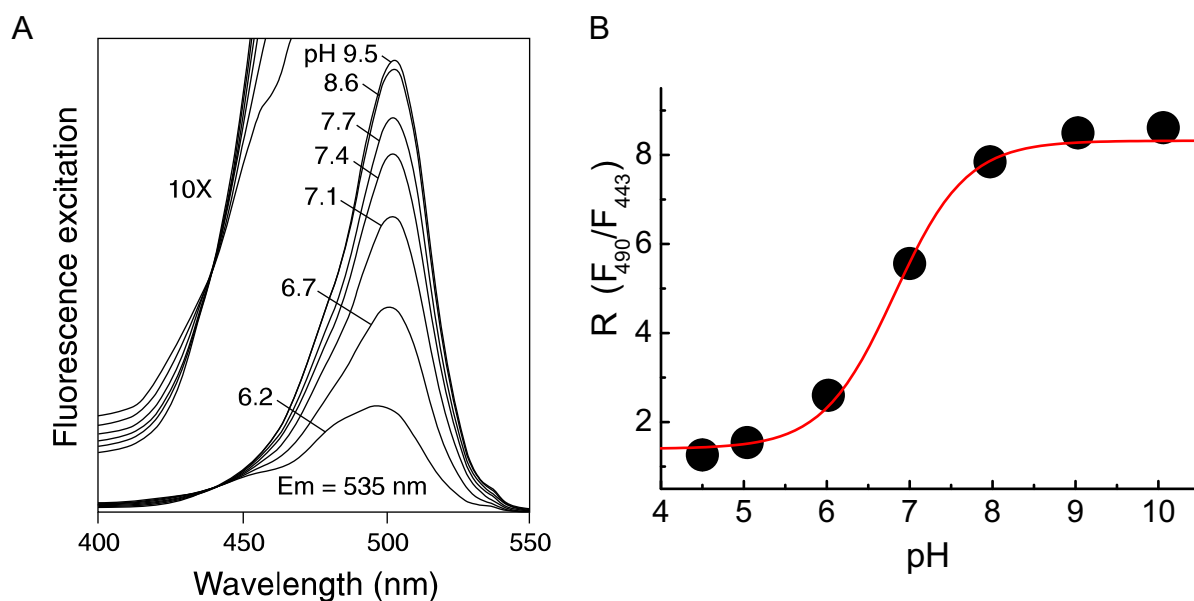
Figure 4.4: BCECF is a ratiometric pH indicator. A. Spectral properties of BCECF (source: Invitrogen), depicting the pH-dependent excitation spectra at a detection wavelength of 535 nm. The isosbestic point is the excitation wavelength, where the light absorption is pH-independent and is shown as an enlarged inset. **B.** Calibration curve for BCECF, obtained by applying 2-µl drops of solutions similar to solution 2 (Table 2, buffers AMPSO, MES and HEPES were used in their appropriate pH ranges) on a coverslip and determining the average F_{490}/F_{443} ratio of 20 measurements. For each data point, 4 drops of solution were measured this way and ratios were averaged. Red line represents fit with Equation 4.

Upon sequential excitation with light of 490 and 443 nm the ratio 490/443 of the respective emissions at 535 nm reports the pH value. A previous calibration with known pH values was conducted by measuring the ratio of BCECF fluorescence in buffers similar to solution 4 (Figure 4.4 B). A fit with Equation 4 can be done and the parameters for R_{min}, R_{max} and pK are obtained.

$$R = \frac{R_{min} + R_{max} \, 10^{\, pH - pK}}{1 + 10^{\, pH - pK}} \qquad \text{Equation 4}$$

$$pH = pk + \log\left(\frac{R - R_{min}}{R_{max} - R}\right) \qquad \text{Equation 5}$$

Equation 5 can be obtained by solving Equation 4 and measured ratios can directly be converted into pH values.

Teflon ring equipped coverslips (see Section 4.3.5) were coated with 1:30 Poly-L-lysine (see Section 4.2.4) for 20 minutes and cells were seeded out 12 hours prior measurements.
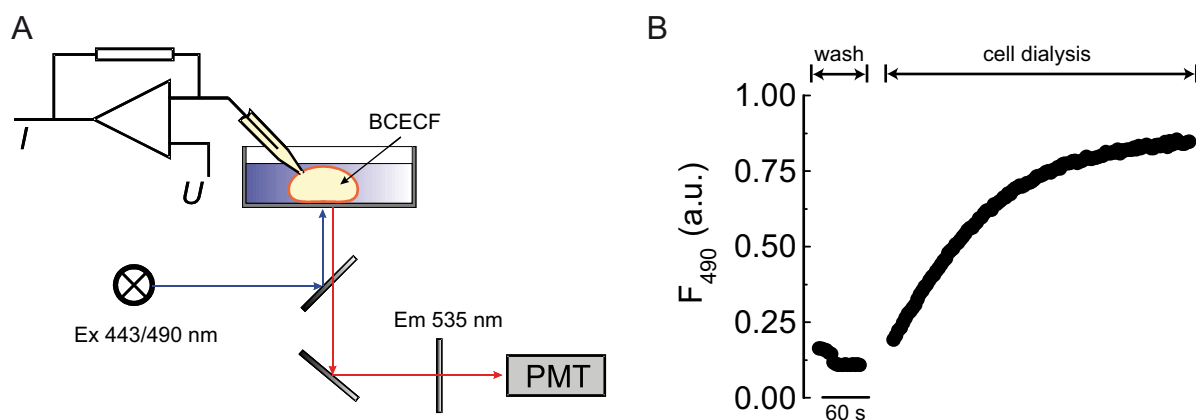
Figure 4.5: A. Schematic representation (courtesy of A.K. Alekov) of the patch clamp fluorometry setup. The cell was filled via the patch pipette with the ratiometric pH-sensitive dye BCECF, which is excited at two wavelengths, provided by a monochromator. The emission light at a single wavelength is detected by a photomultiplier. **B.** Representative time course of BCECF washout from the bath and subsequent dialysis of a cell with pipette solution containing BCECF after opening. Monitored was the fluorescence at 535 nm upon excitation with 490 nm every 5 s.

The UPlanSApo 60X/1.35 oil-immersion objective of the microscope was used and with the ViewFinder a single cell was gated for detecting the fluorescence with the PMT. By inserting the pipette into the solution, dye is flowing into the bath, elevating the fluorescence background. When a gigaseal was established and the cell was slightly lifted up the bath was perfused and the fluorescence was monitored each 5 s until background fluorescence reached its minimum. After opening, the filling of the cell with the dye was monitored and finished after about 5 min (Figure 4.5 B). Proton transport was monitored by applying a voltage pulse to the cell (Figure 4.6 A, upper panel), while simultaneously measuring the total current and the pH of the cytosol. To follow the time course of the pH change, repetitive excitation of the dye at the two wavelengths was carried out (Figure 4.6 A, lower panel) and the fluorescence ratios were calculated and later converted into pH values (Figure 4.6 B). After the depolarizing pulse, the recovery of internal pH at holding voltage was monitored by applying single 443/490 nm excitation pulses every 5 s.

To assess relative uncoupling (see Sections 5.2, 5.9 and 5.10) respective to external Cl^-, the quotients of total transport current and proton flux in one anion can be divided by the respective quotient in external Cl^- (Equation 6).

$$unc_{rel.} = \frac{I_{total}(X^-)}{\Delta pH(X^-)/\Delta t} \cdot \frac{\Delta pH(Cl^-)/\Delta t}{I_{total}(Cl^-)} \qquad \text{Equation 6}$$

This was done cellwise for various voltages and in some designated cases this relative uncoupling was calculated using normalized values to +120 mV in external Cl^-.
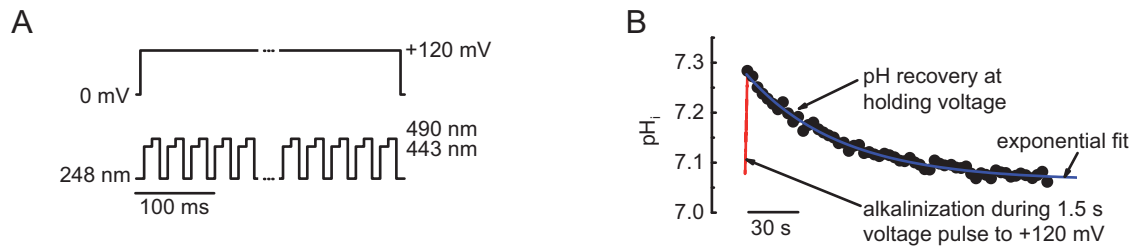
Figure 4.6: Execution of a typical measurement of intracellular pH A. Example for a typical protocol for measuring proton transport. From a holding potential an activating test pulse for 1 to 3 s is applied to the cell (e.g. 0 mV and +120 mV, respectively). During this time, the dye is excited sequentially with two excitation wavelengths 443 and 490 nm for 10 ms each, interrupted by intermediate periods at 248 nm for 10 ms, which is the resting wavelength, where no light is emitted by the monochromator. **B**. pH-dependent fluorescence ratios were converted into pH values (Equation 5) and time courses of depolarization-induced alkalinisation (red line) and subsequent recovery of internal pH at holding potential (circles) are plotted. The recovery can be fitted with a single exponential function (blue line) and describes mainly H^+ flow from the pipette into the cell, but is much slower than the preceding H^+ transport of interest.

4.3.8 Data analysis

Confocal data were analyzed with ImageJ (National Institutes of Health) and the plugin JaCoP [124]. Data analysis of electrophysiological data was performed with a combination of FitMaster (Heka), OriginPro (Originlab Corporation) and Excel (Microsoft). Three dimensional structures and structural alignments were created with Chimera (UCSF) by using PBD structures available. All error bars in graphs denote S.E.M.

5 Results

5.1 ClC-5 endosomes are not labelled by synapto-pHluorin or FITC-transferrin
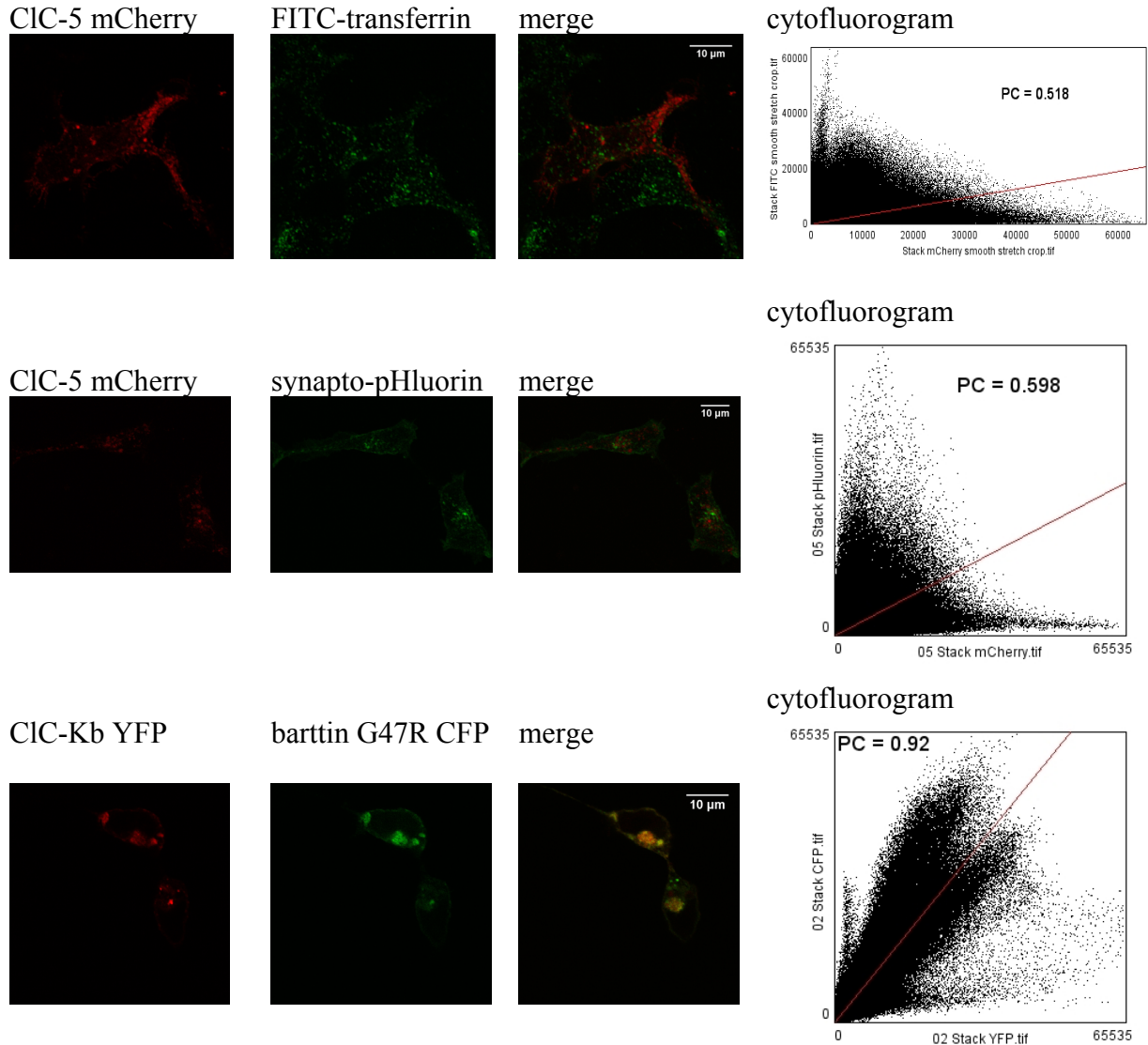
Figure 5.1: Assessment of colocalization of ClC-5 with pH-sensitive dyes. Representative confocal images of HEK293T cells, transiently transfected with ClC-5 mCherry and labelled with FITC-transferrin (**upper row**), HEK293 cells, stably transfected with ClC-5 mCherry and transiently transfected with ratiometric synapto-pHluorin (**middle row**) and HEK293T cells, transiently transfected with ClC-Kb YFP and Barttin G47R CFP (**lower row**). In merged images colocalization is shown in yellow. Right column shows a representative analysis of the respective image stacks, analyzed with JACoP, resulting in a cytofluorogram, where each pixel is plotted according to its fluorescence in both channels with a fitted straight line in red.

In order to estimate the effects of various modifications of ClC transport on endosomal physiology in this work, a quantitative measuring methodology to estimate intravesicular pH was sought.

In previous works which studied the effect of ClC-4 and ClC-5 on endocytosis and the pH of endosomes, synapto-pHluorin [138], [139] or FITC-conjugated transferrin [57], [76]

were used. In those publications, colocalization was either not tested directly or only assessed qualitatively. Synapto-pHluorin has first been used to visualize the exocytotic event of the fusion of synaptic vesicles to the membrane of a neuron [120]. Endosomes can also be labelled from the extracellular side by receptor mediated endocytosis of transferrin [57]. Following this approach in this work, fluorescently labelled ClC-5 was expressed in HEK293T cells. Its colocalization with the aforementioned markers was investigated using confocal microscopy. Subsequently, a quantitative approach, analysing three-dimensional datasets of confocal imaging with the ImageJ plugin JACoP [124] was used to evaluate the degree of colocalization of ClC-5 with selectively targeted pH-sensitive dyes. In order to test the validity of the analysis, two other proteins were also tested: The renal chloride channel ClC-Kb and its accessory subunit barttin, which is amongst other things necessary for membrane targeting of this channel [36]. Cotransfection of ClC-Kb and the G47R mutant of barttin results in mistrafficking and endosomal-like staining and a colocalization was qualitatively shown previously [35]. Upper row in Figure 5.1 shows representative images of cells, transfected with ClC-5 mCherry and labelled with FITC-transferrin. ClC-5 mCherry staining showed a spotty pattern in accordance with its endosomal localization [73], but also membrane staining was seen. FITC-transferrin displayed a similar pattern, only with less membrane staining. Surprisingly however, no colocalization was observed in the merged images. This was also reflected in the quantitative analysis of the corresponding 3D data depicted in the right column with a wide point spread around the fitted line, resulting in a Pearson's coefficient of 0.518, which also reports on absent colocalization. Co-expressing ClC-5 mCherry together with synapto-pHluorin (Figure 5.1, middle row) resulted in a similar fluorescence distribution and the calculated colocalization was similarly low as reflected in the calculated Pearson's coefficient of 0.598. As previously shown in a qualitative approach [35] and as seen in the extensive yellow overlap in the merged picture, there was a large degree of colocalization between ClC-Kb YFP and barttin G47R CFP (Figure 5.1, lower row) with a slightly denser cellular distribution resulting in a value of 0.92 for the Pearson's coefficient. Statistical values of several of those experiments are displayed in Figure 5.2.

A

B

staining	PC
ClC-5 mCherry / synapto-pHluorin	0.56 ± 0.03
ClC-5 mCherry / FITC-transferrin	0.44 ± 0.03
YFP ClC-Kb / G47R Barttin CFP	0.86 ± 0.04
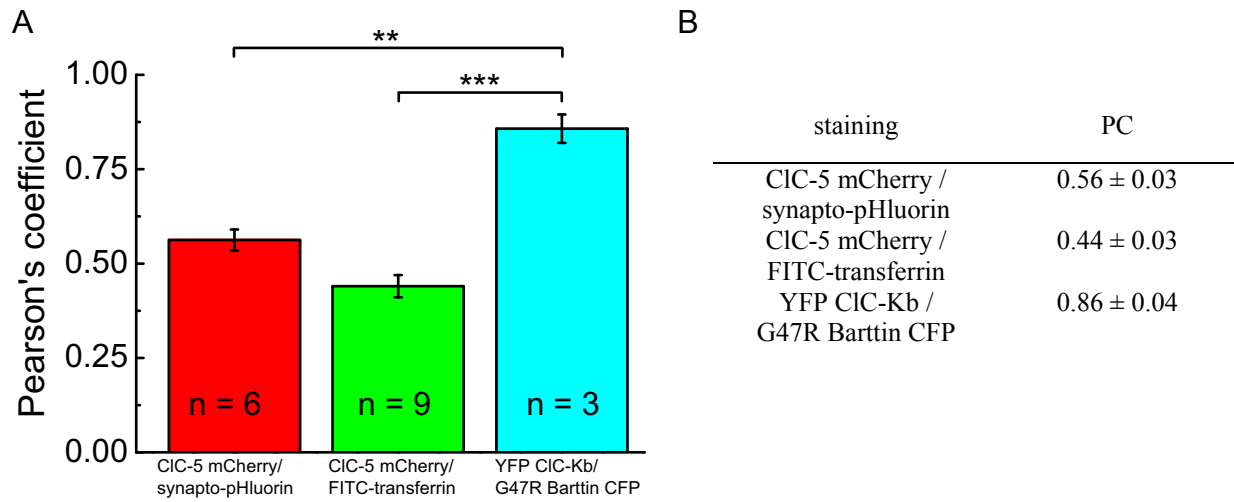
Figure 5.2: Statistical evaluations on colocalization of ClC-5 with synapto-pHluorin or FITC-transferrin. **A** Mean values for Pearson's coefficients (PC) of three double stainings, as indicated, calculated with JACoP from experiments as in Figure 5.1. with statistical values given in **B**. Significant differences were tested using a two-sample t-test Stars (***, p < 0.001; **, p < 0.01).

5.2 Effects of neutral and acidic internal pH on coupled ClC-5 transport
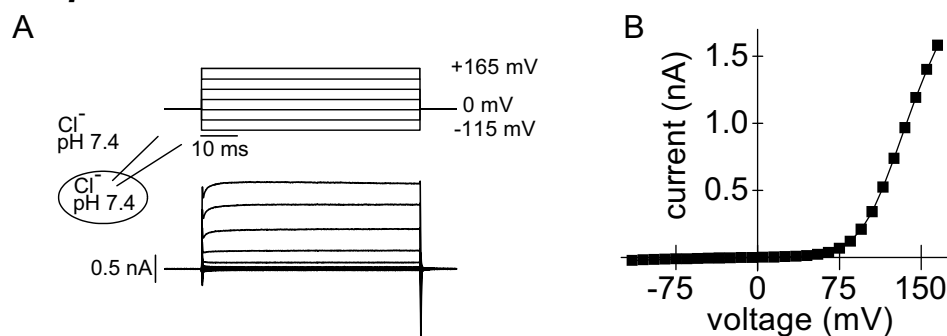
Figure 5.3: Cl⁻ currents mediated by ClC-5 are very outward rectifying with a large transient current at the end of the pulse. A. Voltage protocol and corresponding representative whole-cell current response of a HEK293T cell, expressing ClC-5, measured in standard Cl⁻ solutions (1 and I, see Table 3). For clarity, some intermediate traces were omitted. **B.** Current-voltage relationship of steady-state currents for the measurement depicted in A.

Figure 5.3 A shows a representative recording of ClC-5 mediated Cl⁻ current upon voltage pulses from -115 to +165 mV from a 0-mV holding potential. The measured currents were strongly rectifying with virtually no transport observed in the negative range, whereas pulses more positive than +75 mV resulted in pronounced outward currents, which were absent in nontransfected HEK293 cells (Figure 5.4 B). Following the initial instantaneous rise and the transient capacitive peaks, further time-dependent activation is observed. Pulses back to the holding potential resulted in the appearance of large capacitive peaks that do not depend linearly on the voltage.
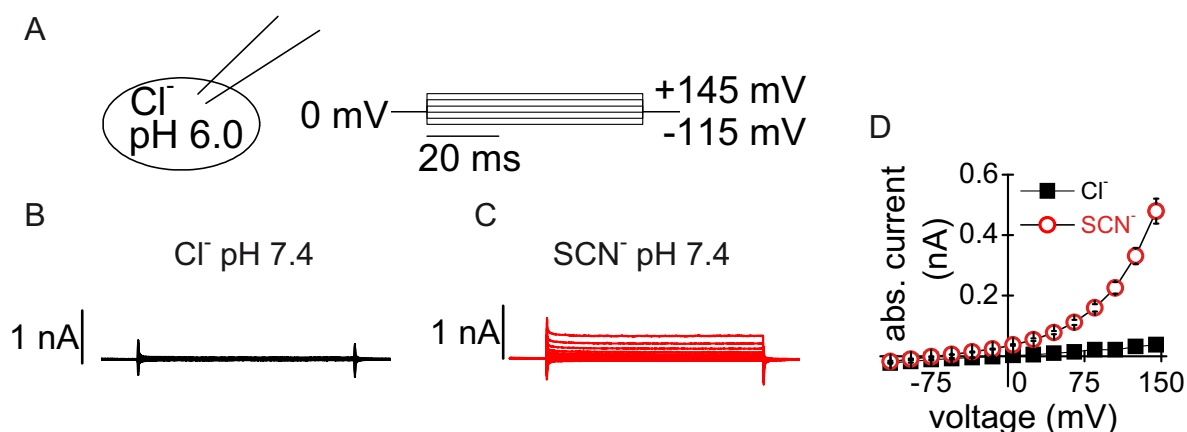
Figure 5.4. **Measurements of nontransfected HEK293 cells show no Cl⁻ and very low endogenous SCN⁻ conductance. A.** Internal pH conditions and voltage protocol used for permeability assays. **B** and **C.** Representative measurements of a nontransfected HEK293 cell, externally sequentially perfused with Cl⁻ and SCN⁻ solutions at pH 7.4 (solutions 2, I and III, see Table 3). **D.** Mean current-voltage relationships of steady-state currents, measured from six cells. (Modified from Grieschat and Alekov, 2012)

Figure 5.5 A and B show measurements of the same HEK293T cell, expressing ClC-5 and being sequentially perfused either with external Cl$^-$ or SCN$^-$ containing solution. As previously shown for ClC-5 expressed in *Xenopus laevis* oocytes [59], external SCN$^-$ evoked much larger outward currents (Figure 5.5 C). The relative current increase was voltage-dependent and in the range of ~7-13 times (Figure 5.5 G, black columns). When the same experiment was performed at internal pH 6.0 this increase of current was dramatically enhanced in a voltage-dependent manner, reaching factors of ~26 to 51 (Figure 5.5 D-G). In those experiments, cells with fairly low expression had to be selected, because otherwise ClC-5 currents in external SCN$^-$ would have become too large to be voltage-clamped reliably.
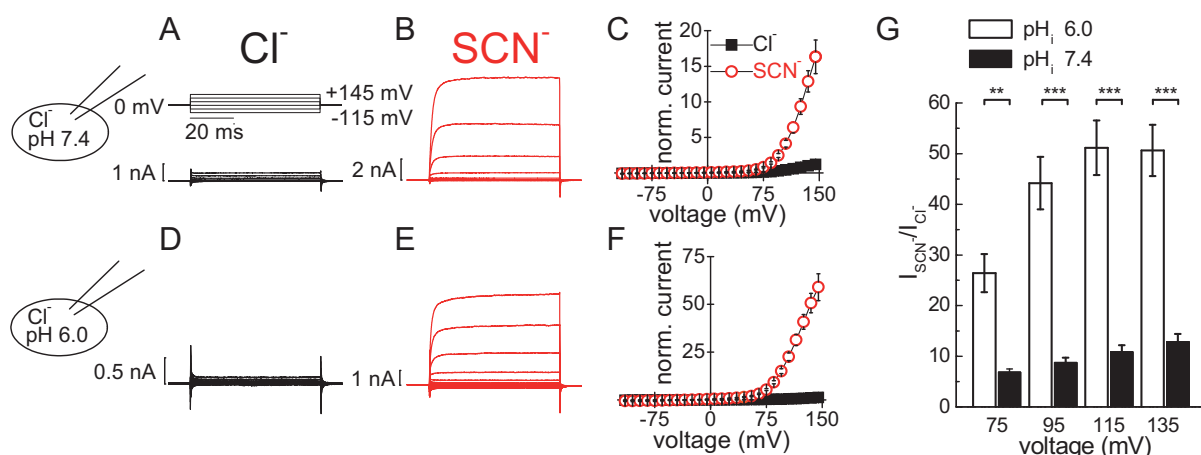
Figure 5.5: Current increase in external SCN$^-$ is dependent on internal pH. **A.** Voltage protocol (**upper panel**) and representative whole-cell measurement of a cell expressing ClC-5 at neutral internal pH. **B.** Recording of the same cell, bathed in SCN$^-$ (solutions 1, I and III, see Table 3). **D** and **E.** Representative recording of a cell externally perfused with Cl$^-$ and SCN$^-$-based solutions, respectively (solutions 2, I and III). **C** and **F.** Current-voltage relationships of experiments shown in A, B, D and E, depicting steady-state currents, normalized to the currents in Cl$^-$ at +135 mV at internal pH 7.4 (**C**) and pH 6.0 (**F**), respectively. **G.** Ratios of current increase upon SCN$^-$ application at different voltages for internal pHs 6.0 and 7.4. Significant differences are indicated by stars (***, p < 0.001; **, p < 0.01, two-sample t-test, n = 10 for pH 7.4, n = 8 for pH 6.0). (Modified from Grieschat and Alekov, 2012)

ClC-5 is a Cl$^-$/H$^+$ antiporter [12], [13] with two Cl$^-$ ions transported in exchange to one proton [79], although different estimates have been published [12], [13]. In previous studies on ClC-5 or the closely related isoform ClC-4, large polyatomic anions such as NO$_3^-$ or SCN$^-$ were shown to convert a certain percentage of ClC transporters in the membrane into "channel mode" [59], [60] which manifested in an increase of anionic current and a decrease of proton movement. Using same approach that Alekov and Fahlke have applied for ClC-4 previously [60], ClC-5 anion/proton antiporter action was investigated here. The ratiometric pH-sensitive fluorescein dye BCECF [137] was used in the pipette solution to report on time-dependent pH

changes. Figure 5.6 A shows a representative measurement of the internal pH at different voltages with Cl⁻ as the external anion.
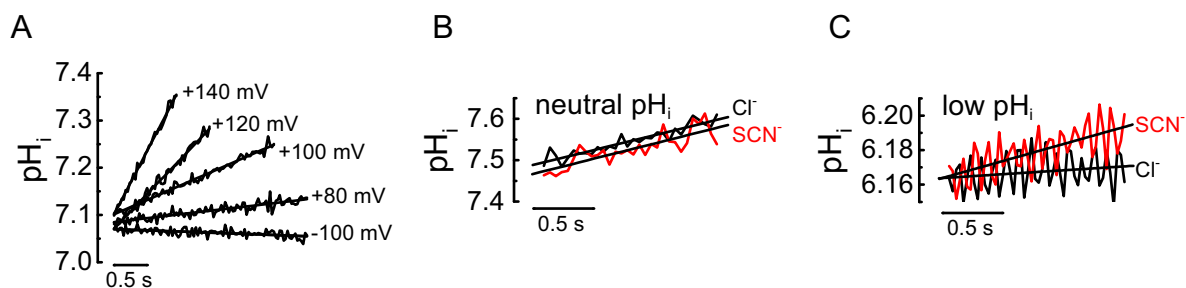
Figure 5.6: External Cl⁻ and SCN⁻ are able to induce voltage-dependent proton transport. A. Representative measurements of the time-course of ClC-5 mediated internal alkalinisation during voltage jumps to different potentials. **B** and **C.** Representative proton transport at +120 mV at symmetric pH 7.4 (**B**) or pH 6.3 (**C**), measured in external Cl⁻ and SCN⁻ (solutions 4 or 5 and V and VII). Lines indicate linear fits to the data. (Modified from Grieschat and Alekov, 2012)

During pulses with voltages higher than +80 mV, a profound alkalinisation of the cytosol was observed, reflecting H^+ transport. A linear regression line was fitted to the data and the slope was used as a quantitative measure proportional to the proton flux. This process showed the same rectification at negative and activation at positive voltages as the ionic transport measured electrophysiologically (Figure 5.7 A and Figure 5.3 A). Exchanging external Cl⁻ for SCN⁻ did not have a significant effect on the proton transport (Figure 5.6 B and Figure 5.7 A) but the strong increase of anionic current can be regarded as transport uncoupling. Therefore, when dividing the current amplitudes and proton fluxes in external SCN⁻ by the values in external Cl⁻ of the same cell (see Equation 6 in Section 4.3.7.4), a relative uncoupling in external SCN⁻ could be calculated (Figure 5.7 C). This resulted in values ranging from ~12 to 17. Surprisingly, when the same experiment was conducted at acidic internal and external pH (Figure 5.6 C and Figure 5.7 B) the proton transport in external SCN⁻ significantly exceeded the proton transport in external Cl⁻. Measurements of internal pH at acidic values were generally noisier and the detected pH changes were smaller (Figure 5.6 C) because the BCECF fluorescence is lower at low pH, resulting in worse signal-to-noise ratios. In addition, the detection sensitivity of the dye is reduced at lower pHs (Figure 4.4 B). And most importantly here again, cells with fairly low ClC-5 expression had to be chosen to achieve SCN⁻ currents that were not too large. The calculation for relative uncoupling in external SCN⁻ revealed a very similar degree of uncoupling compared to measurements in neutral pH (Figure 5.7 D). Thus, the much stronger current increase in external SCN⁻ is not the consequence of a stronger uncoupling. Here, measurements of proton flux also in the acidic pH range were carried out at symmetrical pH to circumvent methodological problems,

whereas current increase experiments (see Figure 5.5) were always done with external pH 7.4. However, this had no qualitative impact on the results, because current increase in SCN⁻ at symmetrical pH 6.3 (Figure 5.8) was very similar to measurements at internal pH 6 and external pH 7.4.
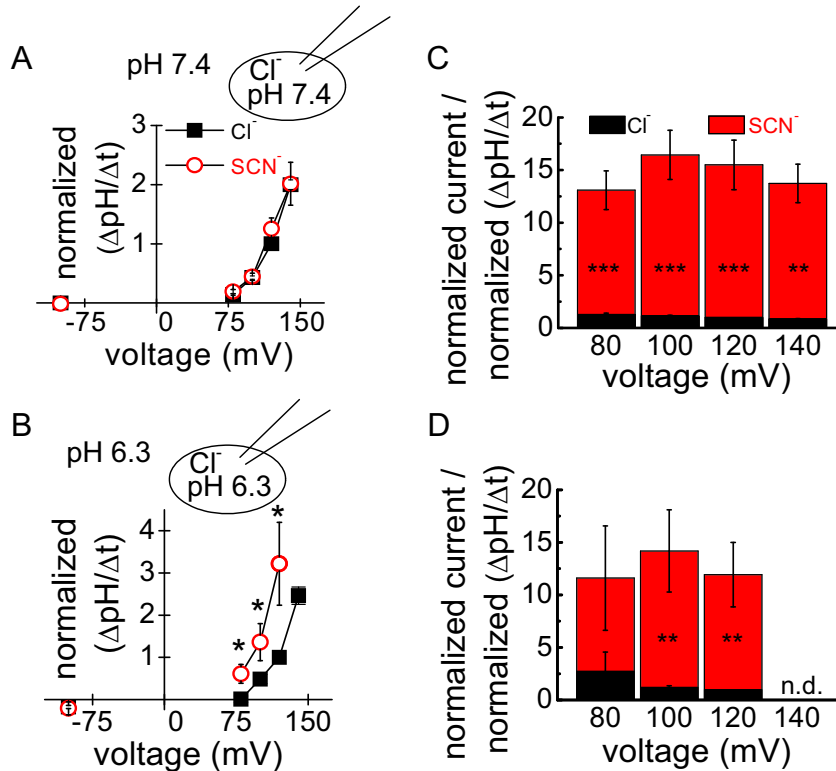
Figure 5.7: Internal protons do not further uncouple proton transport from SCN⁻ transport. A and **B.** Rates of internal pH change in external Cl⁻ and SCN⁻ at symmetrical pH 7.4 (**A**) or pH 6.3 (**B**), normalized to the respective values in Cl⁻ at +120 mV. Rates were obtained from the slopes of linear fits like shown in Figure 5.6. **C** and **D.** Relative uncoupling mediated by external SCN⁻ at different voltages, calculated by the ratio of normalized current to normalized proton flux. Normalization was performed to the values in Cl⁻ at +120 mV. Stars indicate significant differences according to paired t-tests (***, $p < 0.001$; **, $p < 0.01$; *, $p < 0.05$). n.d., not determined. (n = 6-17 for pH 7.4 and n = 4-5 for pH 6.3). (Modified from Grieschat and Alekov, 2012)
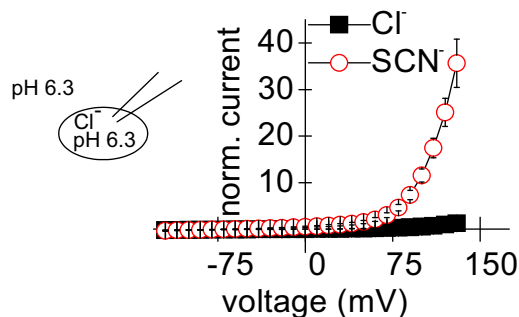
Figure 5.8: Relative current increase by external SCN⁻ at symmetrical pH 6.3. Mean current-voltage relationships of ClC-5 steady-currents in external Cl⁻ and SCN⁻, normalized to the currents at +120 mV in Cl⁻. (Modified from Grieschat and Alekov, 2012)

5.3 Non-stationary noise at neutral and acidic internal pH

Non-stationary noise measurements are well established for estimating unitary conductances in ion channels. It was shown previously for ClC-4 and ClC-5 that also those transporters are valid targets for noise analysis: Zdebik and colleagues [59] proposed the transport activity of ClC-5 to occur in bursts that resemble a channel in the open conformation. Furthermore they showed that the Fourier transformed noise ("power spectrum") follows the $1/f^2$ behaviour of Lorentzian noise, which is commonly attributed to channels. Alekov and Fahlke [60] proposed for ClC-4, that by SCN^- application a large percentage of transporters switch into "channel mode" and thereby permit noise analysis.

To examine the role of internal protons on the strong current increase in external SCN^-, the unitary current amplitude at acidic and neutral pHs was assessed. Using internal I^- [60], [99] slowed down the kinetics of activation to increase the resolution of the method. Figure 5.9 A and B shows representative measurements of two cells at pHs 6.0 and 7.4. Upon voltage pulses to +135 mV, nearly no instantaneous current was seen and the portion of time-dependent current increase was very pronounced. The variance was similarly time-dependent and increased as more ClC proteins were activated over the time range of the voltage pulse. Plots of binned variances versus the currents (Figure 5.9 C and D) appear linear which, according to the theory of noise analysis represents the initial segment of a parabolic function (Equation 1). The short portion of the parabola which was covered by the data suggests that ClC-5 has a very low absolute open probability at this voltage. The initial slope of the parabola reports on the single-channel amplitude and several experiments for pHs 6.0 and 7.4 at +135mV revealed average values of 94.1 ± 6.3 fA and 122.8 ± 15.1 fA, respectively, which were not significantly different.
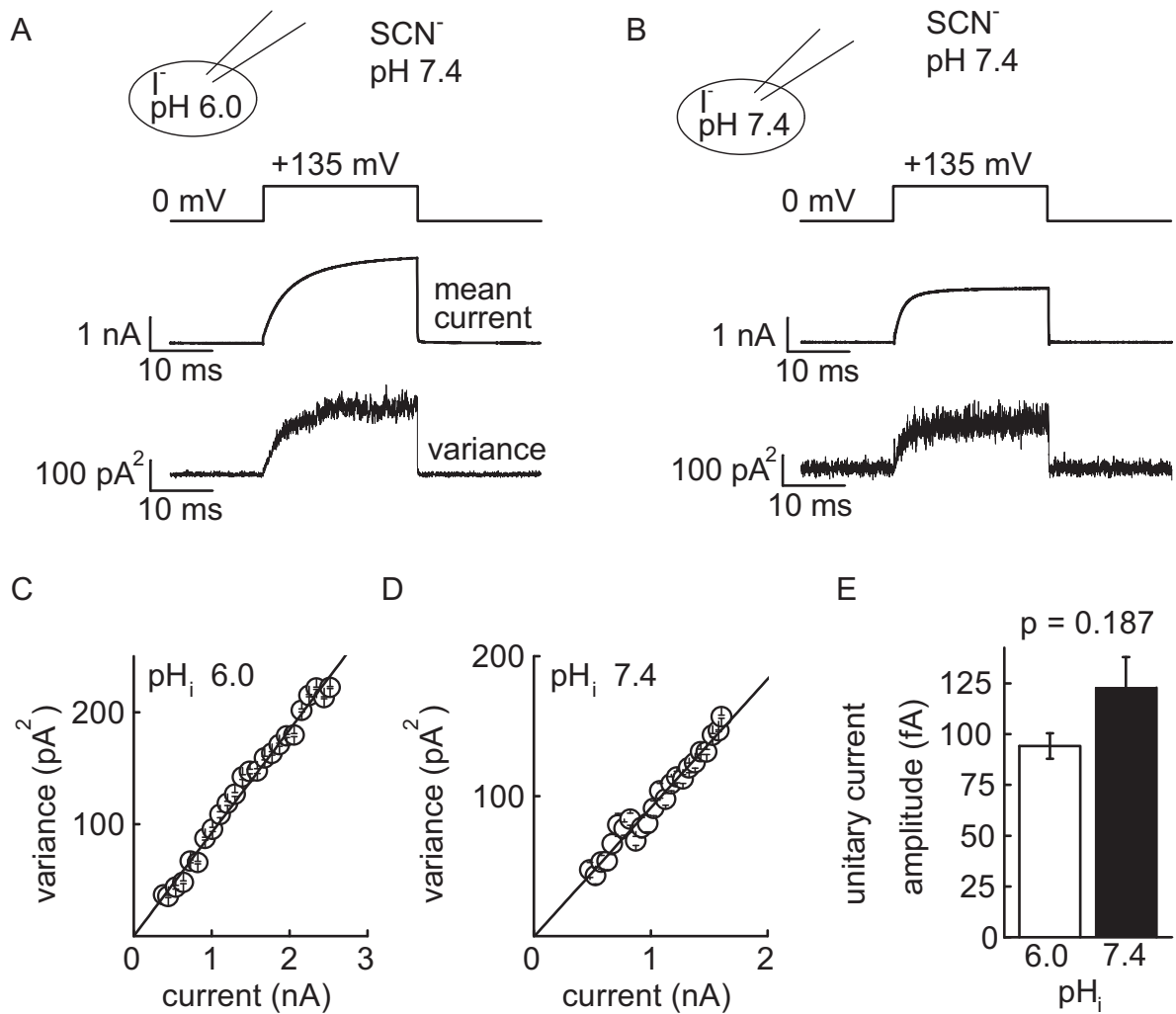
Figure 5.9: ClC-5 unitary amplitude is not significantly modified by internal pH. A and **B**. Ionic conditions for whole-cell noise measurements (solutions 6, 7 and III, see Table 3), voltage protocol and representative recordings for mean current and variance of cells, expressing WT ClC-5, measured at internal pH 6.0 (**A**) or pH 7.4 (**B**), respectively. **C** and **D**. Binned variances plotted against mean current of the cells depicted in A and B with lines obtained from parabolic fits (Equation 1). **E**. Mean unitary current amplitudes from whole-cell noise measurements at pH 6.0 (n = 4) and 7.4 (n = 3). The difference was tested with a two sample t-test. (Modified from Grieschat and Alekov, 2012)

To test the validity of the method and to exclude possible filtering artifacts associated with the whole-cell configuration, also inside-out measurements were performed. Figure 5.10 shows a representative measurement which reports approximately the same single-channel amplitude as elucidated by whole-cell measurements.
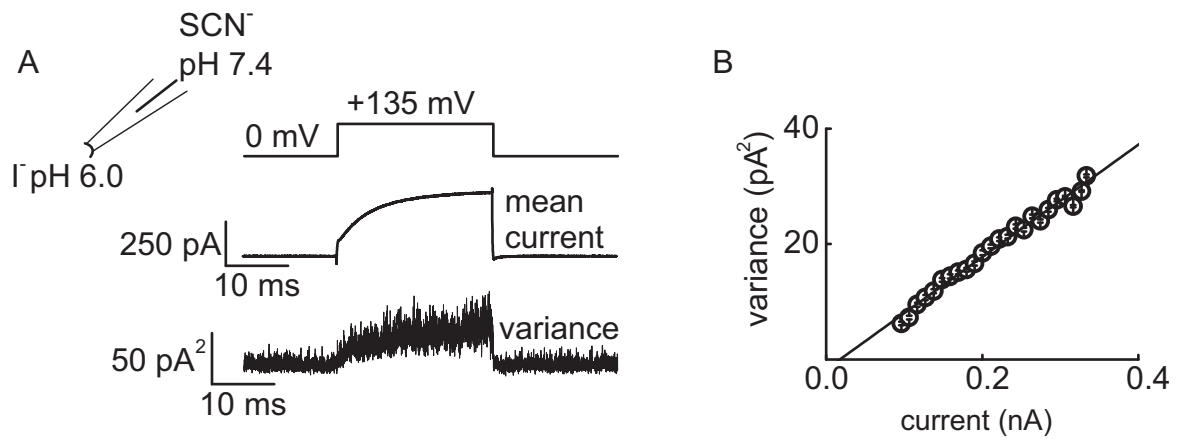
Figure 5.10: Non-stationary noise measurement in inside-out configuration. A. Ionic conditions, voltage protocol, mean current and variance of an inside-out noise measurement of a cell expressing WT ClC-5. **B.** Variance, plotted against the current of the cell depicted in A. The line displays a parabolic fit to Equation 2 and the slope reports a unitary current amplitude of 134 fA. Statistical data of three cells provide a unitary current amplitude of 120 ± 7 fA. (Modified from Grieschat and Alekov, 2012)

5.4 Concentration dependence of ClC-5 currents

The strong current increase upon SCN$^-$ perfusion at acidic internal pH values could be due to altered affinities to the transported anions at the different pHs. External Cl$^-$ and SCN$^-$, respectively, were substituted by equimolar concentration of sodium gluconate to cover a concentration span of 4 to 400 mM. To compensate for the osmolarity and to prevent an excessive electrochemical gradient at high external anion concentrations, internal Cl$^-$ was elevated to 320 mM. Voltage ramp protocols (Figure 5.11 A, upper panel) were used to determine whole-cell current amplitudes at constant perfusion with solutions of respective anion concentrations (Figure 5.11 A, upper panel and B).
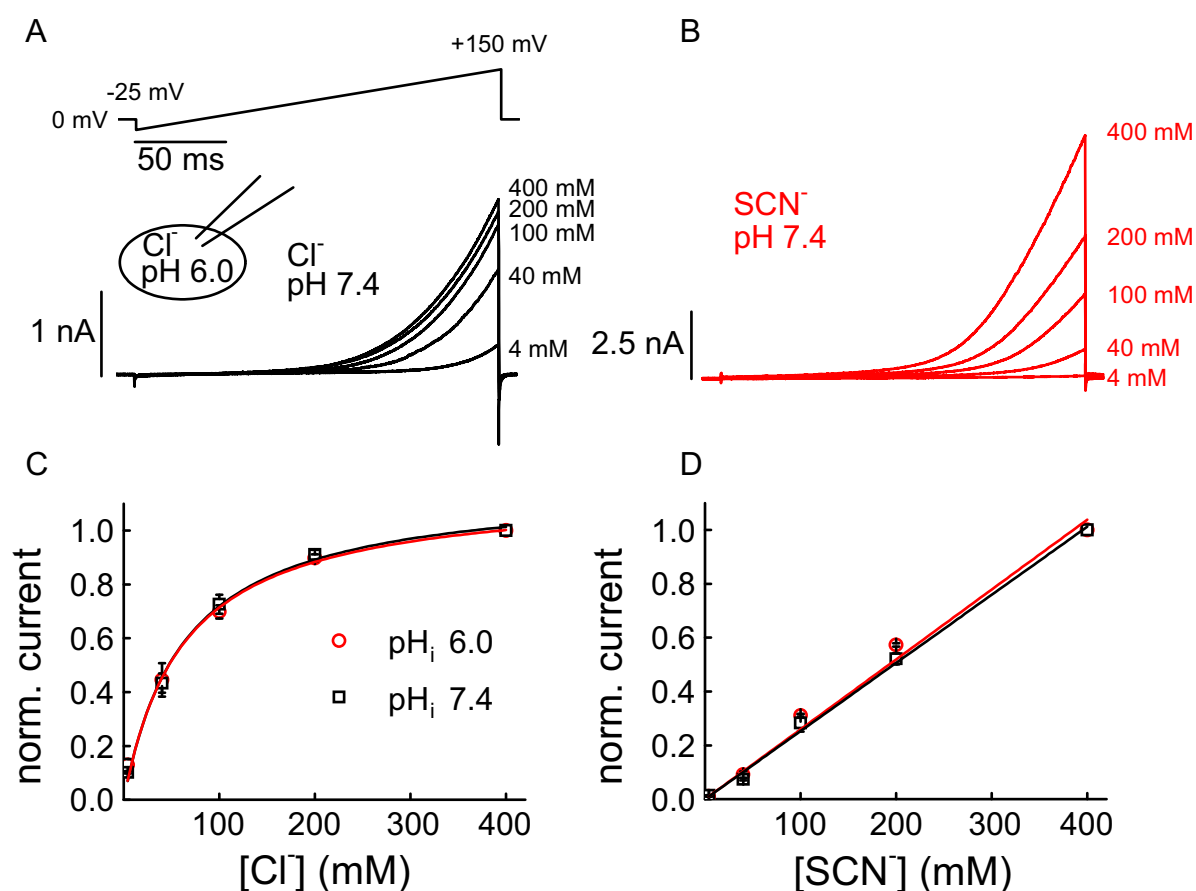
Figure 5.11: Internal pH does not alter apparent K$_d$ values for external Cl$^-$ or SCN$^-$ in ClC-5. A. Voltage ramp protocol for measuring the concentration dependence of currents on external anion concentration and representative whole-cell measurement of a ClC-5 expressing cell, externally perfused with solutions of different Cl$^-$ content and internal Cl$^-$-based solution at pH 6.0 (solutions 9 and VIII – XII, see Table 3). **B.** Representative recording of a cell, externally perfused with different SCN$^-$ concentrations and internal Cl$^-$ at pH 6 (solutions 9 and XIII – XVII). **C and D.** Concentration curves from experiments as in A and B for external Cl$^-$ (**C**) and SCN$^-$ (**D**) at internal pHs 6.0 or 7.4, respectively. Currents were measured at +120 mV of the ramp and normalized to the current at 400 mM external anion concentration. Lines in C represent fits to the Hill equation (Equation 7) with one assumed binding site (Hill coefficient = 1). K_d values for Cl$^-$ are 65 ± 15 mM and 65 ± 9 mM for pHs 6 and 7.4, respectively and not significantly different (two-sample t-test, p = 0.99, n = 4-5). Lines in D are linear regression lines. (Modified from Grieschat and Alekov, 2012)

When solution exchange was completed, indicated by steady current levels, currents at +120 mV were analyzed and plotted against the external anion concentration. The concentration dependence could be fitted with the Hill equation (Hill coefficient = 1),

$$I = \frac{I_{max}[A^-]}{K_d + [A^-]},$$ Equation 7

where I_{max} and K_d designate the saturating current and the apparent dissociation constant, respectively.

Fits to data from individual cells in external Cl⁻ reveal an apparent K_d of 65 mM at both internal pHs, which is similar to values published by another group [140]. As previously published for other ClC transporter isoforms [60], [97] saturating concentration dependence for external SCN⁻ could not be observed and only for visualization linear regression lines were fitted to the data. The slopes of those linear fits show only slight differences at both pHs. Therefore, acidic internal pH does not change the apparent affinities for external anions.

5.5 Voltage dependence of ClC-5 gating

Most ClC proteins show voltage-dependent activation, which means that at different voltages, different numbers of channels can be opened. Therefore, the probability to find a channel in the open conformation changes in a voltage-dependent fashion. This was shown for a number of ClC isoforms, preferably by so-called tail-current analysis: Preconditioning pulses of different voltages are applied to open a certain percentage of channels to reach a steady-state current. A subsequent test pulse of a constant voltage reveals the relative open probability, if the current magnitudes at the time of the test pulse are plotted versus the value of the pre-pulses. If the data are fit with a Boltzmann function (Equation 8), which reports on the behaviour of charged particles in an electric field, the inflection point reports on the voltage of half maximal activation.
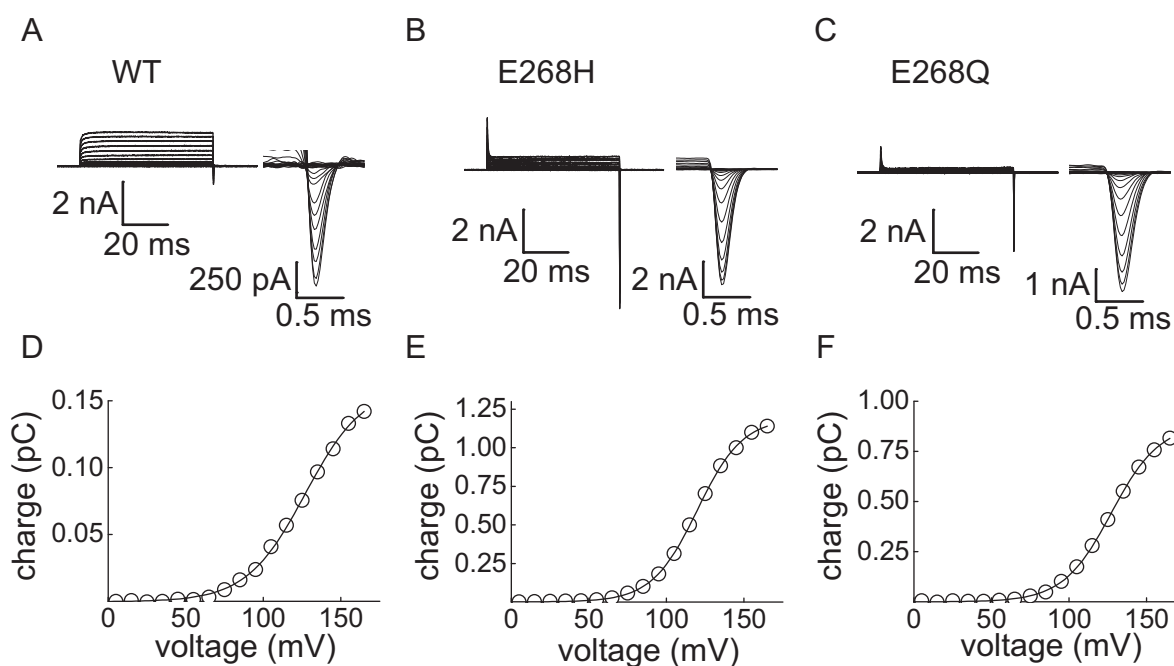
Figure 5.12: ClC-5 displays pronounced nonlinear capacitances. A-C. Representative -P/n leak subtracted whole-cell recordings of WT ClC-5 (**A**) and mutants E268H (**B**) and E268Q (**C**) upon voltage jumps from -115 to +165 mV in Cl⁻ solutions at symmetrical pH 7.4 (solutions 1 and I). The capacitative currents are displayed as enlarged insets. **D-F.** Charge-voltage curves for the cells depicted in A-C. For values positive to 0 mV the area between off-gating curve and baseline was integrated and plotted against the voltage. Solid lines represent fits with the Boltzmann function (Equation 8). (Modified from Grieschat and Alekov, 2012)

In case of ClC-5 this procedure is not feasible for several reasons: First of all, the tail-current analysis requires sufficient current levels, which is not always the case with some mutants. A second reason is the occurrence of large gating currents (Figure 5.12 A-C) which manifest as large transient peaks that superimpose the area of interest at the connection between prepulse

and test pulse and make a determination of relative open probabilities very difficult at most conditions.

However, those gating currents can be used to characterize the voltage dependence of the underlying process. They can be separated from linear capacitances by leak subtraction ([83], see Section 4.3.7.1) and the voltage dependence of either the magnitudes of the peaks or the area under the traces can also be described by a Boltzmann function [141].

$$Q(V) = \frac{Q_{max}}{1 + e^{(V - V_{0.5})/k}}$$ Equation 8

with

$$k = \frac{RT}{zF}$$ Equation 9

In this case, $Q(V)$ is the integral of the off-gating at the respective voltage, Q_{max} is the maximum charge movement, $V_{0.5}$ the voltage of half-maximal activation and k is the slope factor, describing how many elementary charges are displaced during activation through a certain fraction of the membrane and is composed of R, T, F and z which represent the universal gas constant, the absolute temperature and the Faraday constant and the valence, respectively.

The depolarization-activated process that is the origin for the gating currents might be modified by internal protons, and the ClC transporter isoforms possess an internal protonation site: the proton glutamate, which is crucial for coupled transport because here the protons are inserted into the transport cycle [93]. Zdebik *et al.* proposed this insertion to be a voltage-dependent process [59]. Figure 5.12 A-C shows representative leak subtracted whole-cell current traces in Cl⁻ of cells expressing WT ClC-5 and two proton glutamate mutants. In E268H ClC-5 the glutamate is substituted by the also protonatable histidine. However, it has a less acidic pK$_a$, and whereas the glutamate side-chain is negative and becomes neutral upon protonation, the side-chain of histidine is neutral and gains a positive charge, if protonated. The second mutation tested is E268Q with a nonprotonatable glutamine in place of glutamate, which was published to render ClC-5 nonconducting [59]. The wildtype protein (Figure 5.12 A) mediated large anionic outward currents followed by gating currents when the voltage is set back to holding potential. This is the so-called off-gating, first published by Smith *et al.* for ClC-5 [80]. The on-gating upon jumping to positive voltages was often superimposed by ionic current and therefore not visible in wildtype. The mutant E268H ClC-5 (Figure 5.12 B)

also displayed substantial ionic currents, but the proportion of gating current to ionic current was well shifted towards gating currents. An on-gating current was clearly visible upon depolarizing voltage steps. When the proton glutamate was substituted by the nonprotonatable glutamine (Figure 5.12 C), nearly no ionic currents, but pronounced gating currents can be seen under those conditions. When the off-gating currents are integrated and plotted against the voltage (Figure 5.12 D-F), the curves can be fit with the Boltzmann function (Equation 8) and statements on the voltage dependence of depolarization activated gating can be made. For the representative cell expressing wildtype ClC-5 in Figure 5.12 A the voltage of half-maximal activation is ~130 mV, which is comparable to measurements of Smith *et al.*, performed with solutions of similar internal and external Cl⁻ content, respectively [80].

5.6 Voltage-dependent capacitances in ClC-5

Another way to determine the voltage dependence of ClC-5 gating is the measurement of the voltage-dependent cell capacitance, possible with the lock-in extension of the EPC-10 amplifier (see Section 4.3.7.3). Figure 5.13 A shows the ionic conditions and the sinusoidal voltage protocol. As an attempt to minimize possible contamination of the capacitance measurements by ionic currents external Cl⁻ was replaced by the impermeant gluconate ion.
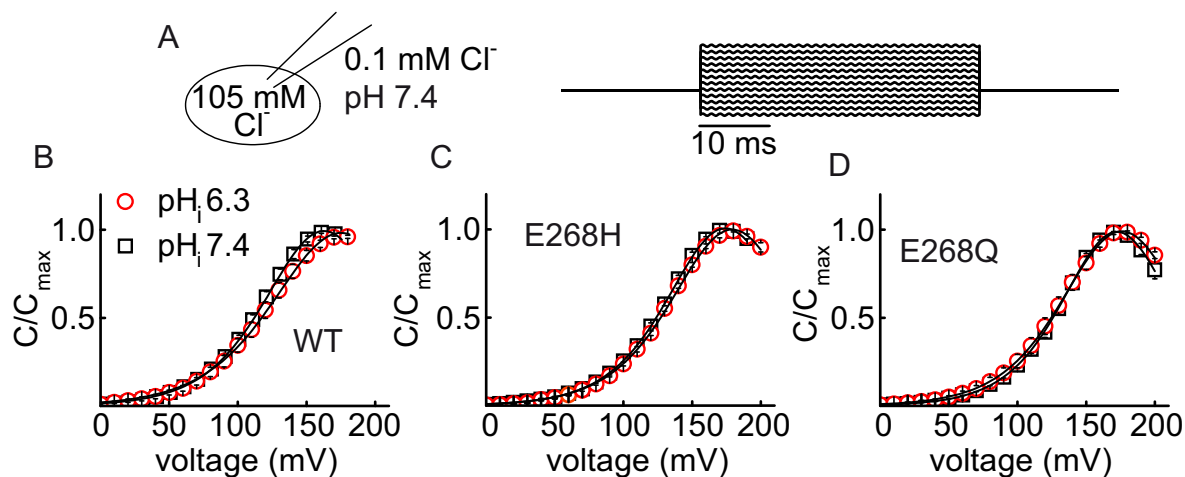
Figure 5.13: Whole-cell capacitance of ClC-5 expressing cells change in a voltage-dependent manner. A. Ionic conditions (solutions 1, 2 and IV, see Table 3) and voltage protocol, used for measuring voltage-dependent capacitance. A sinus stimulus with a peak-to-peak amplitude of 10 mV oscillates at 800 Hz around various test voltages in the positive and negative range. **B-D.** Nonlinear capacitances of WT ClC-5 (**B**) and proton glutamate mutants E268H ClC-5 (**C**) and E268Q ClC-5 (**D**) at pHs 6.3 and 7.4. Changes of capacitance were normalized to the maximum change of capacitance. Lines describe fits to the first derivative to a standard Boltzmann function (Equation 2) and parameters are given in Table 4. (Modified from Grieschat and Alekov, 2012)

Figure 5.13 B-D shows bell-shaped capacitance changes of WT ClC-5 and the aforementioned proton glutamate mutants at acidic and neutral internal pHs. The changes of capacitance are displayed normalized to the maximum change of capacitance and resemble the voltage-dependent capacitance changes of the outer hair-cell motor protein prestin [136]. Depending on the expression, those voltage-dependent changes of capacitance in ClC-5 could add up to 100 percent of capacitance. When the first derivative of a standard Boltzmann function (Equation 2) was fitted to the data, the maximum of the curve reports the voltage for half-maximum activation ($V_{0.5}$). The slope z of the curve gives the apparent number of moved elementary charges e_0 over a fraction of the membrane δ. Parameters for $V_{0.5}$ and z are given in Table 4. The values for $V_{0.5}$ are in the range of 163 to 182 mV and the pH dependence is not very pronounced. Differences between the two pHs are largest for wildtype and smallest for E268Q, but the values for acidic internal pH are always more positive than those for neutral internal pH in wildtype and mutants. Therefore, a shift of the voltage dependence is not very likely to be responsible for the stronger current increase in external SCN⁻.

Furthermore, the merely small shift in voltage dependence upon changing the charge at position 268 argues against this residue to be a part of the voltage sensor responsible for the depolarization-induced activation.

		pH 6.3	pH 7.4	significance p
WT	$V_{0.5}$ **(mV)**	177.8 ± 3.0	163.7 ± 2.4	< 0.005
	z	-0.76 ± 0.02	-0.87 ± 0.01	
	n	12	7	
E268H	$V_{0.5}$ **(mV)**	181.5 ± 2.7	176.2 ± 2.1	0.172
	ST	0.376	< 0.005	
	z	-0.83 ± 0.03	-0.87 ± 0.02	
	n	3	6	
E268Q	$V_{0.5}$ **(mV)**	176.2 ± 2.1	173.5 ± 1.9	0.395
	ST	0.669	0.011	
	z	-0.87 ± 0.03	-0.94 ± 0.04	
	n	6	4	

Table 4: Values for voltages of maximum change of capacitance ($V_{0.5}$) and slope z, obtained from fits to Equation 2 of n individual cells from Figure 5.13 B-D. Significances p between the two pHs and significances ST between WT and mutants for $V_{0.5}$ were calculated with a two-sample t-test.

It is very likely that the appearance of gating currents and nonlinear capacitances have their origin in the same molecular process, associated with activation at positive potentials, because the integration of the capacitance curve reasonably superimposes with the Boltzmann curve of the off-gating of the same cell (Figure 5.14).
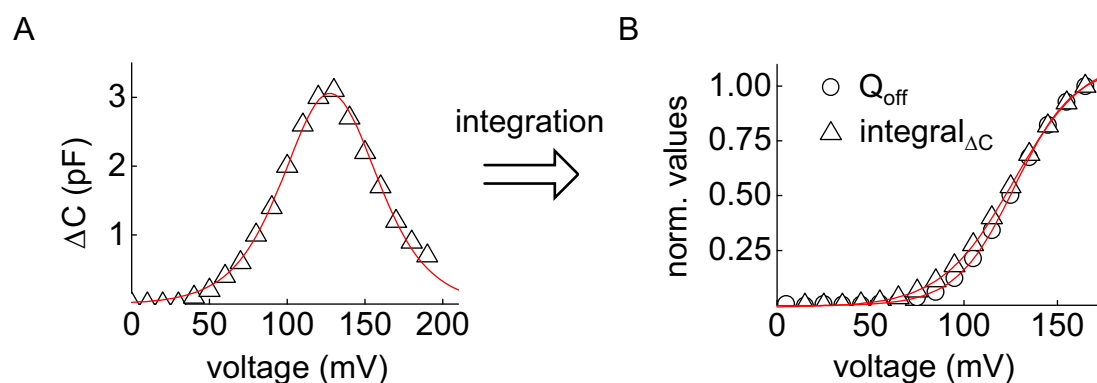
Figure 5.14: Measurements of nonlinear capacitances or gating currents reflect the same voltage-dependent process. A. Measurement of nonlinear capacitances of the cell depicted in Figure 5.12 C. Red line displays fit with the first derivative of a Boltzmann function (Equation 2) **B.** The charge-voltage relationship (Q_{off}) for the same cell (Figure 5.12 F) was normalized to the off-gating charge at +165 mV. The capacitance curve from (A) of the same cell was integrated between 0 and +165 mV, normalized and superimposed to the data of the gating current measurement. Lines represent fits to the Boltzmann equation (Equation 8).

5.7 Regulation of the transport probability of ClC-5

Figure 5.12 shows how mutation of the proton glutamate at the internal side of the protein affected the ratio of gating current to ionic current. To further elucidate the role of the proton glutamate in the regulation of the ratio of gating current to ionic current of ClC-5, internal site-directed modification with a cysteine reactive compound was carried out. Figure 5.15 A shows the voltage protocol and the ionic conditions. Via the patch pipette the negatively charged MTSES (2-sulfonatoethyl methanethiosulfonate) (see Section 4.3.6.1) was used to covalently modify an engineered cysteine replacing glutamate 268. Although cysteine is a protonatable amino acid, the currents which are mediated by E268C ClC-5 resemble the nonconducting mutant E268Q ClC-5, presumably because the relatively high pK_a of 8.0 may predict a high percentage of this residue to be in the neutral protonated form. Directly after opening of the cell, the depicted voltage protocol was applied repeatedly to monitor time-dependent changes. Figure 5.15 B shows a representative -P/n leak subtracted recording.
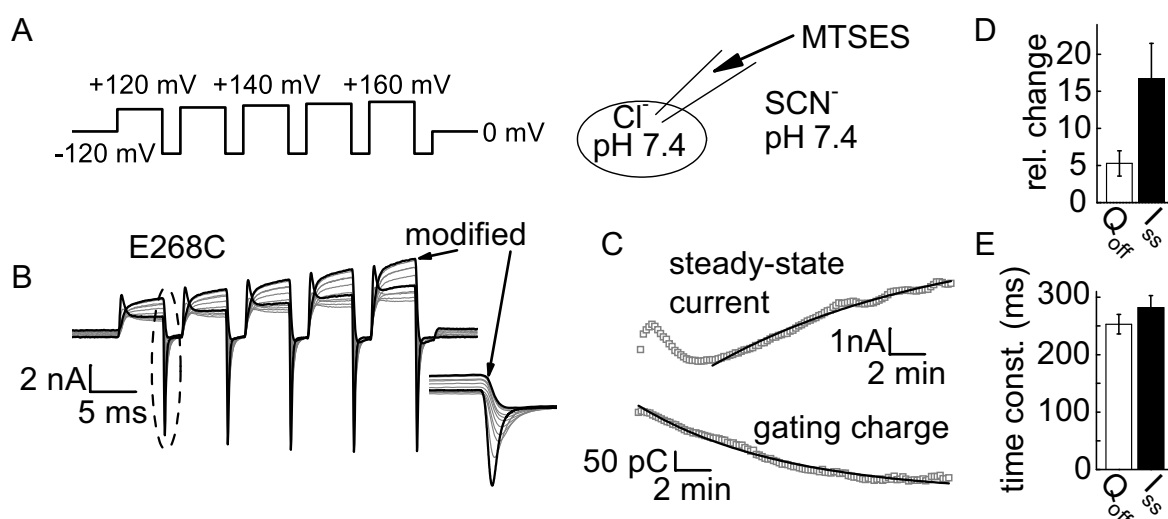
Figure 5.15: The proton glutamate mutant E268C is internally accessible to the charged methanethiosulfonate compound MTSES, which modifies current and gating charge magnitudes. A (left panel). Voltage protocol, applied immediately after opening of the cell, to measure time course of site-directed MTSES modification of cysteine 268 and ionic conditions of the experiment (**right panel,** solutions 1 and III) **B.** Representative -P/n leak subtracted whole-cell recording after opening of a cell expressing E268C ClC-5. Inset shows enlarged ionic currents and gating currents at the encircled segment. **C.** Time-course of steady-state current at the end of the +160 mV pulse (**upper panel**) and gating charge, obtained by integrating the off-gating current at the same voltage (**lower panel**) of the cell shown in (B). Solid lines represent fits to a monoexponential function. **D.** Relative changes of off-gating charge (Q_{off}) and steady-state current (I_{SS}), calculated from initial and final values of 4 experiments like in (B). **E.** Time constants of MTSES induced changes of Q_{off} and I_{SS}, obtained from exponential fits to the data like in C. Measurements and data analysis were performed by A.K. Alekov. (Modified from Grieschat and Alekov, 2012)

The first traces after opening show large on- and off-gating currents and relatively low ionic current magnitudes. This observation reverses with proceeding modification by MTSES – the

gating currents become smaller and ionic current increases – which is well visible in the inset of Figure 5.15 B. Figure 5.15 C displays the time-dependent changes of steady-state current and integrated off-gating current, respectively, at +160 mV. After opening of the cell, the steady-state current first rose, then declined, before a monotonous rising phase began. The first two events can be attributed to equilibration processes with the pipette solution and the long rising phase is a result of the covalent binding of MTSES to the cysteine residue. With similar time dependence the magnitude of the gating charge was decreasing. The modification led to a ~5 times decrease of off-gating current and a ~15 times increase of steady-state current (Figure 5.15 D). It was shown so far that neither the uncoupling (Section 5.2), nor the single channel amplitude (Section 5.3), the anion affinities (Section 5.4) or the voltage dependence (Section 5.5) were changed upon protonation of the internal glutamate at different internal pHs. But changing its properties by MTSES increased ionic current and decreased gating currents, so the gating currents are likely to arise from incomplete transport cycles, which is regulated by glutamate 268.

This inverse relationship between gating current and ionic current, which is also indicated in Figure 5.12, can also lead to an alternative data presentation of Figure 5.13. The quantities of gating charge (C) and ionic current (I) can be written like Equation 10 and Equation 11 and depend on the number of channels (N) in the membrane, the unitary current (i) or unitary gating charge (q) and the probabilities of the transporter to perform complete or incomplete transport cycles (P_C and P_{NC}).

$$C = N \cdot P_{NC} \cdot q \qquad \text{Equation 10}$$

$$I = N \cdot P_C \cdot i \qquad \text{Equation 11}$$

Since the number of transporters and unitary transport rate or charge, respectively, are constant parameters, division of Equation 10 by Equation 11 gives the ratio of the relative probabilities for the transporter to perform complete or incomplete transport cycles. Because E268Q ClC-5 gave only negligible currents, this could only be done for wildtype and mutant E268H ClC-5. Figure 5.16 shows this approach by dividing the capacitances by the ionic steady-state current at +165 mV in external standard Cl⁻ solution and the standard voltage step protocol (Figure 5.3, upper panel). Validating the observation of larger gating current in respect to the ionic currents, the ratio of capacitance to current in symmetrical pH 7.4 was

much larger for E268H (Figure 5.16 B) than in wildtype ClC-5 protein (Figure 5.16 A). Additionally, there was a ~50% reduction of this ratio in wildtype, when the internal pH was lowered to pH 6.3. In E268H ClC-5 the reduction was with ~75% even greater. A nontitratable residue at position 268 (E268Q) does not permit transport and produces the largest gating currents. Thus, it is conceivable that the presence and nature of a protonatable residue at position 268 defines the fraction of transporters to conduct complete transport cycles. As the fraction of incomplete transport cycles decreases at low internal pH, the interaction of protons with glutamate 268 defines the transport probability of ClC-5 which is generally lower for E268H and lowest for E268Q ClC-5.
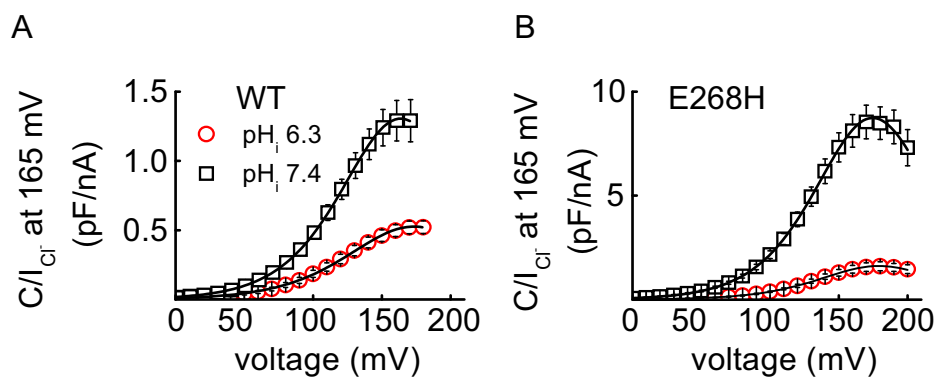
Figure 5.16: Magnitude of change of capacitance depends on internal pH and amino acid at position 268. **A** and **B.** Nonlinear capacitances from Figure 5.13, divided by the steady-state ionic current in external Cl⁻ solution (solution I) at +165 mV for WT ClC-5 (**A**) and E268H ClC-5 (**B**). Lines represent fits to the first equation of a standard Boltzmann function. (Modified from Grieschat and Alekov, 2012)

5.8 The action of internal protons seems to depend on the binding of the gating glutamate to the central ion binding site

Another widely conserved glutamate residue for which protonation is essential for ClC transporter function is glutamate 211 in ClC-5, the so called gating glutamate. Crystal structures of a prokaryotic homologue [86] have shown this glutamate to compete with the anion for a binding site. This was shown in a crystal where a protonated gating glutamate was mimicked through mutation of this glutamate to glutamine, which had swung out to unblock the anion binding site [90]. A recent crystal structure of a eukaryotic ClC transporter [96] shows the external gating glutamate for the first time in a third conformation, bound to a central anion binding site, thereby blocking this position for the anion and being a possible site for the protonation to take place. It was proposed that the protons that neutralize the gating glutamate come from the internal side [93], so here, the effects of internal protons were investigated at mutants, which have a destabilized binding of the gating glutamate to the central anion binding site.

In ClC-5, serine 168 is one of the conserved coordinating amino acids that stabilize the central binding site (serine 107 in EcClC; [86]). Substitution S168P naturally occurs in a plant isoform (proline 160 in AtClCa; [142]) which shows a dramatically different anion specifity and is a NO_3^-/H^+ antiporter in the vacuolar membrane. The aforementioned neutralization of glutamate was here at least partly mimicked by substituting glutamate with cysteine. The effect of internal protons on the current increase in external SCN^- was investigated and Figure 5.17 shows representative whole-cell recordings of cells expressing E211C or S168P, sequentially perfused with external Cl^- and SCN^-, respectively. Similarly to published results for E211A [58], the mutant E211C gives only a small, non rectified current in external Cl^- (Figure 5.17 A), whereas there is a large current increase in external SCN^- (Figure 5.17 B). Measurements for S168P (Figure 5.17 C and D) show a similar result, but Cl^- currents were smaller and rectification was generally stronger than in mutant E211C, which is also in accordance with a previous report [79]. The normalized current-voltage relationships for E211C ClC-5 (Figure 5.17 E, Figure 5.18 A) show a very pronounced current increase in external SCN^- at both internal pHs 6.0 and 7.4. The current increase is not significantly dependent of internal pH and approximately in the range of the current increase of wildtype ClC-5 at internal pH 6.0 (Figure 5.18 C). The relative current increase in S168P ClC-5 in external SCN^- is much larger than in wildtype or E211C ClC-5 (Figure 5.17 F, Figure 5.18 B)

and there is a dependence on internal pH, but less pronounced than in wildtype ClC-5. The current increase at internal pH 7.4 is the same as in WT at internal pH 6.0 (Figure 5.18 C). These results indicate, that a reduced occupancy of the central binding site results in a higher transport probability in external SCN⁻.
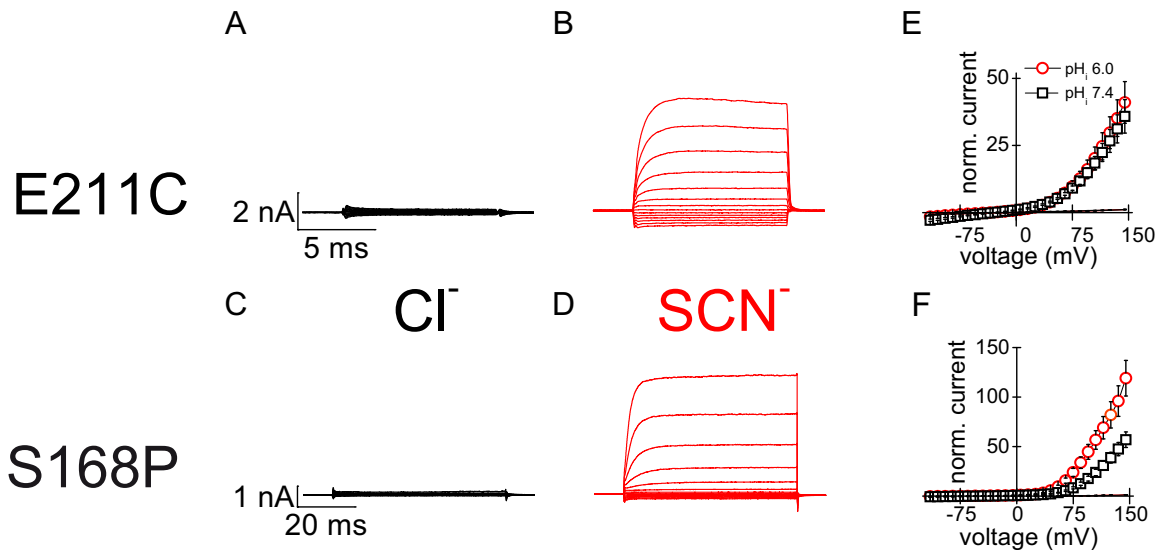
Figure 5.17. External SCN⁻ enhances ionic currents in ClC-5 mutant E211C and S168P more pronounced than in WT ClC-5. A and **B.** Representative whole-cell current recordings of a cell expressing E211C ClC-5, sequentially perfused with external Cl⁻ (**A**) or SCN⁻ (**B**) solution at symmetrical pH 7.4 upon voltage jumps from -115 mV to +145 mV (n = 4). Measurements were carried out by A.K. Alekov. **C.** and **D.** Representative measurements of a cell expressing S168P at the aforementioned conditions (n = 7 and 8 for pH 7.4 and pH 6). **E** and **F.** Normalized currents of E211C (**E**) and S168P (**F**) in pH 6.0 and 7.4. Symbols describe currents in SCN⁻ and Cl⁻ currents are indicated by lines. Normalization was performed to Cl⁻ currents at +135 mV. (Modified from Grieschat and Alekov, 2012)
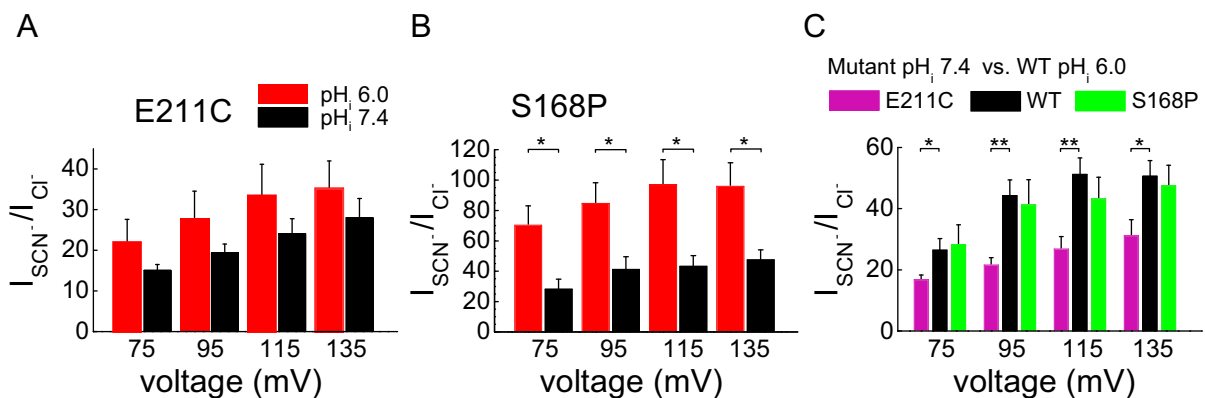
Figure 5.18: In two mutants, current increase in external SCN⁻ at neutral pH are more pronounced, but less pH-dependent than for WT. A and **B.** Ratios of SCN⁻-dependent current increase at various voltages for E211C ClC-5 (**A**) and S168P ClC-5 (**B**), compared at internal pHs 6.0 and 7.4. Data from Figure 5.17. Two-sample t-tests were performed and the asterisk indicates a significant difference ($p < 0.05$). **C.** Comparison of current increase in mutants at internal pH 7.4 (data from A and B) with current increase in WT ClC-5 at internal pH 6.0 (data from Figure 5.5 G) at various voltages. Stars indicate significant differences between mutants and WT (two-sample t-test, **,$p < 0.01$; *, $p < 0.05$). (Modified from Grieschat and Alekov, 2012)

5.9 Selectivity and uncoupling of a proton glutamate mutant

The tendency of residue 268 to be protonated changes the magnitudes of capacitances and varies with internal pH and pK_a of the side chain. But internal pH does not change the relative uncoupling in WT ClC-5. Proton transport and uncoupling by external SCN⁻ was also investigated in the proton glutamate mutant E268H, which is still mediating robust currents in Cl⁻ and SCN⁻ (Figure 5.19 A and B). Currents at neutral internal pH are only augmented by the factor of ~7, when compared at +135 mV (Figure 5.19 C). Like in WT, internal pH 6 evokes a stronger current increase upon SCN⁻ application (Figure 5.19 D and E), the factor of which is ~10 (Figure 5.19 F). Current increases at both internal pHs are therefore less pronounced than in WT. Proton transport in SCN⁻ is slightly higher than in Cl⁻ (Figure 5.19 G, left panel) similarly to WT and with the relative current increases the relative uncoupling is calculated to values between 6 and 8 (Figure 5.19 G, right panel).
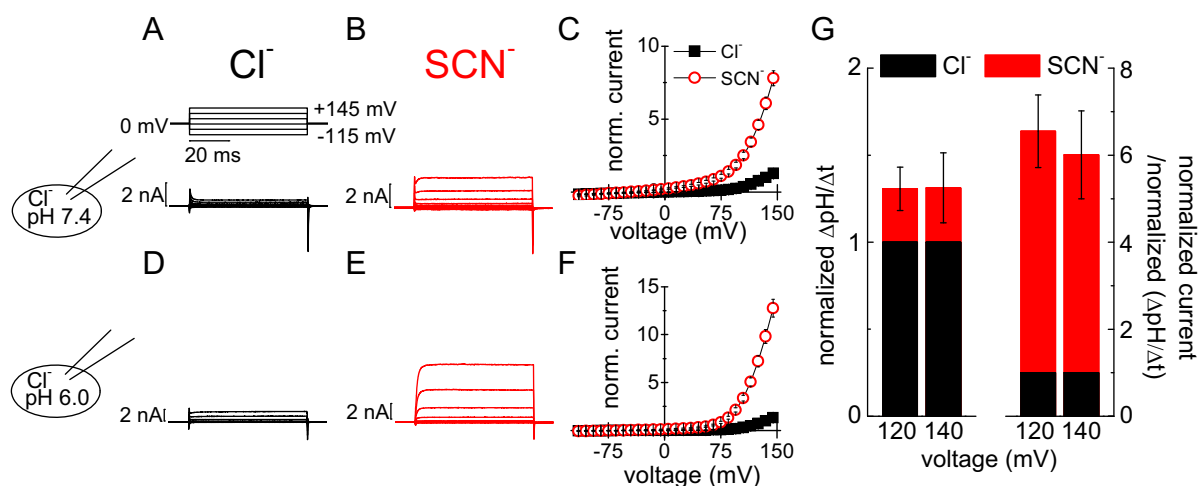
Figure 5.19: Current increase and relative uncoupling in external SCN⁻ is less pronounced in E268H ClC-5 than in WT. **A.** Voltage protocol (**upper panel**) and representative whole-cell measurement of a cell expressing E268H ClC-5 at neutral internal pH. **B.** Recording of the same cell, bathed in SCN⁻ (solutions 1, I and III, see Table 3). **D** and **E**. Representative recording of a cell externally perfused with Cl⁻ and SCN⁻-based solutions, respectively (solutions 2, I and III). **C** and **F**. Current-voltage relationships of experiments shown in A, B, D and E, depicting steady-state currents, normalized to the currents in Cl⁻ at +135 mV at internal pH 7.4 (**C**) and pH 6.0 (**F**), respectively (n = 5-7). **G.** Proton flux in symmetrical pH 7.4 at two voltages (**left panel**), normalized to the proton flux in Cl⁻ at the same voltage and relative uncoupling (**right panel**), calculated by dividing the normalized total transport current by the relative proton flux (Equation 6, n = 9-15).

5.10 Structure-function of the voltage sensor in ClC-5

ClC transporters display profound voltage-dependent activation that is abolished by neutralization of the charge of the so called gating glutamate (glutamate 211 in ClC-5) by mutation [58], [91]. However, the voltage dependence of ClC channels is strongly modulated also by mutations of a variety of other amino acids at different positions in the ClC protein. Of particular importance is the residue next to the gating glutamate – lysine 210 in ClC-5. It is conserved in all mammalian ClC isoforms and has been the subject of previous investigations in ClC-1 [91] and ClC-5 [140]. Yet this residue is not conserved in any crystallized isoform (Figure 5.20).

Figure 5.20: Structure-based multisequence alignment of three crystallized ClC transporter isoforms, with ClC-5 sequence included. Alignment was performed with Chimera using MatchMaker function with default parameters. Structures of CmClC (*Cyanidioschyzon merolae)* and SyClC (*Synechocystis* sp. PCC6803) were aligned to the reference structure of EcClC (*Escherichia coli*) (PDB IDs given in the figure). The ClC-5 sequence was added and aligned with default parameters afterwards. Highlighted by dashed boxes are amino acid positions which are studied for their impact on ClC-5 voltage dependence.

Nevertheless, when superimposing crystal structures of open and closed conformation of EcClC and calculating α-carbon RMSD, also in this isoform the residues adjacent to the gating glutamate at the beginning of helix F seem to experience some form of motion (Figure 5.21).

Figure 5.21: RMSD of two regions between open and closed conformations of EcClC (PDB ID 1OTS and 1OTU). Corresponding residues investigated in this thesis are marked by arrows and labels. RMSD of α-carbons was calculated using Chimera.

In ClC-1 mutations of the corresponding lysine 232 had massive impact on the substrate specifity and the time and voltage dependence of gating. Moreover, the cysteine mutant created a high-affinity binding site for extracellularly applied MTS reagents (see Section 4.3.6.1) [91]. De Stefano *et al.* explored the role of lysine 210 in ClC-5 and also reported altered substrate specifity without changing the degree of uncoupling and a restoration of wildtype behaviour upon MTSET modification [140]. Based on these findings, it appears logical to assume that this position might be important not only for substrate specifity, but also for voltage-dependent gating in ClC-5. The following chapter describes structure-functional investigations, aiming to provide deeper insight into the mechanisms of voltage sensing.
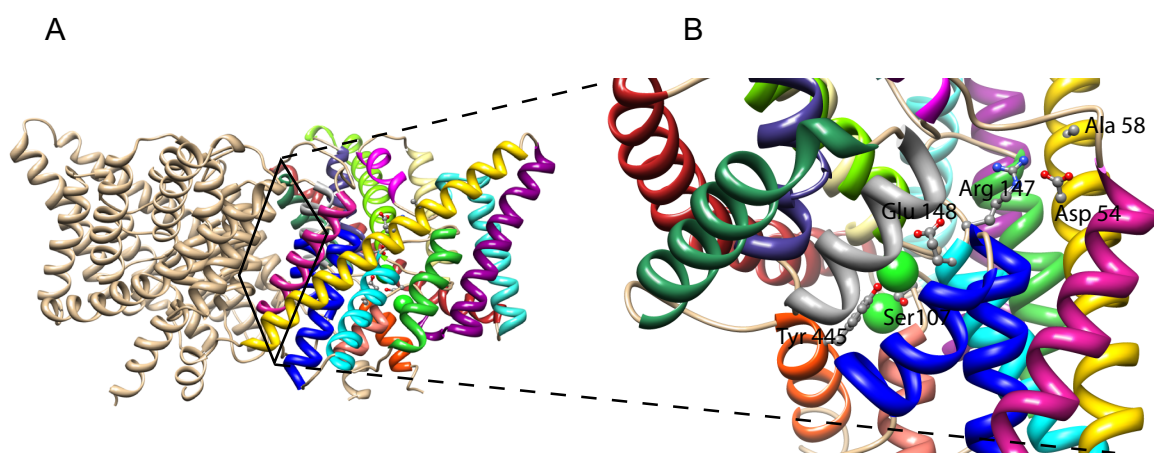
Figure 5.22: Crystal structure of EcClC, showing possible interaction partners for the residue corresponding to lysine 210 in ClC-5. A. Side view of the crystal structure of EcClC (PDB ID 1OTS) with left monomer shown in tan and right monomer with multicoloured helices. **B.** Detailed view at the right monomer from the dimer interface into the protein interior as the black frame indicates. Shown are the gating glutamate Glu 148, bound at the external binding site and the adjacent Arg147 (Glu 211 and Lys 210 in ClC-5) on helix F (cyan) putative interaction partners Asp 54 and Ala 58 (Asp 76 and His 80 in ClC-5) on helix B (yellow). For better orientation Cl$^-$ ions are shown as green spheres, bound to the internal and central binding site with Ser 107 and Tyr 445 stabilizing the central binding site.

Additionally, the crystal structure of EcClC suggests several residues, which might be interaction partners with the residue next to the gating glutamate. The crystal structure of EcClC shows the arginine 147 (lysine 210 in ClC-5) at the N-terminus of helix F protrude back and outwards from the anion pore (Figure 5.22 B) and in proximity to helix B. Two residues on this helix point in the direction of arginine 147. Aspartate 54 (aspartate 76 in ClC-5) is conserved in all human ClC isoforms except ClC-Ka, which has an asparagine at the corresponding position. It is also conserved in EcClC and CmClC (Figure 5.20). One helix turn further towards the extracellular interface, alanine 58 (histidine 80 in ClC-5) is located, a non-conserved amino acid (Figure 5.22 B). The RMSD in the helix B region is fairly low (Figure 5.21) and it might serve as some kind of scaffold. If in ClC-5 a possible interaction of

lysine 210 with residues on helix B can be elucidated, important knowledge about the structure and function of ClC-5 and the differences from other isoforms could be obtained. Also in this case, cysteine modifications and possibly cross-linking might be an appropriate tool.

5.10.1   Substrate specificity and coupling in the K210C ClC-5 mutant
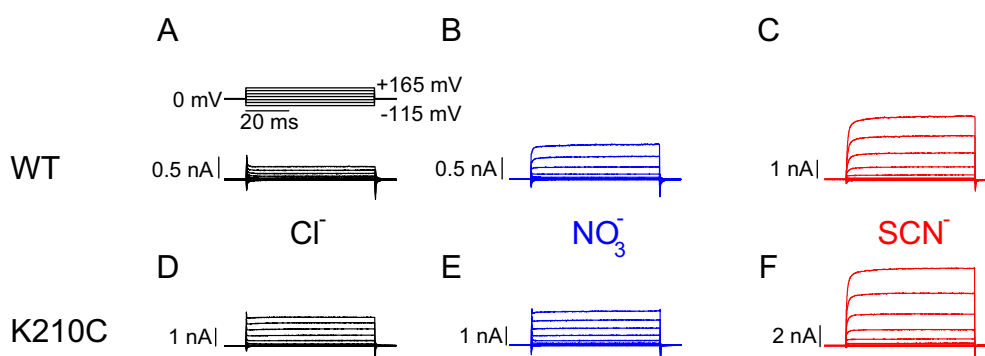
Figure 5.23: Perfusion of NO_3^- and SCN^- leads to different whole-cell current increases in WT and K210C ClC-5 expressing cells. A. Voltage protocol and representative whole-cell measurement of WT ClC-5 at symmetrical pH 7.4. **B.** and **C.** Current traces of the same cell, externally perfused with NO_3^- (**B**) or SCN^-, respectively. **D-F**. Whole-cell current traces, measured at the same cell, expressing K210C ClC-5 with external Cl^- (**D**), NO_3^- (**E**), or SCN^- (**F**) solutions (solutions 1, I , II and III, see Table 3).

To investigate the effects of K210 on the interaction of ClC-5 with the transported substrates, whole-cell measurements in external solutions containing variable anions were performed. Representative whole-cell currents of cells, expressing either WT ClC-5 or K210C ClC-5 and externally perfused with Cl^-, NO_3^- or SCN^--containing solutions are shown in Figure 5.23. Macroscopically, the currents in K210C ClC-5 (Figure 5.23 D-F) were under all tested conditions very rectifying, similar to currents elicited from cells expressing WT ClC-5 (Figure 5.23 A-C). However, in contrast to NO_3^- currents in WT (Figure 5.23 B and Figure 5.24 A) which were about 3 times larger than Cl^- currents, there was essentially no current increase when external Cl^- was exchanged for NO_3^- in K210C. This is in accordance with previously published results [140]. The currents in external SCN^- were ~6 times higher than in Cl^- for K210C ClC-5, thus demonstrating much less current increase, compared to WT ClC-5.
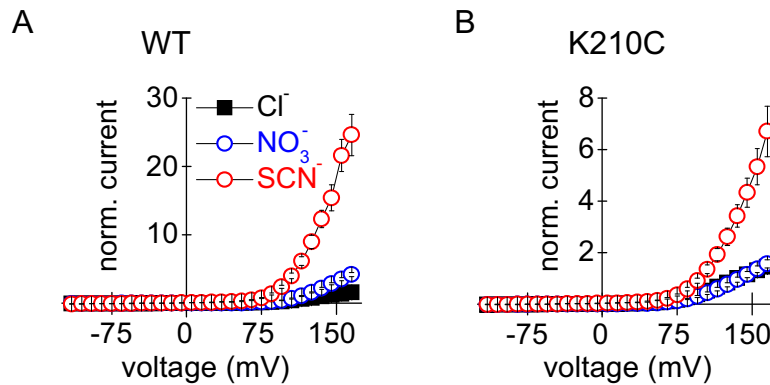
Figure 5.24: SCN⁻ and NO₃⁻ mediate less current increase in K210C ClC-5 than in wildtype. A and **B.** Steady-state current-voltage relationships of WT (**A**) and K210C ClC-5 (**B**), normalized to currents at +135 mV in Cl⁻, obtained from experiments like shown in Figure 5.23. Data for Cl⁻ and SCN⁻-measurements in (A) are mostly taken from Figure 5.5 (n = 7-17 for WT and n = 6 for K210C).

Larger external anions were found to uncouple ClC transport. There exist therefore two different explanations for the observed effects. On one hand, the mutant K210C ClC-5 might exhibit a higher selectivity for transporting NO_3^- and SCN^- when compared to the wildtype, while preserving the stoichiometry of the anion/proton antiport. Alternatively, transport coupling might be also altered, resulting in a much better coupling between the anion and proton transport even for larger anions in the mutant than in the WT. To discriminate between these two possibilities, here, the relative proton transport activity of wildtype and K210C ClC-5 in external NO_3^- was measured via pH-dependent fluorescence changes of intracellularly perfused BCECF (Figure 5.25). Robust time- and voltage-dependent pH changes could be observed for wildtype and mutant in both Cl⁻ and NO_3^- (Figure 5.25 C and D, Figure 5.26 B). Proton transport was larger in Cl⁻. The additional current increase in NO_3^- for wildtype results in a ~5-9 times uncoupling, relative to Cl⁻, which corresponds to previously published results [79]. A similar relative decrease of proton transport, compared to wildtype data, but unchanged total transport current results in a relative uncoupling of ~3 for the K210C ClC-5 mutant. This contradicts previous results for the similar mutant K210A ClC-5, which was reported to demonstrate an unaltered degree of uncoupling compared to wildtype [140].
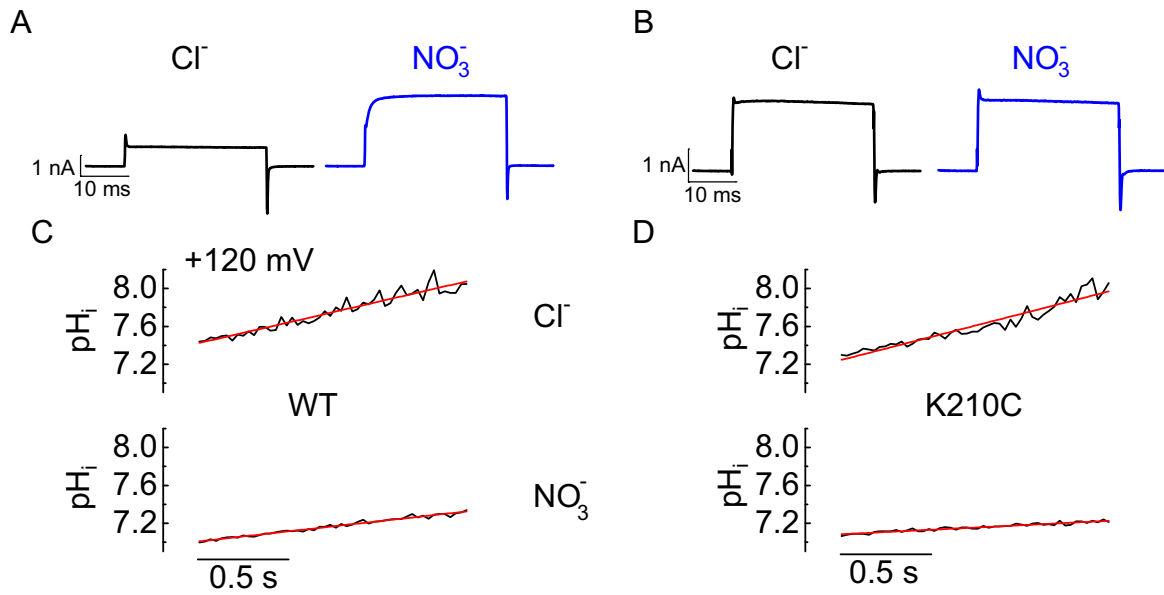
Figure 5.25: WT and K210C ClC-5 transport protons in both external Cl⁻ and NO₃⁻. A and **B.** Representative whole-cell current traces at +120 mV of the same cells expressing WT (**A**) or K210C (**B**) in external Cl⁻ or NO₃⁻ at symmetrical pH (solutions 4 and V or VI). **C** and **D.** Representative time-dependent internal alkalinisation of the cells from A and B during a 1.5-s +120-mV pulse in external Cl⁻ (**upper panel**) or NO₃⁻ (**lower panel**), monitored by pH-dependent BCECF fluorescence. Solid lines are linear fits to the data.
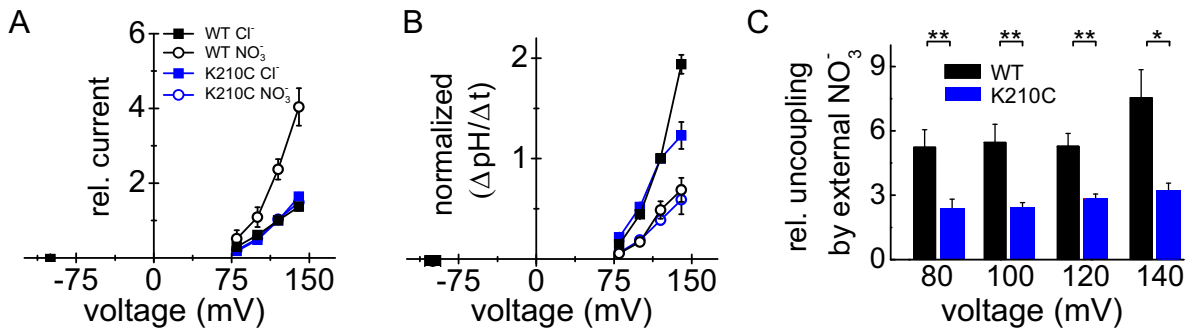
Figure 5.26: NO₃⁻-mediated uncoupling is less pronounced in K210C ClC-5. A. Transport current from experiments like Figure 5.25 A and B at various voltages. Currents were normalized to the currents in Cl⁻ at +120 mV. **B.** Proton fluxes, obtained from the slopes of linear fits to data like in Figure 5.25 C and D and normalized to the proton fluxes in Cl⁻ at +120 mV. **C.** Relative uncoupling by external NO₃⁻, as a ratio of total transport current to proton flux in NO₃⁻, divided by the respective ratio in Cl⁻ at the same voltage. Significance of differences was tested with a two-sample t-test (**,$p < 0.01$; *, $p < 0.05$, n = 7-10 for WT; 7-14 for K210C)

5.10.2 Effects of K210 mutations on the voltage dependence of ClC-5

As shown for example in Section 5.5, the removal of external Cl⁻ was chosen to prevent possible contaminating effects of ionic currents on capacitance measurements. But this maneuver shifted voltage dependence to very positive values, which might impede analysis. To circumvent Cl⁻ removal and the problems associated with this, the majority of the following experiments was conducted on the background of the nonconducting E268Q mutant, because this mutant showed only little differences to the wildtype concerning voltage dependence (Figure 5.13) and additionally demonstrated very pronounced nonlinear capacitances. Moreover, voltage dependence was further left-shifted by using an internal solution with reduced Cl⁻ content [80], [143]. This allowed even better resolving of the right shoulder of the capacitance curve and thereby greatly improved the analysis of voltage dependence of K210 mutants.

K210R substitutes the native residue for the arginine found in the EcClC isoform and K210C with its aforementioned property to be available for MTS modification are interesting candidates for investigations on voltage-dependent gating. Figure 5.27 A-C shows representative leak-subtracted whole-cell measurements for E268Q ClC-5 and two double mutants K210C/E268Q and K210R/E268Q with nearly no ionic currents and well defined gating currents. While for E268Q ClC-5 the amplitudes of on-gating currents were smaller than of off-gating currents, this behaviour is reversed in the K210R/E268Q double mutant. For K210C/E268Q the magnitudes for on- and off-gating currents were approximately the same size. However, both double mutants displayed additional initial off-gating currents at negative potentials, when jumping from -30 mV holding potential to test potentials. From this, it can be concluded, that a certain percentage of double mutant transporters were already activated at -30 mV. Such an assumption might also explain why gating currents were generally smaller for the double mutants than in E268Q, because not all transporters were deactivated. In fact, capacitance curves shown in Figure 5.27 D report markedly shifted voltage dependence for both double mutants, with pronounced voltage-dependent capacitance increase even at negative voltages. Table 5 summarizes the values for half-maximal activation and the apparent charge, which is displaced during depolarization obtained by fitting Equation 2 to the data. Mutation K210C shifted the value for half-maximal activation by ~30 mV towards less depolarizing values, whereas K210R introduced ~50 mV shift, relative to single mutant E268Q. Values for z had a reduced magnitude for double mutants, in the sequence of left-shift of the voltage dependence.
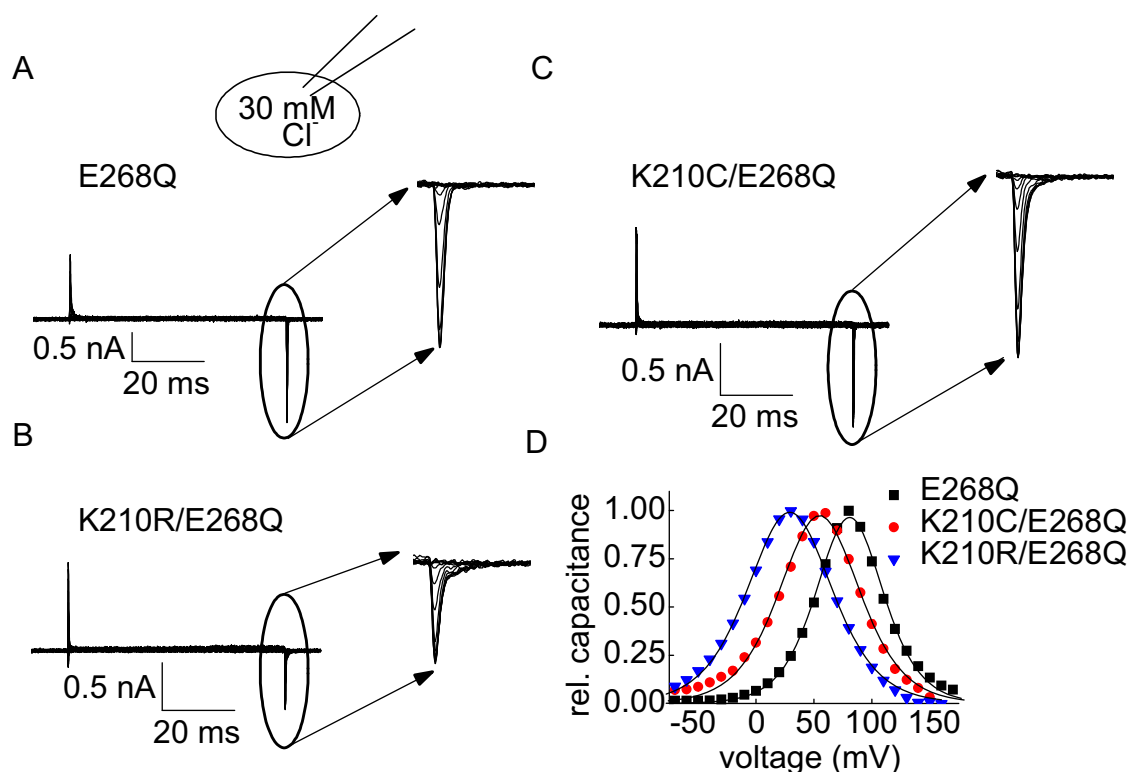
Figure 5.27: Nonlinear capacitances in double mutants of E268Q ClC-5 show shifted voltage dependence. **A-C.** Representative -P/n leak subtracted whole-cell recordings of HEK293T cells expressing E268Q (**A**), K210C/E268Q (**B**) or K210R/E268Q ClC-5 (**C**) at 30 mM internal Cl⁻ and symmetrical pH 7.4 (solutions 10 and I). Cells were held at -30 mV and voltage pulses from -115 to +165 mV were applied. **D.** Normalized nonlinear capacitances, measured at the same ionic conditions. Lines represent fits to the first derivative of the Boltzmann function. Parameters are given in Table 5.

	E268Q	**K210C/E268Q**	**K210R/E268Q**
$V_{0.5}$ **(mV)**	80.7 ± 0.6	51.4 ± 3.7	29.1 ± 1.0
z	-1.31 ± 0.01	-1.10 ± 0.02	-1.04 ± 0.01
n	17	14	16

Table 5: Parameters for fits to data summarized in Figure 5.27 D and numbers of single experiments.

A cysteine in place of lysine 210 was previously shown to be accessible to extracellular modification with MTS reagents as well in ClC channels as in ClC-5 [91], [140]. In K210C ClC-5, MTSET could restore the anion selectivity of the wildtype [140]. Therefore, a similar strategy was applied here, to investigate the effects of such modifications on voltage-dependent gating. Additionally, metal cations are a useful tool to study the accessibility of engineered cysteines [144]. Therefore, the effects of extracellular Cd^{2+} were also studied. To ensure, that the observed effects of externally applied compounds are indeed effects on the

introduced cysteine, they were all tested on the single mutant E268Q ClC-5, as shown in Figure 5.28 A. Neither extracellular application of MTSET nor CdCl$_2$ had significant effects on the voltage dependence or the slope of the capacitance curve of E268Q ClC-5 therefore only little nonspecific effects could further be expected.
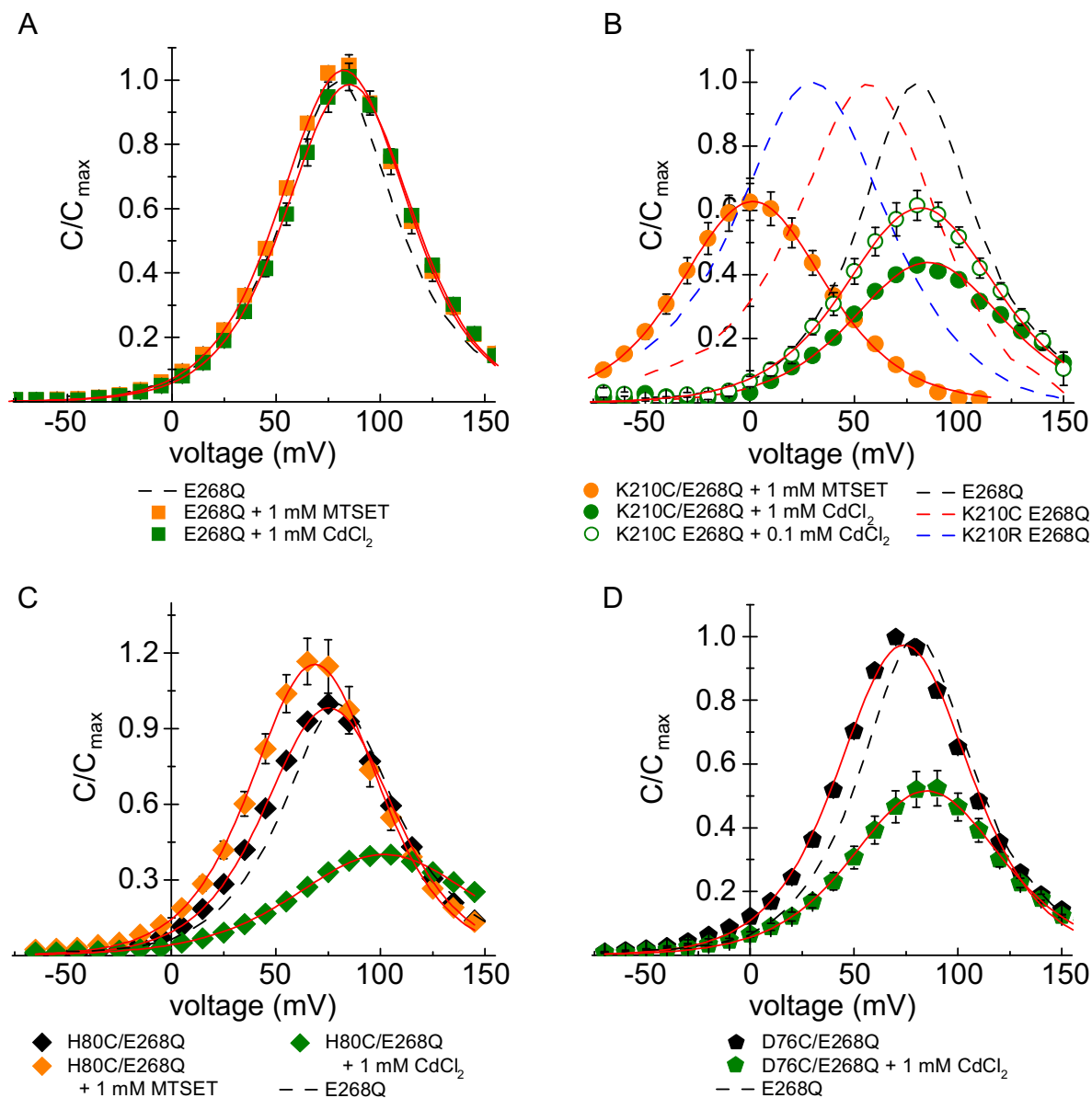
Figure 5.28: Modification of engineered cysteines H80C and K210C by extracellular MTSET and CdCl$_2$ causes a shift of voltage-dependent activation. A-C. Nonlinear capacitances of E268Q (**A**) K210C/E268Q (**B**), H80C/E268Q (**C**) and D76C/E268Q (**D**). Measurements were performed with 30 mM internal and 155 mM external Cl$^-$ (solutions 10 and I, see Table 3) in presence or absence of extracellular MTSET or CdCl$_2$. For comparison, E268Q, K210R/E268Q and unmodified K210C/E268Q from Figure 5.27 D are shown as dashed lines and normalization was performed to the maximum capacitance values of the unmodified forms of the respective mutants. Solid lines represent fits to the first derivative of the Boltzmann function. Parameters are given in Table 6 and Table 7.

Modification of K210C/E268Q by 1 mM MTSET resulted in a ~45-mV left-shift, accompanied by a 40-percent reduction of nonlinear capacitance (Figure 5.28 B, orange circles). The opposite effect resulted from modification with 0.1 mM CdCl$_2$. Here, the voltage

dependence of E268Q (Table 5) was restored but the magnitude of the slope was reduced and the size of capacitance change decreased (Figure 5.28 B, open circles). An increase of the concentration of extracellular $CdCl_2$ had merely small additional effect on voltage dependence and slope, but the size of the capacitances was decreased to a larger extent (Figure 5.28 B, green circles).

[compound] (mM)	E268Q		K210C/E268Q		
	1 MTSET	1 CdCl$_2$	1 MTSET	0.1 CdCl$_2$	1 CdCl$_2$
$V_{0.5}$ (mV)	82.4 ± 1.0	85.2 ± 0.9	5.7 ± 4.1	81.7 ± 1.4	85.5 ± 2.0
z	-1.24 ± 0.03	-1.25 ± 0.02	-1.14 ± 0.03	-1.07 ± 0.04	-1.00 ± 0.03
n	5	4	14	4	5

Table 6: Parameter values for fits with the first equation of a Boltzmann function to the data presented in Figure 5.28 A and B

Thus, MTSET application did not restore the behaviour of the single mutant, as previous results suggested [140], but rather the divalent metal cation Cd^{2+} abolished the effects of the additional mutation K210C on voltage dependence. It is seen in the EcClC crystal that the side-chain of the corresponding arginine in EcClC does not protrude into the anion binding pocket, but is directed backwards (Figure 5.22). Homology modelling proposed two residues, sporting charged or partially charged side-chains that might be in close proximity to the side chain of lysine 210 in ClC-5. Cysteine mutations of those residues aspartate 76 or histidine 80, respectively, were also tested for external accessibility and possible effects of modification. Figure 5.28 C demonstrates that mutation H80C mediated only a mild 5-mV shift of voltage dependence with respect to E268Q ClC-5 (Table 7), but allowed external modification, not possible without the cysteine substitution.

[compound] (mM)	H80C/E268Q			D76C/E268Q	
	-	1 MTSET	1 CdCl$_2$	-	1 CdCl$_2$
$V_{0.5}$ (mV)	75.5 ± 0.9	68.6 ± 0.2	103.3 ± 3.3	79.1 ± 0.5	84.7 ± 1.1
z	-1.24 ± 0.02	-1.26 ± 0.02	-0.87 ± 0.03	-1.21 ± 0.04	-1.06 ± 0.02
n	11	3	4	4	4

Table 7: Parameter values for fits with the first equation of a Boltzmann function to the data presented in Figure 5.28 C and D.

Compared to K210C/E268Q, MTSET modification of H80C/E268Q (Figure 5.28 C, orange rhombi) caused a smaller left-shift, but the capacitance compared to the unmodified form was

slightly increased in contrast to the strong decrease in K210C/E268Q. $CdCl_2$ mediated the same 30-mV right-shift like in K210C/E268Q associated with the same percentage of capacitance decrease, but because H80C/E268Q is only slightly shifted relative to E268Q, in this case no restoration of this behaviour was achieved E268Q (Figure 5.28 C, green rhombi). Voltage for half-maximal activation is much more positive than for E268Q alone.

The double mutant D76C/E268Q showed the same voltage dependence as the single E268Q mutant, but the slope was slightly reduced (Figure 5.28 D). The possibility for modification was also tested on the mutant D76C/E268Q by applying 1 mM extracellular $CdCl_2$ (Figure 5.28 D, green pentagons) and only a shift of voltage dependence in the range of 5 mV, like in E268Q was provoked. In contrast, unlike in E268Q, a reduced change of capacitance was noticed.

Noteworthy, in contrast to covalent MTS modification, which is only reversible after the application of reducing agents like dithiothreitol [140], the effect of $CdCl_2$ application was nearly instantly reversible and was mainly dependent of the speed of removal (Figure 5.29).
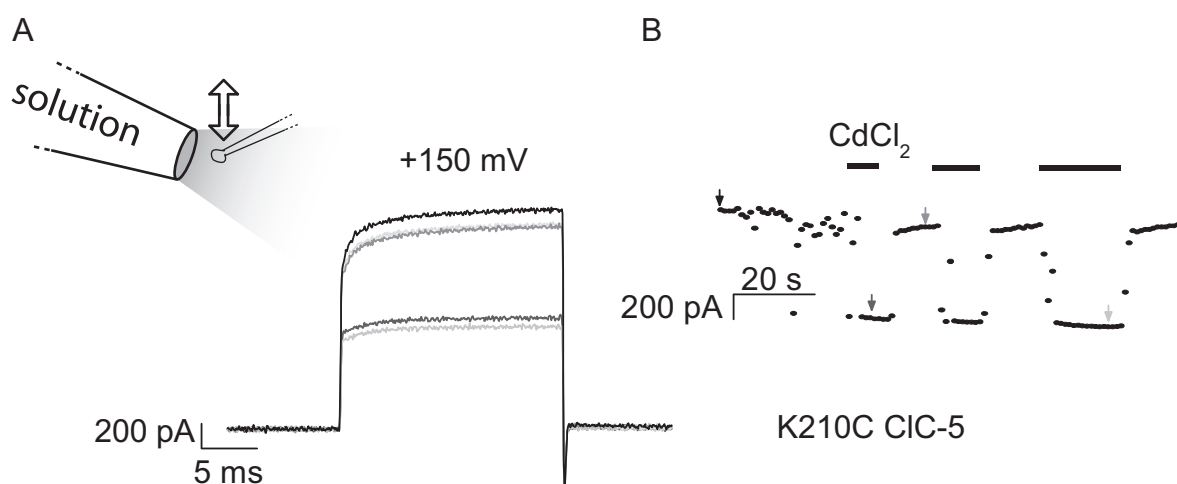
Figure 5.29: Effect of extracellular $CdCl_2$ is instantaneous and readily reversible. A. Schematic display of local perfusion and representative –P/n leak-subtracted current traces at +150 mV of a cell expressing K210C ClC-5 in Cl⁻ solutions 10 and I. Traces were recorded at time points indicated in B at corresponding gray shades, when the cell was driven in and out of a stream of solution, supplemented with 1 mM $CdCl_2$. **B.** Steady-state current amplitudes for the cell shown in A, recorded in 1-s intervals. Arrows indicate time points of current traces shown in A and black bars are the periods the cell was exposed to $CdCl_2$.

5.10.3 Effects of internal and external anions on the gating of E268Q and K210R/E268Q ClC-5

Reduction of the internal Cl⁻-concentration shifts the voltage dependence of ClC transporters to less depolarizing values [80], [143]. That means internal chloride can be considered as a voltage-dependent blocker. This indicates the existence of an internal ion binding site that directly modifies the following voltage-dependent transitions. Measurements of nonlinear capacitances at three different internal Cl⁻ concentrations were performed in HEK293T cells expressing either E268Q ClC-5 or the voltage-shifted K210R/E268Q ClC-5 double mutant (Figure 5.30 A and B).
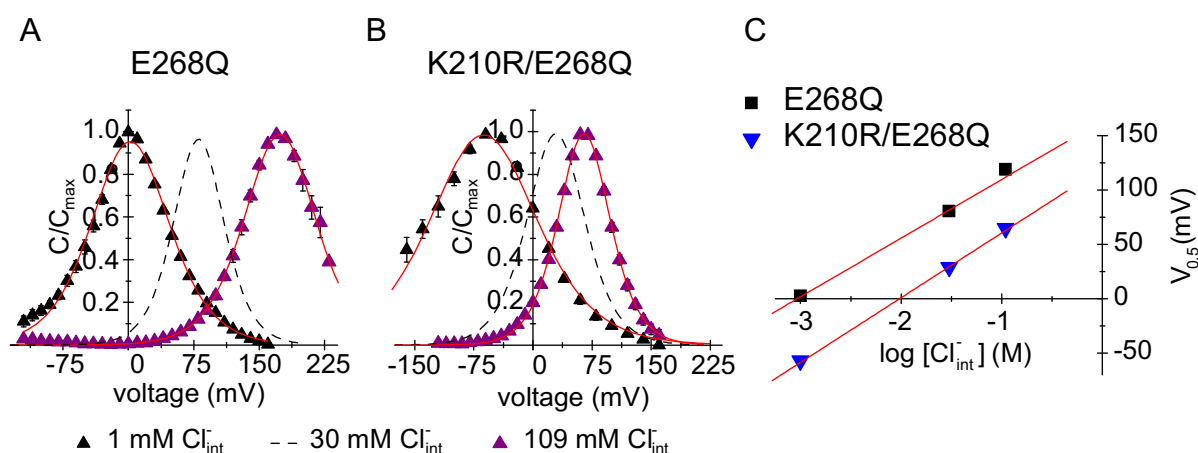
Figure 5.30: Nonlinear capacitances are shifted by internal [Cl⁻] and mutation K210R changes apparent K_d for internal Cl⁻. A and B. Normalized nonlinear capacitances of E268Q (**A**) and K210R/E268Q ClC-5 (**B**) at different internal Cl⁻ concentrations (solutions 1, 10, 11 and I) at symmetrical pH 7.4. Solid lines are fits of the first derivative of the Boltzmann function (for parameters see Table 8). Dashed lines describe data from Figure 5.27 D for comparison. **C.** Summary of midpoints of capacitance curves from Table 8 plotted against the decadic logarithm of the internal Cl⁻ concentration. Lines represent linear fits to the data and report on the apparent K_d for internal Cl⁻ at 0 mV.

	[Cl⁻int] (mM)	1	30	105
	$V_{0.5}$ (mV)	2.8 ± 1.1	80.7 ± 0.6	118.7 ± 1.9
E268Q	z	-0.88 ± 0.02	-1.31 ± 0.01	-1.27 ± 0.00
	n	6	17	4
	$V_{0.5}$ (mV)	-57.0 ± 1.5	29.1 ± 0.4	64.9 ± 1.1
K210R/E268Q	z	-0.62 ± 0.03	-1.04 ± 0.01	-1.15 ± 0.03
	n	4	16	5

Table 8: Values for voltages of maximum change of capacitance ($V_{0.5}$) and slope z, obtained from fits to Equation 2 of n individual cells from Figure 5.30. Data for 30 mM are taken from Table 5.

At 1 mM internal Cl⁻ the half-maximal voltage of activation ($V_{0.5}$) for E268Q was strongly left-shifted to ~0 mV (Figure 5.30 A), whereas the additional mutation K210R shifted this

value to -60 mV (Figure 5.30 B). Additionally, the slope of the capacitance curve was reduced, more pronounced in the double mutant (Table 8). Compared to 30 mM internal Cl⁻, an elevated concentration of 109 mM shifted voltage dependence towards more depolarizing values and the slope was only little altered in E268Q ClC-5, whereas its value was increased for K210R/E268Q. Analogous to the interpretation of Orhan *et al.* for ClC-4, also for ClC-5 it can be conceived that internal anions mediate a voltage-dependent block, which can be described by the following reaction scheme:
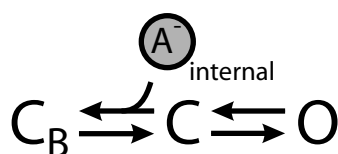
$$C_B \rightleftharpoons \overset{A^-_{internal}}{C} \rightleftharpoons O \qquad \text{Scheme 2}$$

$$P_{NOC} = \cfrac{1}{1 + \cfrac{[A]_{in}}{K_d(0)} \exp^{\frac{z\delta FV}{RT}}} \qquad \text{Equation 12}$$

According to the model, internal anions (A⁻) serve as voltage-dependent blocker and the activation of transport cycles can only be initiated after chloride first unbinds from the closed transporter (C_B). The mathematical description of this model has been provided previously elsewhere [143], [145]. It predicts that when anion binding and unbinding is fast (i.e. the observed rate-limiting reaction is the C-O transition), the half-maximal activation of ClC-5 should depend exponentially on the Cl⁻ concentration (Equation 12). Accordingly, plotting these values against the decadic logarithm of the internal Cl⁻ concentration should result in a linear dependence. Indeed, this was the case as well for E268Q, as for the double mutants K201R E268Q ClC-5. The X-axis intercept in this plot provides according to Equation 12 the apparent binding affinity (K_d) of ClC-5 for internal anions. This procedure reveals a value of approximately 1 mM E268Q ClC-5, whereas the apparent binding affinity for the double mutant K210R/E268Q is 10 mM. Therefore, a mutation at the outer vestibule of the anion pore affects the affinity for internal anions.

Analogously to the previous experiments, the effects of external anions on E268Q ClC-5 and on the double mutant K210R/E268Q were tested. In accordance to the effects described for ClC channels but also for some of the mammalian ClC transporters, depleting extracellular Cl⁻ shifted the voltage dependence to more depolarizing values, imposing that binding of external anions favours voltage-dependent activation. Depleting extracellular Cl⁻

shifts the voltage dependence to more depolarizing values. Figure 5.31 shows capacitance curves for E268Q and K210R/E268Q with 0.1 mM external Cl^-. Values for 155 mM Cl^- from Figure 5.27 D were used for normalization and are presented as dashed lines.
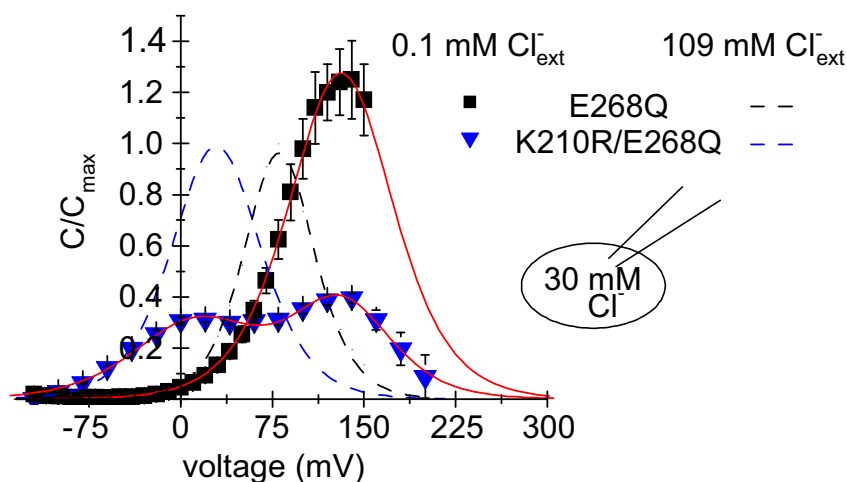
Figure 5.31: Removal of external Cl^- enhances and shifts nonlinear capacitances in E268Q, whereas a double bell-shaped capacitance curve in K210R/E268Q becomes visible. Nonlinear capacitances of E268Q and K210R/E268Q ClC-5, measured with 30 mM internal Cl^- and external Cl^- reduced to 0.1 mM at symmetrical pH 7.4 (solutions 10 and IV). For comparison, dashed lines represent the fits to data in 155 mM Cl^-_{ext} from Figure 5.27 D. Solid lines represent fits to the first derivative of a standard Boltzmann function (E268Q) or the sum of two of such functions (K210R/E268Q). Parameters are given in Table 9.

	E268Q	**K210R/E268Q**
$V_{0.5}$ **(mV)**	130.4 ± 2.1	131.4 ± 1.8
z	-0.91 ± 0.02	-0.95 ± 0.22
$V_{0.5}$ **(mV)**		10.3 ± 4.6
z		-0.76 ± 0.03
n	3	4

Table 9: Mean parameter values for trace fitting of one (E268Q) or the sum of two (K210R/E268Q) derivatives of the standard Boltzmann function to n individual cells from Figure 5.31.

For E268Q, voltage-dependent changes of capacitance were larger and shifted towards more depolarizing values by ~50 mV and the value for z decreased from -1.31 to -0.91 e_0 (Table 9). Removing external Cl^- decreased nonlinear capacitances of K210R/E268Q dramatically but also led to the appearance of a second local maximum in the capacitance curve. The change of capacitance was distributed over a much broader voltage span and on single-cell level the relative magnitude of left maximum varied, but was usually the smaller of both. The voltage dependence of the nonlinear capacitances could be fitted with the sum of two derivatives of a standard Boltzmann function with parameters are given in Table 9. The right maximum had

same voltage dependence as E268Q (similar $V_{0.5}$ and z). The left maximum was at 10 mV with a slope of -0.76 e_0.

5.10.4 Gating kinetics of ClC-5 and K210/E268Q mutants

As seen in Figure 5.27 an additional mutation at position 210 changed the appearance of gating currents and the voltage dependence of nonlinear capacitances with respect to the single mutant E268Q. This was also true for modifications of the cysteine substitution of lysine 210. To analyze if there is also a difference of kinetics of the depolarization activated process that gives rise to gating currents, the time dependence of those currents can be studied using so called *envelope protocols* [143], [146](Figure 5.32 A, upper panel). During this protocol, depolarizing pulses of a certain voltage for incrementing durations are applied to the cell. With increasing time, more ClC-5 transporters are activated and those contribute to the off-gating charge at the end of the pulse, measured after a jump to -100 mV. Plotting the integral of the off-gating currents (Q_{off}) versus the time of the depolarizing pulse, reports on the activation kinetics at the respective voltage. A preceding constant reference pulse of +150 mV was included in all protocols and was used for normalization.
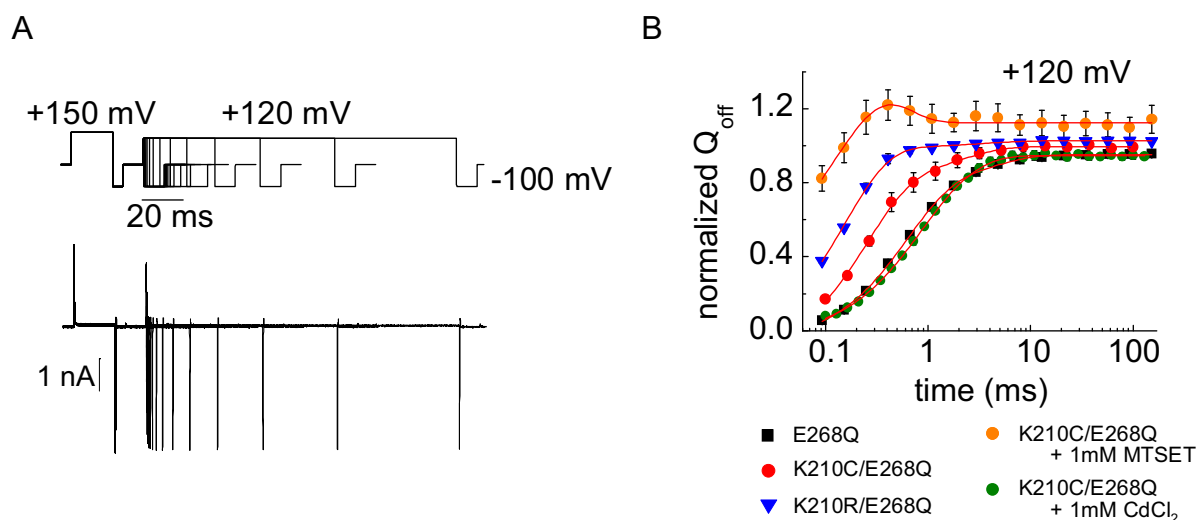
Figure 5.32: Envelope protocols report altered time courses of off-gating charge movement. A. Envelope protocol (**upper panel**) and representative recording of a HEK293T cell, expressing E268Q ClC-5 (solution 10 and I). From the holding potential, a +150-mV step was applied, followed by a test pulse of -100 mV to elicit a large off-gating current which was used for normalization. After this, voltage pulses of different voltages (here: +120 mV) were applied for incrementing durations at each sweep before jumping to -100 mV. The off-gating currents of those voltage jumps were integrated normalized to the integrated gating current at +150 mV. **B.** Normalized time-dependent development of off-gating charges after activation at +120 mV for various mutants and external modifications, as indicated. For clarity, some points were omitted. Red lines represent exponential fits with one or two exponentials.

Figure 5.32 A (lower panel) shows a representative recording of time-dependent development of off-gating currents of E268Q ClC-5 at +120 mV. Mean normalized values for measurements of this and other mutants at this voltage are summarized in Figure 5.32 B.

Gating charges develop in an exponential manner. Figure 5.33 shows detailed the activation time courses of WT ClC-5 (Figure 5.33 A) and the various mutations (Figure 5.33 B, C, E) and cysteine modifications (Figure 5.33 D and F) at different voltages and time constants and amplitudes are shown in Figure 5.34. In some cases, gating currents at +30 mV were too small to provide a reliable analysis and were therefore omitted. Although wildtype ClC-5 mediates, in contrast to the mutants measured here, substantial transport currents, gating currents could be recorded and time dependence could be fitted with double exponential functions (Figure 5.33 A). Fast (τ_1) and slow (τ_2) time constants were in the range 0.3-0.4 and 2.0-3.5 ms, respectively (Figure 5.34 A). Mutant E268Q ClC-5 (Figure 5.33 C) reached higher Q_{off} values than wildtype, which can not be attributed to left-shifted voltage dependence, resulting in larger gating currents already at lower voltages. However, the voltage dependence of the mutant is shifted at most towards more depolarized values (see Table 4). Voltage-dependent time constants for this mutant were slowed down to values of 0.6-1.0 and 4.3-7.7 ms for τ_1 and τ_2, respectively (Figure 5.34 C). The double mutant K210C/E268Q (Figure 5.33 B) exhibited already at +30 mV well-defined off-gating currents, and the values for +120 mV reached the same magnitude as at the preceding +150 mV reference pulse, which, however, can be due to the left shift of voltage dependence. The time dependence was faster than in mutant E268Q and had values similar to wildtype, disregarding measurements at +60 mV, showing quite large errors (Figure 5.34 B). When this mutant was modified by 1 mM external $CdCl_2$ (Figure 5.33 D, Figure 5.34 D), kinetics became slower, resembling the behaviour of the single mutant E268Q (superimposed in Figure 5.32 B). This probably reflects the restoration of the voltage dependence to E268Q values, mediated by $CdCl_2$ as demonstrated before in this work (Figure 5.28 and Table 7). The double mutant K210R/E268Q (Figure 5.33 E) that strongly shifted the voltage dependence towards less depolarizing voltages demonstrated also smaller time constants for the fast component, which further diminished at high voltages (Figure 5.34 E). The magnitude of gating currents was already at 25% at the beginning, explained by the left-shifted voltage dependence – even at the holding potential a certain percentage of ClC are activated and deactivate subsequently during the -100-mV test pulse. Interestingly, the magnitude of gating currents at +90 and +120 mV reached the same steady-state value, which was also the same magnitude as at +150 mV. This finding was even more distinct in the MTSET-modified form of K210C/E268Q (Figure 5.33 F), exhibiting a very strong voltage dependence of τ_1, which was the fastest of all measured time constants at +120 mV (Figure 5.34 F).
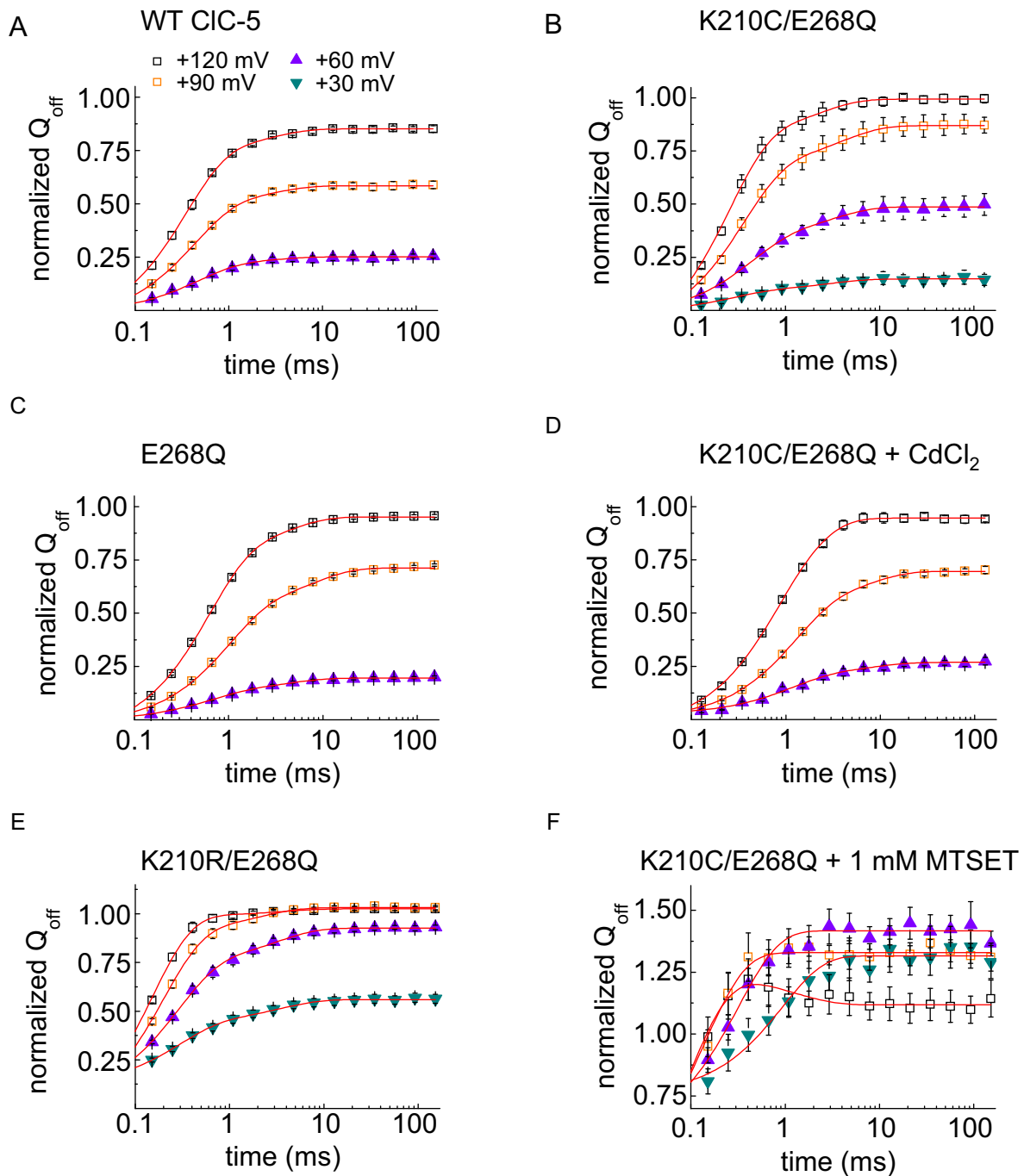
Figure 5.33: Normalized time courses of off-gating currents at various voltages, measured using the same solutions and envelope protocols similar as shown in Figure 5.32 A, upper panel. The time-variable voltage step was carried out at different voltages and charges were normalized to the +150 mV reference pulse, included in each sweep. Red lines are mono- or biexponential fits and time constants and amplitudes are depicted in Figure 5.34. (n = 3-7).

Very importantly here, τ_2, which was only visible above +90 mV, had negative amplitude and describes therefore a form of deactivation, which was also time- and voltage-dependent. This deactivation was stronger at more positive voltages in a way, that the 10-ms reference pulse of +150 mV evoked less off-gating currents than all of the other tested voltages, which therefore reached values above 1 after less than 1 ms (Figure 5.34 F). Also, gating currents at +120 mV

first increased and then decreased and reached lower steady-state values than the other voltages (Figure 5.33 F). Both can be seen in a representative measurement in Figure 5.35. The described behaviour could also be observed at +90 mV and in the mutant K210R/E268Q at +120 mV and seems to be therefore dependent on the voltage range where those mutants activate.
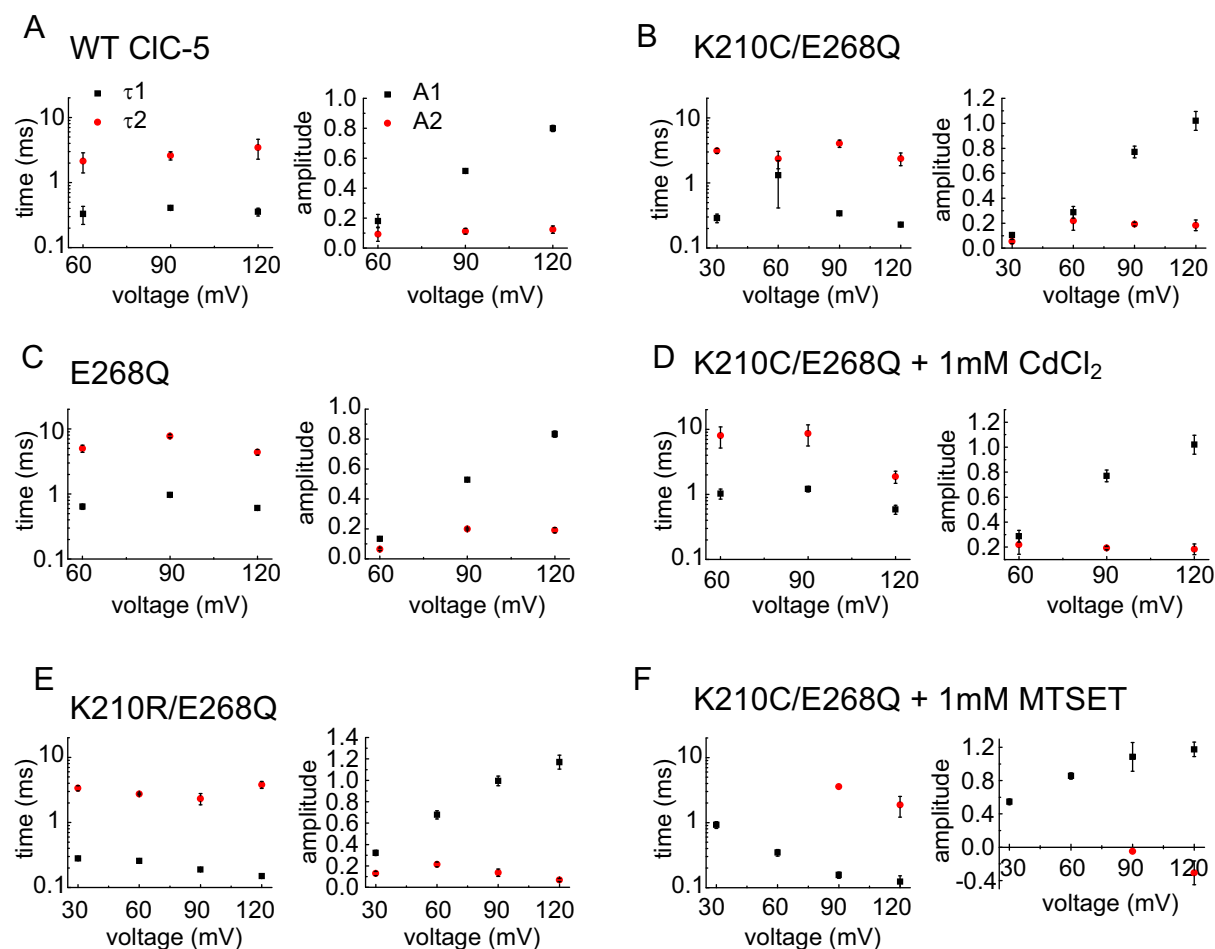
Figure 5.34: Mean voltage-dependent time constants and amplitudes of exponential fits for development of off-gating currents from Figure 5.33. Time constants are displayed on a logarithmic scale.
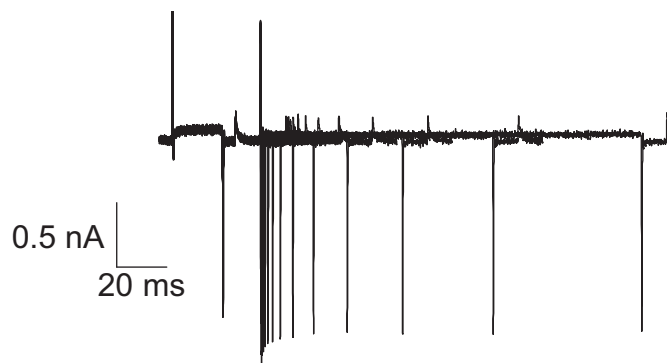
Figure 5.35: Off-gating currents can display a form of time- and voltage-dependent depletion. Representative whole-cell measurement of a HEK293T cell expressing K210C/E268Q ClC-5 after modification with 1 mM MTSET, recorded at +120 mV under the conditions shown in Figure 5.32.

5.10.5   Voltage-dependent modification of K210C ClC-5 by MTSET

Because the residue modified by MTSET – K210C – is directly adjacent to the gating glutamate and mutations were shown here to directly modify voltage dependence, also a voltage dependence of modification is conceivable. Yang and Horn demonstrated the voltage-dependent movement of the voltage sensing S4 domain of the skeletal muscle sodium channel by determining reaction rate constants of covalent MTSET modification of a cysteine mutant [147]. They proposed a simple model assuming that the exposure of the cysteine in the S4 domain to the outside is a fast and voltage-dependent first order transition and that the subsequent binding of MTSET to the cysteine is a slow second order reaction and voltage-independent:

$$\text{Cys}_{in} \underset{\beta(V)}{\overset{\alpha(V)}{\rightleftharpoons}} \text{Cys}_{out} \xrightarrow{[MTSET]k_{on}} \text{Cys-SET} \qquad \text{Scheme 3}$$

(fast) (slow)

According to their model the rate of modification is linearly dependent on the concentration. They further assumed that the cysteine is located outside the electric field, so that the local MTSET concentration is not affected by it.

MTSET modification of K210C/E268Q ClC-5 induces a pronounced left shift of capacitances (see Section 5.10.2 and Figure 5.28 B) and the magnitude of gating currents decreased. This decrease was monitored to assess rates of modificati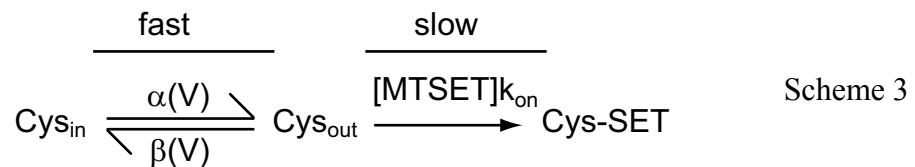on. Figure 5.36 B shows time courses of modification of K210C ClC-5 by 1 mM external MTSET from observation of the charge of the off-gating (Q_{off}) at +120 mV at four different holding voltages. Gating currents decreased monoexponentially with rate constants (i.e. reciprocal time constants) increasing with higher voltage (Figure 5.36 D). Even at -70 mV, a decrease of off-gating current was detectable

The concentration dependence was assessed at +70 mV (Figure 5.36 C) and plotting rate constants versus the concentration reveals a saturating behaviour (Figure 5.36 D) and not a linear relationship, as predicted by the model of Yang and Horn.
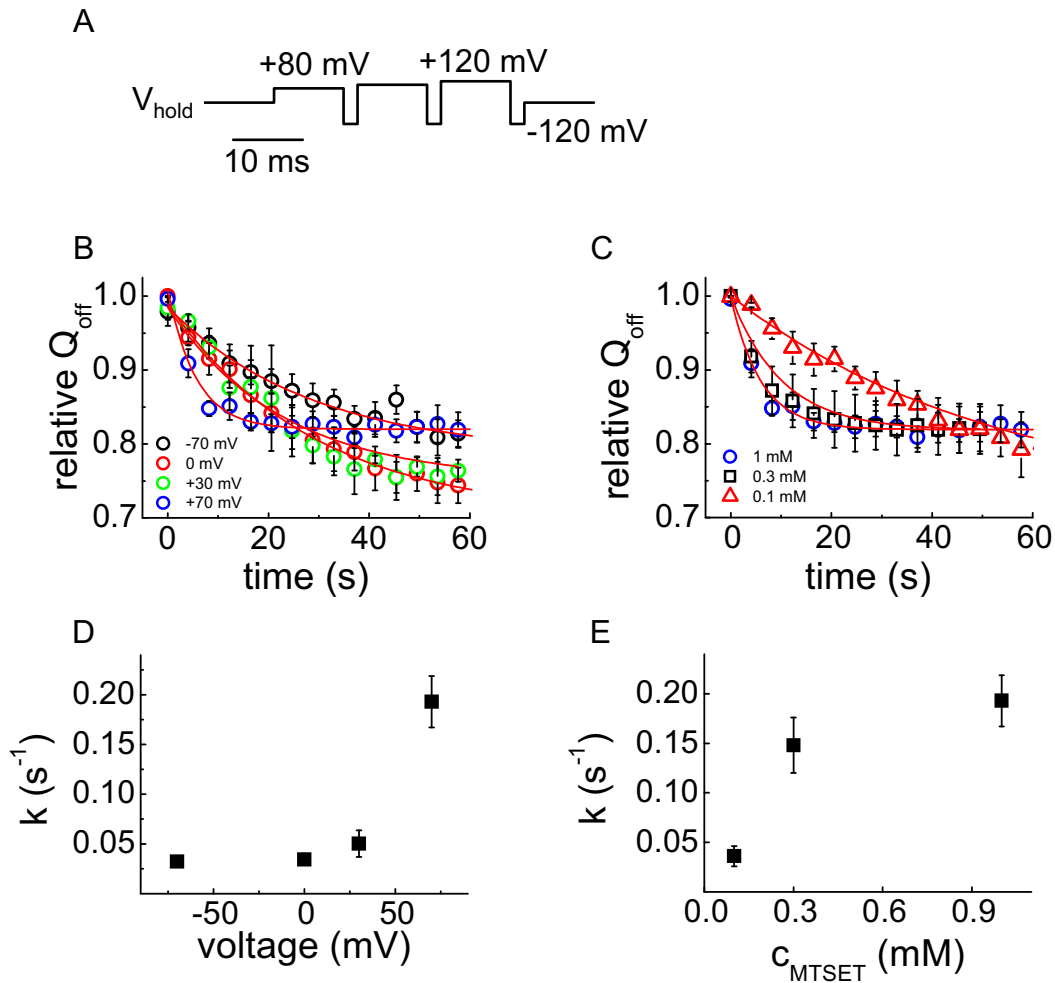
Figure 5.36: MTSET modification of K210C ClC-5 is voltage- and concentration-dependent. A. Voltage protocol, used to follow time course of MTSET modification. V_{hold} was varied for measuring voltage dependence of modification. The off-gating charge upon the +120 mV voltage jump to -120 mV was monitored and the protocol was applied in 2-s intervals. **B** and **C.** Time course of MTSET modification at different holding voltages (**B**) or different MTSET concentrations (**C**). Values were normalized to the off-gating charges before modification took place. Concentration-dependent modification (B) was measured at +70 mV and data for 1 mM MTSET come from (A). For clarity, some intermediate data points were omitted. Red lines represent monoexponential fits to the data. **D** and **E.** Time constants for exponential fits, displayed as rate constants versus the holding voltage (**D**) and the MTSET concentration (**E**), respectively.

5.11 Functional specialization of ClC transporters with respect to the voltage-dependent gating and nonlinear capacitances

The presence of gating currents in ClCs was first detected in ClC-5 [80], but other ClC transporter isoforms also display those nonlinear capacitances. The low membrane insertion upon heterologous expression of ClC-3 in the past has handicapped electrophysiological access and contradicting and ambiguous reports have been published. Zhao *et al.* [148] have found a dileucine cluster in the N-Terminus of ClC-3 which acts as a retention signal and when those amino acids are mutated to alanine (ClC-3_{13-19A}), substantial membrane insertion was achieved [148]. When expressed in HEK293T cells and measured using the whole-cell patch clamping technique, robust outwardly rectifying Cl$^-$ currents could be observed (Figure 5.37 A) similar to ClC-5 with pronounced on- and off-gating currents. Although gating currents could not be observed in previous works on ClC-4 [60], [143], a closer examination of leak-subtracted recordings demonstrated the existence of those currents in this isoform, too (Figure 5.37 B). As in ClC-5, the voltage-dependent development can be described with a Boltzmann function. Also, by applying sinusoidal protocols and by utilizing the lock-in functionality of the patch clamp amplifier, voltage-dependent changes of whole-cell capacitances in ClC-3, -4 and -5 could be recorded under the same conditions and compared (Figure 5.37 C). When normalized to the Cl$^-$ currents at +135 mV, large differences in capacitance magnitudes can be seen, which were also reflected in the size of the gating currents in whole-cell recordings. Compared to ClC-3 and ClC-5 gating currents as well as changes in capacitance were tiny, but voltage dependence resembled ClC-3, which had the highest normalized capacitances. ClC-5 ranges between the other isoforms in the size of capacitances, but voltage dependence is strongly shifted towards depolarizing voltages.
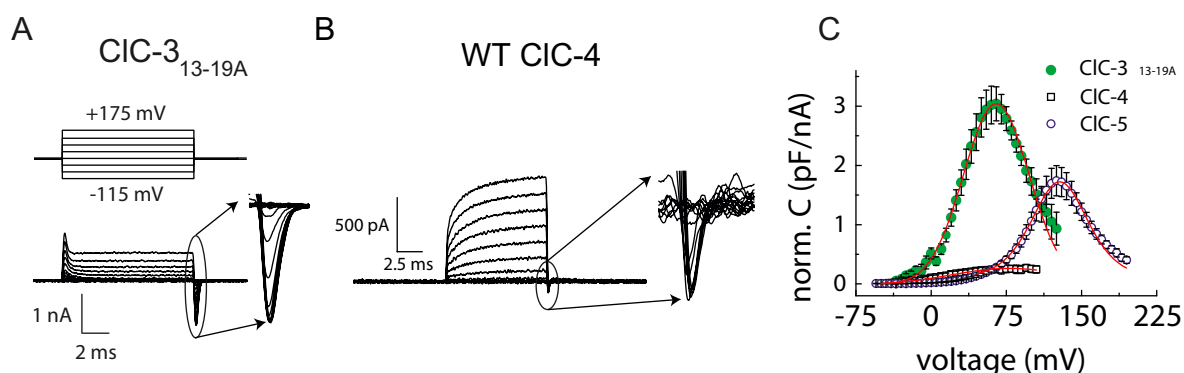
Figure 5.37: ClC-3 and ClC-4 also display nonlinear capacitances which differ from ClC-5 with respect to magnitude and voltage dependence. **A.** and **B.** Voltage protocol and representative –P/n leak subtracted whole-cell recordings (solutions 12 and XVIII) of a cell expressing ClC-3, bearing a mutation for enhanced plasma membrane insertion (**A**) or ClC-4 (**B**). Depicted as enlarged insets are the off-gating currents. **C.** Capacitance curves of ClC-3 to -5, normalized to the current at +135 mV. Red lines represent fits to the first derivative of a standard Boltzmann function (Equation 2). ClC-3 and ClC-4 measurements were performed by R. Guzman and A.K. Alekov, respectively. (Modified from Guzman *et al.* (submitted))

6 Discussion

6.1 Fluorescent Measurements of endosomal pH

Mammalian cells are characterized by a variety of morphologically and functionally different intracellular organelles, but ClC-5 is localized mainly in the plasma membrane and in a subpopulation of early endosomal vesicles. Elucidating the physiological effects of disease-causing mutations or other modifications of ClC-5 function, like chloride concentration, anion species or pH, requires therefore the existence of pH markers that predominantly report the acidity of the endosomes in which ClC-5 is also present. The standard methodology to perform such investigations is to use endosomal markers with conjugated pH-sensitive dyes. Two markers are very often used for such investigations of ClC transporter function – FITC conjugated transferrin [57] or VAMPII-fused pHluorin (synapto-pHluorin)[120], [138], [139]. The aim of measuring the pH of endosomes containing ClC-5 therefore included the necessity to quantify the extent of colocalization of ClC-5 with the two aforementioned markers using 3D confocal microscopy.

The experiments reveal, that FITC-transferrin did not colocalize to a substantial degree with ClC-5 (Section 5.1). Similarly, the co-expression of ClC-5 and the VAMPII-fused pHluorin (synapto-pHluorin) also resulted in a very low degree of colocalization. Such lack of colocalization is not surprising, because ClC-5 is mainly part of the endocytotic pathway whereas VAMPII is associated mainly with exocytosis [121], [122]. Although ClC-5 containing endosomes demonstrated a similar staining pattern as synapto-pHluorin containing endosomes, these vesicles seem to belong to two different populations.

A partial colocalization of ClC-4 and ClC-5 was previously shown in transfected Caco-2 cells [56], but the extent of colocalization between FITC-transferrin and ClC-5 was not quantified. These authors showed later that ClC-4 is an important determinant of transferrin uptake in mouse fibroblasts [62]. It seems therefore logical to assume that most of the FITC-transferrin uptake occurs due to endogenous activity in HEK293 cells and the compartments containing endocytosed transferrin are different from those, in which both overexpressed ClC-5 and ClC-4 are localized.

Hara-Chikuma and colleagues [76] measured endosomal pH in proximal tubule (PT) cells of normal and ClC-5 knock-out mice. Compared to wildtype mice, they reported a higher pH value in early endosomes of knock-out mice, measured with transferrin-conjugated dyes, but an unchanged pH of late endosomes, labelled by α_2-macroglobulin-conjugated dyes. However, only endosomal-like staining by immunofluorescence in wildtype cells, along with

substantial plasma membrane staining in knock-out mice was reported but the colocalization of ClC-5 and the applied pH indicators was not quantified.

Smith *et al.* utilized synapto-pHluorin to quantify the effects of various Dent's disease mutations [138]. Colocalization to organelle markers was assessed in a semi-quantitative manner based on 2D images but co-staining with ClC-5 and synapto-pHluorin was not performed. These authors detected ClC-5 in both early and late endosomes in transfected HEK-MSR cells, yet the latter of which was shown before not to acidify in a ClC-5 dependent manner [76]. The experiments revealed a higher endosomal pH in HEK-MSR cells transfected with Dent's disease mutants when compared to cells transfected with WT ClC-5, however, other Dent's disease mutants had the opposite effect in decreasing endosomal pH. A similar approach was used to demonstrate that ClC-5 is able to directly acidify endosomes when the V-type ATPase is blocked [139]. In this case however, immunofluorescent images revealed qualitatively partially overlapping localization of ClC-5 and synapto-pHluorin.

The lack of colocalization in presented in this thesis and the data of Hara-Chikuma *et al.* showing no effect of ClC-5 knock-out on the pH of late endosomes suggests that pH measurements with this synapto-pHluorin are likely to be contaminated with acidification facilitated by other conductances. As an alternative, different experimental systems (native mouse PT cells vs. transfected HEK cells) might account for the discrepancies, which make a direct qualitative measurement of colocalization of ClC-5 and the respective dyes even more plausible.

The results here show that two of the most commonly used markers for investigating endosomal acidity – FITC-conjugated transferrin and synapto-pHluorin – are not optimally suitable for investigating ClC-5 function. They further suggest that a careful 3D assessment of the colocalization of the used pH marker and ClC-5 in the particular expression system are essential for performing quantitative investigations of the physiological role of this isoform. They also demonstrate the need of developing new sensors for measuring endosomal acidification with higher specificity to the different endosomal subpopulations. Another possibility to overcome the problems associated with poor colocalization is to develop techniques in which acidity is dynamically measured at the single vesicle level with online colocalization to the corresponding ClC protein.

6.2 The proton glutamate E268 regulates transport probability of ClC-5

This work provides insights into the mechanism of voltage sensing and regulation of transport probability. Smith and Lippiat were the first to describe the presence of gating currents in ClC-5 and used them to describe voltage dependence. In analogy to Santos-Sacchi [136], additionally, here the voltage dependence was also assessed by measuring the capacitance changes, mediated by ClC-5 upon depolarization. Furthermore, the process underlying gating currents is likely to be the same that activates ionic currents because Smith and Lippiat [80] demonstrated that the conductance-voltage relationship of WT ClC-5 closely resembles the charge-voltage relationship of the non-conducting E268A ClC-5 in terms of shape and voltage dependence. As suggested in this thesis, the presence of gating currents and nonlinear capacitances represent the same molecular process and can therefore be used synonymous.

The ratio between nonlinear capacitances and ionic transport differed strongly depending on one hand on the internal pHs and on the other on the biochemical properties of the side chain of the amino acid at position 268. This amino acid is strongly conserved among the ClC transporters and is postulated to be at the intracellular end of the proton conduction pathway [59], [93]. Results presented in this thesis indicate that a readily protonatable residue at this position and/or high internal $[H^+]$ reduced the capacitance but increased the probability of transport, not only in coupled mode, but also in uncoupled mode, without changing the degree of uncoupling. The reason for this was, however, neither a shift of voltage dependence of the process activated by depolarizing voltages (Section 5.6) nor altered affinities for the transported substrates (Section 5.4). Likewise, the single channel amplitude in external SCN^- remained unchanged by a better supply of internal H^+ (Section 5.3), which was also published for NO_3^- by another group [79], suggesting that internal protons do not increase unitary transport rates independent on the nature of the transported anion. Altogether, the aforementioned results show that internal protons modulate a different gating process. This process regulates the transport probability of ClC-5, but is different from the prominent depolarization-activated gating, manifested in its voltage dependence of the nonlinear capacitances and gating charge movements. In ClC-4 the depolarization activated gating process is similarly independent of internal pH [143] and an additional gating process was detected at hyperpolarization which corroborates the notion that ClC transporter gating is a complex voltage and substrate-dependent process.

Based on the recently published ClC structure showing the gating glutamate occupying the central anion binding site S_{cen} [96], it can be postulated that ionic transport

requires this residue to first unbind from S_{cen}. The binding of the negative side chain is strong, but it is weakened by the transfer of one proton to the gating glutamate at this site. Accordingly, when the gating glutamate is substituted by cysteine, which is far less protonatable, the effects of internal protons are absent. Additional support for this hypothesis is provided by the findings that S168P, which destabilizes the binding of anions or of the gating glutamate to the central binding site, reduces sensitivity to internal pH (Section 5.8).

The results presented here, in conjunction with the solved structures of EcClC and CmClC [90], [96] can be used to create a simple schematic model, explaining the occurrence of the gating currents in ClC transporters (Figure 6.1).
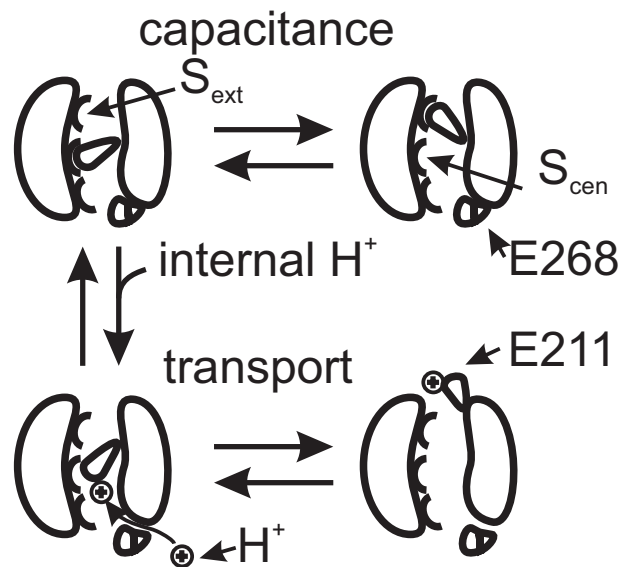
Figure 6.1: Theoretical model scheme on the generation of voltage-dependent capacitance mediated by ClC-5. The gating glutamate E211 can be protonated when it accepts a proton at the central binding site, delivered by the proton glutamate 268. The protonated gating glutamate swings out and this complete transport process does not generate capacitance. When the protonation can not be accomplished, the nonprotonated gating glutamate is only able to oscillate between the central and external binding site in a voltage-dependent manner and creates capacitance without transport. The internal proton supply and/or the properties of the residue at position 268 determine the proportion of completed and incomplete transport-cycles and thereby the magnitude of nonlinear capacitances and ionic currents. (From Grieschat and Alekov, 2012)

The model describes the movement of the gating glutamate between the central (S_{cen}) and the external (S_{ext}) anion binding sites and the external solution: when the gating glutamate is bound at the central binding site it can accept a proton delivered by the proton glutamate and subsequently swing out. The transport cycle can proceed and no capacitance is generated. When one imagines voltage-dependent gating charge movement it becomes graspable that a protonated and therefore neutral gating glutamate cannot contribute to this. In accordance with this assumption, gating currents could not be detected upon substitution of the gating glutamate by the neutral alanine [80] or the mostly protonated and therefore neutral cysteine (Figure 5.17 A). Conversely, when no transport is possible, because the proton glutamate is

mutated to glutamine and is unable to protonate the gating glutamate, the negatively charged side chain is only able to switch between both closed conformations, (S_{cen}, S_{ext}). This restricted conformational change is responsible for the observed capacitance changes. The pronounced gating currents seen in the transporting WT ClC-5 do not contradict the postulated model, because the absolute open probability of this isoform is very low, as determined by non-stationary noise analysis (Section 5.3). In addition, a protonatable residue with a higher pK_a of the side chain (e.g. histidine) in place of the proton glutamate has a lower tendency to pass the proton on to the gating glutamate and the model predicts larger capacitances in this case, which are also experimentally observed for this mutant (Figure 5.12). According to the presented scheme, also a higher internal proton concentration facilitates the proton transfer from the proton to the gating glutamate and leads to low capacitance, which is also confirmed in the experiments (Figure 5.16).

Several unexplained experimental findings reported by other groups can be easily explained by the model postulated here. For example, it becomes clear why, in contrast to mammalian ClC transporters, the bacterial isoform EcClC is still able to mediate uncoupled Cl^- flux when the proton glutamate is neutralized. The gating glutamate in EcClC might be bound more weakly at S_{cen}, which would result in much higher probability to swing to S_{ext} and be protonated from the external side, thereby opening the conduction way for Cl^-.

It should be finally noted that there are findings that might not fully agree with the model presented in Figure 6.1. On one hand, mutation E268H not only shifts the ratio of transport to capacitance (i.e. alters transport probability), but also changes the degree of uncoupling by external SCN^- (see Section 5.9). The model predicts however no qualitative difference between a higher pK_a of the proton glutamate 268 side chain or a higher internal proton concentration. Unfortunately, the method used to measure proton flux in this work is not suitable to accurately quantify absolute coupling stoichiometries and therefore, only relative uncoupling with respect to Cl^- upon external SCN^- application was determined. So it is not possible to discriminate, if in E268H ClC-5 SCN^- uncouples less efficiently than in WT or if Cl^- transport *per se* is less coupled to H^+ movement. An investigation on the coupling efficiencies of various proton glutamate mutants of EcClC [149] left this parameter nearly unchanged compared to wildtype. However, the different behaviour of proton glutamate mutants of EcClC and ClC-5 with nonprotonatable residues at this position makes the direct transfer of these results very difficult.

The results concerning proton transport in external SCN^- presented in this thesis differ from results in ClC-4 [60] and results of another group which expressed analyzed ClC-5 in

Xenopus laevis oocytes [59], reporting strong decrease of H^+ flux upon SCN^- application. The differences to ClC-4 can be easily explained, based on the much higher overall transport probability of this isoform [60]. In this case, the maximum possible 100% transport probability is much earlier reached and application of external SCN is not able to induce a further increase, but only uncouples transport. The differences to the results of Zdebik *et al.* are on the other hand most probably due to differences in the expression system. The internal conditions are not exactly known and cannot be controlled in *Xenopus* oocytes but can be of crucial importance. For example, in this work and from others it is shown that lower internal Cl^- concentration will result in increased transport probability.

6.3 Lysine 210, positioned in the immediate proximity of the gating glutamate, alters anion/proton antiport coupling and voltage dependence of ClC-5

In order to characterize the function of lysine 210 in ClC-5 transport, one experiment shown here, investigated possible effects on transport coupling in various external substrates.

The residue next to the gating glutamate was subject of previous investigations in ClC-1 [91] and also in ClC-5 [140] and in both cases strong impact on the anion selectivity was reported. WT ClC-1 favours in terms of conduction Cl^- to NO_3^-, whereas the corresponding mutation K231A reverses this behaviour [91]. ClC-5 prefers in terms of transport specificity the large uncoupling anion NO_3^- over Cl^-, but mutation K210A shifts this behaviour well towards Cl^- [140]. This tendency was also seen for the mutant K210C ClC-5 in the same publication, where NO_3^- currents were slightly decreased compared to Cl^- currents. This is in agreement with results presented in this thesis, also reporting about the same current magnitudes for external Cl^- and NO_3^-

Measuring proton transport, De Stefano *et al.* reported a relative uncoupling of ~3-4 in external NO_3^- for both the K210A mutant and wildtype, denoting only an altered substrate specifity [140]. However, this finding partly contrasts with results in this thesis. Here, mutant K210C ClC-5 mediates NO_3^- currents with about the same magnitude as Cl^- currents, but uncoupling in NO_3^- was less pronounced than in wildtype (Section 5.10.1). This value was also ~3 and therefore comparable to K210A, yet relative uncoupling in wildtype reached values of ~5-7 in measurements presented in this thesis. This value is supported by previous results from the same group, using a different method to determine the absolute coupling stoichiometries in Cl^- and NO_3^- [79]. For WT ClC-5 they reported a 2 to 1 Cl^-/H^+

stoichiometry and a 12-22 to 1 NO_3^-/H^+ stoichiometry, which results in 6-12 times relative uncoupling – values much different than the recently published ones [140] and comparable to the values presented in this thesis for the wildtype. Therefore, the unchanged uncoupling detected by De Stefano *et al.* [140] could be due to insensitivities of the chosen method. Unfortunately, as mentioned before, the method used in this thesis is not capable to determine absolute transport stoichiometries. Therefore, the mutation K210C could bring about stronger NO_3^-/H^+ coupling or weaker Cl^-/H^+ coupling to mediate the detected relative uncoupling.

De Stefano and colleagues postulated no change of voltage dependence of Cl^- currents in K210A and only a small change for K210C but they gained this notion merely by comparing current magnitudes at two different voltages and not by quantifying $V_{0.5}$, as pursued in this thesis. For K210R they assessed a stronger alteration of voltage dependence, which is consistent to the result presented here. Although in this thesis, the nonconducting double mutant K210C/E268Q was used to determine voltage dependence, previous experiments (Figure 5.13) showed that the additional proton glutamate mutation does not alter voltage dependence dramatically.

6.4 The effects of mutations and modification at position 210 are diverse and suggest complex amino acid interactions

It is obvious, that the properties of the side chain adjacent to the gating glutamate modifies voltage sensing of ClC-5 (Section 5.10.2), but it is puzzling what the determinants are. The conservative mutation of lysine to arginine (both possess long, either neutral or positively charged residues) shifts voltage dependence much more than the shorter and neutral or negative cysteine. Furthermore, when this cysteine is modified by the MTSET, this elongation and reintroduction of positive charge does not restore the properties similar to the long and positively charged lysine, but shifts the voltage dependence by another 50 mV towards hyperpolarizing voltages.

In contrast, extracellular application of Cd^{2+} restores voltage dependence and kinetics of activation to values very similar to those of E268Q (Figure 5.28 and Figure 5.33). It could be hypothesized that Cd^{2+} assumes a transient binding to the deprotonated sulfhydryl group and still possesses positive charge to somehow mimic the properties of the native lysine. However, magnitudes of capacitances and gating currents are not restored to the large values of E268Q. From those results of site-directed cysteine modification, neither clear effects of charge, nor of size can be deduced. It appears therefore that the amino acid at position 210 does not directly move in the membrane electric field and serves as a part of the voltage

sensor of ClC-5, but interacts with other amino acids and the specific energy of this interaction modulates voltage-dependent gating. Possible candidates for such interactions are residues from the external part of helix B (see Figure 5.22) and namely with amino acids histidine 80 and aspartate 76, which are located only 3-5 Å away from K210. In addition, it is possible that the residue at position 210 does not interact with a single partner, but with different ones, depending on the size of the substituted residue. Because of this, depending on which amino acid is the interaction partner, the same charge can have a dramatically different effect. Nevertheless, the strong effects of mutations at this position on voltage dependence and selectivity argue that not only movements of the gating glutamate take place during transport.

The effects of cysteine modification were two-fold – MTSET modification of K210C/E268Q shifted the voltage dependence to hyperpolarized values, along with a decrease of capacitance (Section 5.10.2), when normalized to the data of the unmodified cysteine mutant. This might be explained by a higher baseline capacitance at a given holding potential – The strong left-shift of $V_{0.5}$ to 0 mV in MTSET modified K210C/E268Q (Figure 5.28 B) would lead to a certain percentage of activated ClC-5 even at -30 mV holding potential, and therefore cause a quite high capacitance. Only the remaining nonactivated ClC could contribute to the voltage-dependent increase nonlinear capacitance, rendering the bell-shaped curve shallower. This assumption is however inconsistent with the reduction of capacitance, when the voltage dependence is shifted to more positive values by Cd^{2+}, which should result in more transporters contributing to the capacitance at the same given holding potential. Similar inconsistency is observed also for the H80C/E268Q double mutant, for which MTSET increased the capacitance, along with slightly shifting the voltage dependence to less positive voltages. Furthermore in D76C/E268Q, Cd^{2+} strongly decreases capacitance without dramatic voltage shift. In K210C/E268Q the decrease of capacitance seems to exhibit a different dependence on the Cd^{2+} concentration than the left-shift of voltage dependence does. All these observations indicate a complex process, which is strongly dependent on the position of the substituted amino acid in the protein. At least in case of Cd^{2+} the diverse effects could also be linked to the divalent nature of the cation or to the possible voltage dependence of instantaneous binding and unbinding. It can not be concluded yet, if K210 interacts with residues of helix B, but cross-linking experiments in the future might be the answer to this.

6.5 Voltage-dependent kinetics of ClC-5 activation are associated with simultaneous deactivation

The kinetics of activation of ClC-5 can directly be linked to the voltage dependence of activation. Mutants or modification, which shifted the voltage dependence to less positive values activated with a smaller time constants (τ_1 and τ_2, Section 5.10.4). *Vice versa*, right-shift upon Cd^{2+} modification of K210C/E268Q slowed activation kinetics down to values similar to the absence of the cysteine substitution the same way as voltage-dependence was restored. Apparently also a third process has to be taken into account which is best seen at the most left-shifted MTSET-modified K210C/E268Q – gating charge reduction (inactivation) that is time- and voltage-dependent (Figure 5.33 and Figure 5.35).

This process of deactivation resembles the gating charge immobilization of cation channels, for example the Shaker K^+ channel of *Drosophila* where this voltage- and time-dependent behaviour was also shown [150]. The effect in this potassium channel was strongly dependent on the holding voltage and could be abolished by mutational deletion of a portion of the N-terminus. Because cation channels and Cl^- transporters share no homology, a conclusion on a molecular correlate in ClC-5 is not possible. Further insight might be gained however from future investigations on the dependence of the nonlinear capacitances and holding voltage of the experiment.

6.6 Voltage-dependent gating presumably involves movement of helix F

The accessibility for covalent MTS modification of the cysteine substituted residue next to the gating glutamate was published before for ClC-1 [91] and also for ClC-5 [140], and in this thesis, the voltage dependence of modification was assessed, which was faster at depolarizing voltages (Section 5.10.5). Thus, additionally to the shifted voltage dependence of K210 mutants, voltage-dependent MTSET modification indicates that movements not only of the gating glutamate but of the whole helix are involved in the gating process. One could imagine that, when the protonated gating glutamate 211 swings out, movements of Helix F occur, which alter the orientation of residue 210, which is localized in the loop at the beginning of this helix and subsequently exposed to the solution at depolarizing voltage.

Modification was shown to take place at all tested voltages. This raises several possibilities. Perhaps, even at -70 mV a fraction of K210C/E268Q ClC-5 proteins are activated, which could be the case, because also in the negative voltage range nonlinear capacitance is evoked (Figure 5.27 D). Alternatively, K210C might never be completely

excluded from the external solution, even at nonactivating voltages. As a third possibility, the short voltage pulses to determine Q_{off} could be sufficient to cause exposal and subsequent modification, which indeed was shown to be fast for thiols in aqueous solution with a rate of 10^5 M^{-1} sec^{-1} [132].

The model of Yang and Horn [147] (Scheme 3), previously used to describe voltage-dependent MTS modifications, predicts a linear dependence between modification rate and MTSET concentration, which seems not to be the case for modification of K210C ClC-5. This indicates that not all of the assumptions for the validity of this model hold.

6.7 Mutation K210R at the external interface reduces blocking effect of internal anions

Attempting to explain the observed shifts in the voltage dependence for various mutations of lysine 210, the apparent binding affinities of ClC-5 for internal anions were assessed in this thesis. Mutation K210R increased the K_d value 10-fold, indicating that conformational changes at the extracellular edge of the pore directly modulate the binding of internal anions (Section 5.10.3). The blocking action of internal anions on ClC-5 might be explained by assuming that Cl^- binding to the internal binding site disfavours the binding of the negative gating glutamate to the central binding site by electrical repulsion [143]. *Vice versa* this can be a reason for the elevated apparent K_d for internal Cl^- in the mutant K210R/E268Q – The mutation shifts voltage dependence to less depolarized voltages because the gating glutamate can reach the central binding site easier and a Cl^- ion at the internal binding site cannot bind with the high affinity as in WT. Feng *et al.* [151] reported a much slower transport in CmClC, when the gating glutamate is substituted by a shorter aspartate, which is supposed to more difficultly reach the internal binding site (S_{int}).

The apparent binding constant for internal Cl^- was previously assessed for ClC-4 to be 800 µM [143] and is very similar to values reported here for E268Q ClC-5. It is however unclear, whether the observed effects are caused by Cl^- binding to the internal or the central binding site S_{int} or S_{cen} (Figure 3.5). The values for these two mammalian ClC transporters differ profoundly from values published for the prokaryotic EcClC, which were measured using isothermal titration calorimetry (ITC) and reporting a $K_d > 20$ mM for the Cl^- affinity of the internal binding site [94]. Interestingly, this group determined the affinity of the central binding site to be 700 µM for Cl^-. It is therefore possible that either the experiments presented here report the binding affinities of internal Cl^- to the central binding site, or alternatively binding affinities might differ profoundly between the mammalian and bacterial isoforms.

6.8 Mutation K210R might mediate voltage-dependent transitions that result in bi-phasic voltage sensing

Measurements with reduced external Cl⁻ showed increased and right-shifted bell-shaped capacitance for the single mutant E268Q whereas the double mutant K210R/E268Q featured a double bell-shaped capacitance curve (Figure 5.31). This behaviour is presumably not directly connected to the left-shift of voltage dependence of K210R/E268Q, because the even further shifted MTSET-modified K210C/E268Q does not show this behaviour upon removal of extracellular Cl⁻.

In analogy to Santos-Sacchi [136] the increase of capacitance can be regarded as the generation of a dipole in a certain direction upon depolarization, until $V_{0.5}$ is reached. After this voltage, the dipole is reorienting, which leads to reduction in membrane capacitance. In this framework, the double-peak behaviour of mutation K210R/E268Q is interpreted as a repeated reorientation of the protein dipole moment (Figure 6.2).
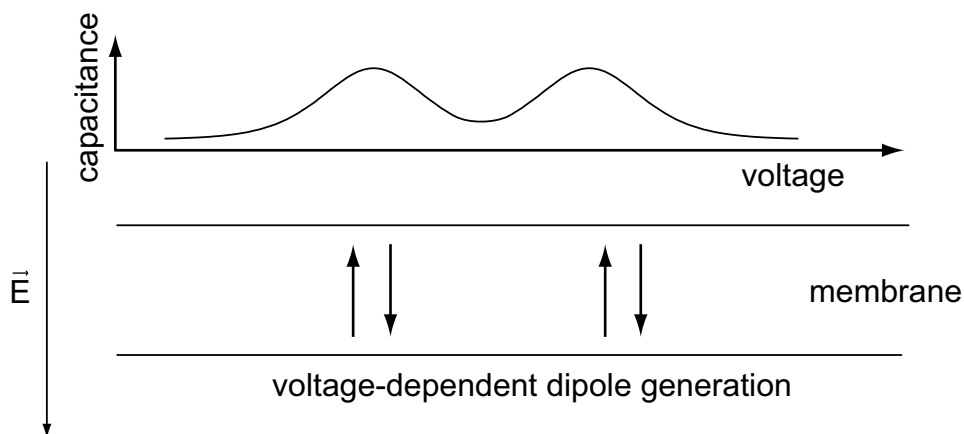
Figure 6.2: Voltage-dependent dipole generation opposes the electric field and elevates capacitance. Shown is the direction of the electric field (E) and parallel components of the generated dipoles, either in direction or opposing the direction of the electric field. The direction and magnitude is voltage dependent and weakens or strengthens the electric field, leading to increase or decrease of membrane capacitance. Mutation K210R might lead to a voltage-dependent repeat of this dipole movement.

Since the external electric field obviously does not change its orientation during this process, the observed reorientation cannot be simplistically explained by a reversed movement direction of charged amino acids in the protein (i.e. the gating glutamate 211) and more complex mechanisms should be discussed to encounter for the experimental findings. One possibility is that hypothetic interactions of lysine 210 with other residues serve as a spring, opposing the movements of the gating glutamate. For the double bell-shaped capacitance

curve it might be thinkable, that in one voltage range K210R might interact with certain residues in helix B and arrange for the voltage-dependent action of the gating glutamate. When higher voltages are applied, the arginine 210 might switch its interaction partners, which might change the interaction energy manifested in the model as reduced spring constant. Such switches would allow accordingly a reversal of the movement direction of the gating glutamate, thereby creating a second event of dipole formation.

Although no clear role can be attributed to the nature of the substituted side-chain concerning charge and length, one can speculate that the bifurcated guanidinium group of arginine has more opportunities to find other reaction partners than lysine. As a consequence, it can initially interact with one partner residue in the low voltage range and then it interacts with the same partner like lysine would do and result in the same voltage dependence as E268Q (Figure 5.31). Deciphering the structural basis from existing ClC crystals is obstructed by the poor conservation of the residue next to the gating glutamate (Figure 5.20) – arginine in ClC-ec1, tryptophan in CmClC and phenylalanine in SyClC. In the future, scanning analysis with cross-linkable residues in helix B might provide further evidence for the validity of this very speculative mechanism.

6.9 Physiological importance of gating currents and nonlinear capacitances of mammalian ClC transporters

Gating currents and nonlinear capacitances can be used as an unambiguous hallmark of ClC transporter activity to discriminate them from endogenous or somehow upregulated conductances, which might be the origin of contradicting ClC-3 reports in the past. Particularly by mutation of the proton glutamate, ClC-3, -4 and -5 demonstrated significant gating currents and nonlinear capacitances, but of different magnitudes (Section 5.11). ClC-3 demonstrated largest, ClC-4 lowest changes of capacitance and ClC-5 ranges in the middle. Applying the model from (Section 6.2), it can be stated, that ClC-3 is the "worst" transporter of all three, while ClC-4 is the "best" transporter. This is reflected in the absolute open probabilities, which was previously determined for ClC-4 by non-stationary noise analysis to be ~50% [60]. Non-stationary noise analysis under the same ionic conditions shown in this thesis reveals a much smaller absolute open probability for ClC-5, which is reflected in larger gating currents.

Those three ClCs are intracellularly localized transporters, apparently with the same task of shunting against high positive voltage in endosomes, caused by the V-type ATPase. Yet large differences concerning voltage dependence and transport probability argue for specializations of each isoform to different intracellular compartments. In those organelles,

very diverse concentrations of protons and Cl$^-$ are present, which may be accompanied by different transmembrane voltages (Figure 3.2). The membrane capacitance influences the number of charges which is needed to impose a certain membrane potential [152]. It may be speculated that "bad" ClC transporters, that act as "good" capacitors elevate the membrane capacitance to lower transmembrane voltage, normally opposing further acidification. Thereby they might be able to provide an electrical shunt without actually transporting ions. Compartments with conditions requiring charge transport for shunting might be the operational area of the "good" transporters.

7 References

[1]   B. Hille, *Ion Channels of Excitable Membranes*, 3rd Edition. Sinauer Associates Inc 2, 2001.

[2]   F. J. Sigworth, "Voltage gating of ion channels," *Q. Rev. Biophys.*, vol. 27, no. 1, pp. 1–40, 1994.

[3]   F. Sachs, "Stretch-activated ion channels: what are they?," *Physiology (Bethesda)*, vol. 25, no. 1, pp. 50–56, 2010.

[4]   E. A. Barnard, "Receptor classes and the transmitter-gated ion channels," *Trends Biochem. Sci.*, vol. 17, no. 10, pp. 368–374, 1992.

[5]   D. C. Gadsby, "Ion channels versus ion pumps: the principal difference, in principle," *Nat. Rev. Mol. Cell Biol.*, vol. 10, no. 5, pp. 344–352, 2009.

[6]   O. Jardetzky, "Simple Allosteric Model for Membrane Pumps," *Nature,* vol. 211, no. 5052, pp. 969–970, 1966.

[7]   N. C. Danbolt, "Glutamate uptake," *Prog. Neurobiol.*, vol. 65, no. 1, pp. 1–105, 2001.

[8]   A. L. Harris, "Emerging issues of connexin channels: biophysics fills the gap," *Q. Rev. Biophys.*, vol. 34, no. 3, pp. 325–472, 2001.

[9]   Y. Maulet, R. C. Lambert, S. Mykita, J. Mouton, M. Partisani, Y. Bailly, G. Bombarde, and A. Feltz, "Expression and targeting to the plasma membrane of xClC-K, a chloride channel specifically expressed in distinct tubule segments of Xenopus laevis kidney," *Biochem. J.*, vol. 340 (Pt 3), pp. 737–743, 1999.

[10]   T. J. Jentsch, T. Friedrich, A. Schriever, and H. Yamada, "The CLC chloride channel family," *Pflugers Arch.,* EJP., vol. 437, no. 6, pp. 783–795, 1999.

[11]   A. Accardi and C. Miller, "Secondary active transport mediated by a prokaryotic homologue of ClC Cl- channels," *Nature*, vol. 427, no. 6977, pp. 803–807, 2004.

[12]   A. Picollo and M. Pusch, "Chloride/proton antiporter activity of mammalian CLC proteins ClC-4 and ClC-5," *Nature*, vol. 436, no. 7049, pp. 420–423, 2005.

[13]   O. Scheel, A. A. Zdebik, S. Lourdel, and T. J. Jentsch, "Voltage-dependent electrogenic chloride/proton exchange by endosomal CLC proteins," *Nature*, vol. 436, no. 7049, pp. 424–427, 2005.

[14]   J. J. Matsuda, M. S. Filali, K. A. Volk, M. M. Collins, J. G. Moreland, and F. S. Lamb, "Overexpression of CLC-3 in HEK293T cells yields novel currents that are pH dependent," *Am. J. Physiol.-Cell Ph.*, vol. 294, no. 1, pp. C251–C262, 2008.

[15]   A. R. Graves, P. K. Curran, C. L. Smith, and J. A. Mindell, "The Cl-/H+ antiporter ClC-7 is the primary chloride permeation pathway in lysosomes," *Nature*, vol. 453, no. 7196, pp. 788–792, 2008.

[16]   T. J. Jentsch, "CLC Chloride Channels and Transporters: From Genes to Protein Structure, Pathology and Physiology," *Crit. Rev. Biochem. Mol.* vol. 43, no. 1, pp. 3–36, 2008.

[17]   M. M. White and C. Miller, "A voltage-gated anion channel from the electric organ of Torpedo californica," *J. Biol. Chem.*, vol. 254, no. 20, pp. 10161–10166, 1979.

[18]   K. Steinmeyer, C. Ortland, and T. J. Jentsch, "Primary structure and functional expression of a developmentally regulated skeletal muscle chloride channel," *Nature*, vol. 354, no. 6351, pp. 301–304, 1991.

[19]   C. Fahlke, R. Rüdel, N. Mitrovic, M. Zhou, and A. L. George Jr, "An aspartic acid residue important for voltage-dependent gating of human muscle chloride channels," *Neuron*, vol. 15, no. 2, pp. 463–472, 1995.

[20]   A. H. Bretag, "Muscle chloride channels," *Physiol. Rev.*, vol. 67, no. 2, pp. 618–724, 1987.

[21] C. Fahlke, "Chloride channels take center stage in a muscular drama," *J. Gen. Physiol.,* vol. 137, no. 1, pp. 17–19, 2011.

[22] M. C. Koch, K. Steinmeyer, C. Lorenz, K. Ricker, F. Wolf, M. Otto, B. Zoll, F. Lehmann-Horn, K. H. Grzeschik, and T. J. Jentsch, "The skeletal muscle chloride channel in dominant and recessive human myotonia," *Science*, vol. 257, no. 5071, pp. 797–800, 1992.

[23] M. Pusch, K. Steinmeyer, and T. J. Jentsch, "Low single channel conductance of the major skeletal muscle chloride channel, ClC-1," *Biophys. J.*, vol. 66, no. 1, pp. 149–152, 1994.

[24] F. Lehmann-Horn and K. Jurkat-Rott, "Voltage-gated ion channels and hereditary disease," *Physiol. Rev.*, vol. 79, no. 4, pp. 1317–1372, 1999.

[25] A. Thiemann, S. Gründer, M. Pusch, and T. J. Jentsch, "A chloride channel widely expressed in epithelial and non-epithelial cells," *Nature*, vol. 356, no. 6364, pp. 57–60, 1992.

[26] C. Saint-Martin, G. Gauvain, G. Teodorescu, I. Gourfinkel-An, E. Fedirko, Y. G. Weber, S. Maljevic, J. P. Ernst, J. Garcia-Olivares, and C. Fahlke, "Two novel CLCN2 mutations accelerating chloride channel deactivation are associated with idiopathic generalized epilepsy," *Hum. Mutat.*, vol. 30, no. 3, pp. 397–405, 2009.

[27] M. Pusch, S. E. Jordt, V. Stein, and T. J. Jentsch, "Chloride dependence of hyperpolarization-activated chloride channel gates," *J. Physiol. (Lond.)*, vol. 515 (Pt 2), pp. 341–353, 1999.

[28] S. E. Jordt and T. J. Jentsch, "Molecular dissection of gating in the ClC-2 chloride channel," *EMBO J.*, vol. 16, no. 7, pp. 1582–1592, 1997.

[29] M. R. Bösl, V. Stein, C. Hübner, A. A. Zdebik, S. E. Jordt, A. K. Mukhopadhyay, M. S. Davidoff, A. F. Holstein, and T. J. Jentsch, "Male germ cells and photoreceptors, both dependent on close cell-cell interactions, degenerate upon ClC-2 Cl(-) channel disruption," *EMBO J.*, vol. 20, no. 6, pp. 1289–1299, 2001.

[30] J. Blanz, M. Schweizer, M. Auberson, H. Maier, A. Muenscher, C. A. Hübner, and T. J. Jentsch, "Leukoencephalopathy upon disruption of the chloride channel ClC-2," *J. Neurosci.*, vol. 27, no. 24, pp. 6581–6589, 2007.

[31] G. C. Scheper, C. G. M. van Berkel, L. Leisle, K. E. de Groot, A. Errami, T. J. Jentsch, and M. S. Van der Knaap, "Analysis of CLCN2 as candidate gene for megalencephalic leukoencephalopathy with subcortical cysts," *Genet. Test. Mol. Bioma.*, vol. 14, no. 2, pp. 255–257, 2010.

[32] S. Kieferle, P. Fong, M. Bens, A. Vandewalle, and T. J. Jentsch, "Two highly homologous members of the ClC chloride channel family in both rat and human kidney," *Proc. Natl. Acad. Sci. U.S.A.*, vol. 91, no. 15, pp. 6943–6947, 1994.

[33] S. Uchida, S. Sasaki, T. Furukawa, M. Hiraoka, T. Imai, Y. Hirata, and F. Marumo, "Molecular cloning of a chloride channel that is regulated by dehydration and expressed predominantly in kidney medulla," *J. Biol. Chem.*, vol. 268, no. 6, pp. 3821–3824, 1993.

[34] R. Estévez, T. Boettger, V. Stein, R. Birkenhäger, E. Otto, F. Hildebrandt, and T. J. Jentsch, "Barttin is a Cl- channel beta-subunit crucial for renal Cl- reabsorption and inner ear K+ secretion," *Nature*, vol. 414, no. 6863, pp. 558–561, 2001.

[35] A. G. H. Janssen, U. Scholl, C. Domeyer, D. Nothmann, A. Leinenweber, and C. Fahlke, "Disease-Causing Dysfunctions of Barttin in Bartter Syndrome Type IV," *J. Am. Soc. Nephrol.*, vol. 20, no. 1, pp. 145–153, 2009.

[36] U. Scholl, S. Hebeisen, A. G. H. Janssen, G. Müller-Newen, A. Alekov, and C. Fahlke, "Barttin modulates trafficking and function of ClC-K channels," *Proc. Natl. Acad. Sci. U.S.A.*, vol. 103, no. 30, pp. 11411–11416, 2006.

[37] D. B. Simon, R. S. Bindra, T. A. Mansfield, C. Nelson-Williams, E. Mendonca, R. Stone, S. Schurman, A. Nayir, H. Alpay, A. Bakkaloglu, J. Rodriguez-Soriano, J. M. Morales, S. A. Sanjad, C. M. Taylor, D. Pilz, A. Brem, H. Trachtman, W. Griswold, G. A. Richard, E. John, and R. P. Lifton, "Mutations in the chloride channel gene, CLCNKB, cause Bartter's syndrome type III," *Nat. Genet.*, vol. 17, no. 2, pp. 171–178, 1997.

[38] C. Fahlke and M. Fischer, "Physiology and pathophysiology of ClC-K/barttin channels," *Front. Physiol.*, vol. 1, p. 155, 2010.

[39] R. Birkenhäger, E. Otto, M. J. Schürmann, M. Vollmer, E. M. Ruf, I. Maier-Lutz, F. Beekmann, A. Fekete, H. Omran, D. Feldmann, D. V. Milford, N. Jeck, M. Konrad, D. Landau, N. V. Knoers, C. Antignac, R. Sudbrak, A. Kispert, and F. Hildebrandt, "Mutation of BSND causes Bartter syndrome with sensorineural deafness and kidney failure," *Nat. Genet.*, vol. 29, no. 3, pp. 310–314, 2001.

[40] T. J. Jentsch, "Chloride and the endosomal–lysosomal pathway: emerging roles of CLC chloride transporters," *J. Physiol.*, vol. 578, no. 3, pp. 633–640, 2007.

[41] I. Mellman, "Endocytosis and molecular sorting," *Annu. Rev. Cell Dev. Biol.*, vol. 12, pp. 575–625, 1996.

[42] N. D. Sonawane and A. S. Verkman, "Determinants of [Cl-] in recycling and late endosomes and Golgi complex measured using fluorescent ligands," *J. Cell Biol.*, vol. 160, no. 7, pp. 1129–1138, 2003.

[43] G. Borsani, E. I. Rugarli, M. Taglialatela, C. Wong, and A. Ballabio, "Characterization of a human and murine gene (CLCN3) sharing similarities to voltage-gated chloride channels and to a yeast integral membrane protein," *Genomics*, vol. 27, no. 1, pp. 131–141, 1995.

[44] M. Kawasaki, M. Suzuki, S. Uchida, S. Sasaki, and F. Marumo, "Stable and functional expression of the ClC-3 chloride channel in somatic cell lines," *Neuron*, vol. 14, no. 6, pp. 1285–1291, 1995.

[45] M. Hara-Chikuma, B. Yang, N. D. Sonawane, S. Sasaki, S. Uchida, and A. S. Verkman, "ClC-3 chloride channels facilitate endosomal acidification and chloride accumulation," *J. Biol. Chem.*, vol. 280, no. 2, pp. 1241–1247, 2005.

[46] D. Duan, C. Winter, S. Cowley, J. R. Hume, and B. Horowitz, "Molecular identification of a volume-regulated chloride channel," *Nature*, vol. 390, no. 6658, pp. 417–421, 1997.

[47] J. J. Matsuda, M. S. Filali, M. M. Collins, K. A. Volk, and F. S. Lamb, "The ClC-3 Cl-/H+ Antiporter Becomes Uncoupled at Low Extracellular pH," *J. Biol. Chem.*, vol. 285, no. 4, pp. 2569–2579, 2009.

[48] L. Wang, W. Ma, L. Zhu, D. Ye, Y. Li, S. Liu, H. Li, W. Zuo, B. Li, W. Ye, and L. Chen, "ClC-3 is a candidate of the channel proteins mediating acid-activated chloride currents in nasopharyngeal carcinoma cells," *Am. J. Physiol.-Cell Ph.*, vol. 303, no. 1, pp. C14–23, 2012.

[49] M. Kawasaki, S. Uchida, T. Monkawa, A. Miyawaki, K. Mikoshiba, F. Marumo, and S. Sasaki, "Cloning and expression of a protein kinase C-regulated chloride channel abundantly expressed in rat brain neuronal cells," *Neuron*, vol. 12, no. 3, pp. 597–604, 1994.

[50] P. Huang, J. Liu, A. Di, N. C. Robinson, M. W. Musch, M. A. Kaetzel, and D. J. Nelson, "Regulation of human CLC-3 channels by multifunctional Ca2+/calmodulin-dependent protein kinase," *J. Biol. Chem.*, vol. 276, no. 23, pp. 20093–20100, Jun. 2001.

[51] X. Li, T. Wang, Z. Zhao, and S. A. Weinman, "The ClC-3 chloride channel promotes acidification of lysosomes in CHO-K1 and Huh-7 cells," *Am. J. Physiol.-Cell Ph.*, vol. 282, no. 6, pp. C1483–C1491, 2002.

[52] F. J. Miller Jr, M. Filali, G. J. Huss, B. Stanic, A. Chamseddine, T. J. Barna, and F. S. Lamb, "Cytokine activation of nuclear factor κB in vascular smooth muscle cells requires signaling endosomes containing Nox1 and ClC-3," *Circ. Res.*, vol. 101, no. 7, pp. 663–671, 2007.

[53] S. M. Stobrawa, T. Breiderhoff, S. Takamori, D. Engel, M. Schweizer, A. A. Zdebik, M. R. Bösl, K. Ruether, H. Jahn, A. Draguhn, R. Jahn, and T. J. Jentsch, "Disruption of ClC-3, a chloride channel expressed on synaptic vesicles, leads to a loss of the hippocampus," *Neuron*, vol. 29, no. 1, pp. 185–196, 2001.

[54] L. W. Dickerson, D. J. Bonthius, B. C. Schutte, B. Yang, T. J. Barna, M. C. Bailey, K. Nehrke, R. A. Williamson, and F. S. Lamb, "Altered GABAergic function accompanies hippocampal degeneration in mice lacking ClC-3 voltage-gated chloride channels," *Brain Res.*, vol. 958, no. 2, pp. 227–250, 2002.

[55] M. A. van Slegtenhorst, M. T. Bassi, G. Borsani, M. C. Wapenaar, G. B. Ferrero, L. de Conciliis, E. I. Rugarli, A. Grillo, B. Franco, H. Y. Zoghbi, and A. Ballabio, "A gene from the Xp22.3 region shares homology with voltage-gated chloride channels," *Hum. Mol. Genet.*, vol. 3, no. 4, pp. 547–552, 1994.

[56] R. Mohammad-Panah, C. Ackerley, J. Rommens, M. Choudhury, Y. Wang, and C. E. Bear, "The chloride channel ClC-4 co-localizes with cystic fibrosis transmembrane conductance regulator and may mediate chloride flux across the apical membrane of intestinal epithelia," *J. Biol. Chem.*, vol. 277, no. 1, pp. 566–574, 2002.

[57] R. Mohammad-Panah, R. Harrison, S. Dhani, C. Ackerley, L.-J. Huan, Y. Wang, and C. E. Bear, "The chloride channel ClC-4 contributes to endosomal acidification and trafficking," *J. Biol. Chem.*, vol. 278, no. 31, pp. 29267–29277, 2003.

[58] T. Friedrich, T. Breiderhoff, and T. J. Jentsch, "Mutational Analysis Demonstrates That ClC-4 and ClC-5 Directly Mediate Plasma Membrane Currents," *J. Biol. Chem.*, vol. 274, no. 2, pp. 896–902, 1999.

[59] A. A. Zdebik, G. Zifarelli, E.-Y. Bergsdorf, P. Soliani, O. Scheel, T. J. Jentsch, and M. Pusch, "Determinants of Anion-Proton Coupling in Mammalian Endosomal CLC Proteins," *J. Biol. Chem.*, vol. 283, no. 7, pp. 4219 –4227, 2008.

[60] A. K. Alekov and C. Fahlke, "Channel-like slippage modes in the human anion/proton exchanger ClC-4," *J. Gen. Physiol.*, vol. 133, no. 5, pp. 485–496, 2009.

[61] T. Suzuki, T. Rai, A. Hayama, E. Sohara, S. Suda, T. Itoh, S. Sasaki, and S. Uchida, "Intracellular localization of ClC chloride channels and their ability to form hetero-oligomers," *J. Cell. Physiol.*, vol. 206, no. 3, pp. 792–798, 2006.

[62] R. Mohammad-Panah, L. Wellhauser, B. E. Steinberg, Y. Wang, L. J. Huan, X. D. Liu, and C. E. Bear, "An essential role for ClC-4 in transferrin receptor function revealed in studies of fibroblasts derived from Clcn4-null mice," *J. Cell Sci.*, vol. 122, no. 8, p. 1229, 2009.

[63] S. Brandt and T. J. Jentsch, "ClC-6 and ClC-7 are two novel broadly expressed members of the CLC chloride channel family," *FEBS Lett.*, vol. 377, no. 1, pp. 15–20, 1995.

[64] M. Poët, U. Kornak, M. Schweizer, A. A. Zdebik, O. Scheel, S. Hoelter, W. Wurst, A. Schmitt, J. C. Fuhrmann, R. Planells-Cases, S. E. Mole, C. A. Hübner, and T. J. Jentsch, "Lysosomal storage disease upon disruption of the neuronal chloride transport protein ClC-6," *Proc. Natl. Acad. Sci. USA.*, vol. 103, no. 37, pp. 13854–13859, 2006.

[65] I. Neagoe, T. Stauber, P. Fidzinski, E.-Y. Bergsdorf, and T. J. Jentsch, "The late endosomal ClC-6 mediates proton/chloride countertransport in heterologous plasma membrane expression," *J. Biol. Chem.*, vol. 285, no. 28, pp. 21689–21697, 2010.

[66] U. Kornak, D. Kasper, M. R. Bösl, E. Kaiser, M. Schweizer, A. Schulz, W. Friedrich, G. Delling, and T. J. Jentsch, "Loss of the ClC-7 chloride channel leads to osteopetrosis in mice and man," *Cell*, vol. 104, no. 2, pp. 205–215, 2001.

[67] P. F. Lange, L. Wartosch, T. J. Jentsch, and J. C. Fuhrmann, "ClC-7 requires Ostm1 as a beta-subunit to support bone resorption and lysosomal function," *Nature*, vol. 440, no. 7081, pp. 220–223, 2006.

[68] T. Stauber and T. J. Jentsch, "Sorting motifs of the endosomal/lysosomal CLC chloride transporters," *J. Biol. Chem.*, vol. 285, no. 45, pp. 34537–34548, 2010.

[69] L. Leisle, C. F. Ludwig, F. A. Wagner, T. J. Jentsch, and T. Stauber, "ClC-7 is a slowly voltage-gated 2Cl-/1H+-exchanger and requires Ostm1 for transport activity," *EMBO J.*, vol. 30, no. 11, pp. 2140–2152, 2011.

[70] G. Novarino, S. Weinert, G. Rickheit, and T. J. Jentsch, "Endosomal Chloride-Proton Exchange Rather Than Chloride Conductance Is Crucial for Renal Endocytosis," *Science*, vol. 328, no. 5984, pp. 1398–1401, 2010.

[71] S. Weinert, S. Jabs, C. Supanchart, M. Schweizer, N. Gimber, M. Richter, J. Rademann, T. Stauber, U. Kornak, and T. J. Jentsch, "Lysosomal Pathology and Osteopetrosis upon Loss of H+-Driven Lysosomal Cl- Accumulation," *Science*, vol. 328, no. 5984, pp. 1401–1403, 2010.

[72] K. Steinmeyer, B. Schwappach, M. Bens, A. Vandewalle, and T. J. Jentsch, "Cloning and Functional Expression of Rat CLC-5, a Chloride Channel Related to Kidney Disease," *J. Biol. Chem.*, vol. 270, no. 52, pp. 31172–31177, 1995.

[73] W. Günther, A. Lüchow, F. Cluzeaud, A. Vandewalle, and T. J. Jentsch, "ClC-5, the chloride channel mutated in Dent's disease, colocalizes with the proton pump in endocytotically active kidney cells," *Proc. Natl. Acad. Sci. USA*, vol. 95, no. 14, p. 8075, 1998.

[74] S. E. Lloyd, S. H. Pearce, S. E. Fisher, K. Steinmeyer, B. Schwappach, S. J. Scheinman, B. Harding, A. Bolino, M. Devoto, P. Goodyer, S. P. Rigden, O. Wrong, T. J. Jentsch, I. W. Craig, and R. V. Thakker, "A common molecular basis for three inherited kidney stone diseases," *Nature*, vol. 379, no. 6564, pp. 445–449, 1996.

[75] N. Piwon, W. Gunther, M. Schwake, M. R. Bosl, and T. J. Jentsch, "ClC-5 Cl--channel disruption impairs endocytosis in a mouse model for Dent's disease," *Nature*, vol. 408, no. 6810, pp. 369–373, 2000.

[76] M. Hara-Chikuma, Y. Wang, S. E. Guggino, W. B. Guggino, and A. S. Verkman, "Impaired acidification in early endosomes of ClC-5 deficient proximal tubule," *Biochem. Biophys. Res. Commun.*, vol. 329, no. 3, pp. 941–946, 2005.

[77] W. Günther, N. Piwon, and T. J. Jentsch, "The ClC-5 chloride channel knock-out mouse-an animal model for Dent's disease," *Pflugers Arch.,* EJP, vol. 445, no. 4, pp. 456–462, 2003.

[78] S. J. Scheinman, "X-linked hypercalciuric nephrolithiasis: clinical syndromes and chloride channel mutations," *Kidney Int.*, vol. 53, no. 1, pp. 3–17, 1998.

[79] G. Zifarelli and M. Pusch, "Conversion of the 2 Cl−/1 H+ antiporter ClC-5 in a NO3−/H+ antiporter by a single point mutation," *EMBO J.*, vol. 28, no. 3, pp. 175–182, 2009.

[80] A. J. Smith and J. D. Lippiat, "Voltage-dependent charge movement associated with activation of the CLC-5 2Cl-/1H+ exchanger," *FASEB J.*, vol. 24, no. 10, pp. 3696–3705, 2010.

[81] A. L. Hodgkin and A. F. Huxley, "A quantitative description of membrane current and its application to conduction and excitation in nerve," *J. Physiol. (Lond.)*, vol. 117, no. 4, pp. 500–544, 1952.

[82] C. M. Armstrong and F. Bezanilla, "Currents related to movement of the gating particles of the sodium channels," *Nature*, vol. 242, no. 5398, pp. 459–461, 1973.

[83] C. M. Armstrong and F. Bezanilla, "Charge movement associated with the opening and closing of the activation gates of the Na channels," *J. Gen. Physiol.*, vol. 63, no. 5, pp. 533–552, 1974.

[84] C. Miller and M. M. White, "Dimeric structure of single chloride channels from Torpedo electroplax," *Proc. Natl. Acad. Sci. USA*, vol. 81, no. 9, p. 2772, 1984.

[85] R. Dutzler, "A structural perspective on ClC channel and transporter function," *FEBS Lett.*, vol. 581, no. 15, pp. 2839–2844, 2007.

[86] R. Dutzler, E. B. Campbell, M. Cadene, B. T. Chait, and R. MacKinnon, "X-ray structure of a ClC chloride channel at 3.0 A reveals the molecular basis of anion selectivity," *Nature*, vol. 415, no. 6869, pp. 287–294, 2002.

[87] A. Bateman, "The structure of a domain common to archaebacteria and the homocystinuria disease protein," *Trends. Biochem. Sci.*, vol. 22, no. 1, pp. 12–13, 1997.

[88] C. P. Ponting, "CBS domains in CIC chloride channels implicated in myotonia and nephrolithiasis (kidney stones)," *J. Mol. Med.*, vol. 75, no. 3, pp. 160–163, 1997.

[89] T. Schmidt-Rose and T. J. Jentsch, "Transmembrane topology of a CLC chloride channel," *Proc. Natl. Acad. Sci. USA*, vol. 94, no. 14, p. 7633, 1997.

[90] R. Dutzler, E. B. Campbell, and R. MacKinnon, "Gating the Selectivity Filter in ClC Chloride Channels," *Science*, vol. 300, no. 5616, pp. 108–112, 2003.

[91] C. Fahlke, H. T. Yu, C. L. Beck, T. H. Rhodes, and A. L. George, "Pore-forming segments in voltage-gated chloride channels," *Nature*, pp. 529–531, 1997.

[92] S. Waldegger and T. J. Jentsch, "Functional and structural analysis of ClC-K chloride channels involved in renal disease," *J. Biol. Chem.*, vol. 275, no. 32, pp. 24527–24533, 2000.

[93] A. Accardi, M. Walden, W. Nguitragool, H. Jayaram, C. Williams, and C. Miller, "Separate ion pathways in a Cl-/H+ exchanger," *J. Gen. Physiol.*, vol. 126, no. 6, pp. 563–570, 2005.

[94] A. Picollo, M. Malvezzi, J. C. D. Houtman, and A. Accardi, "Basis of substrate binding and conservation of selectivity in the CLC family of channels and transporters," *Nat. Struct. Mol. Biol.*, vol. 16, no. 12, pp. 1294–1301, 2009.

[95] C. Miller and W. Nguitragool, "A provisional transport mechanism for a chloride channel-type Cl^-/H^+ exchanger," *Phil. Trans. R. Soc. B*, vol. 364, no. 1514, pp. 175–180, 2009.

[96] L. Feng, E. B. Campbell, Y. Hsiung, and R. MacKinnon, "Structure of a Eukaryotic CLC Transporter Defines an Intermediate State in the Transport Cycle," *Science*, vol. 330, no. 6004, pp. 635 –641, 2010.

[97] W. Nguitragool and C. Miller, "Uncoupling of a CLC Cl−/H+ Exchange Transporter by Polyatomic Anions," *J. Mol. Biol.*, vol. 362, no. 4, pp. 682–690, 2006.

[98] C. G. Vanoye and A. L. George, "Functional characterization of recombinant human ClC-4 chloride channels in cultured mammalian cells," *J. Physiol.*, vol. 539, no. 2, pp. 373–383, 2002.

[99] S. Hebeisen, H. Heidtmann, D. Cosmelli, C. Gonzalez, B. Poser, R. Latorre, O. Alvarez, and C. Fahlke, "Anion permeation in human ClC-4 channels," *Biophys. J.*, vol. 84, no. 4, pp. 2306–2318, 2003.

[100] A. Accardi, S. Lobet, C. Williams, C. Miller, and R. Dutzler, "Synergism between halide binding and proton transport in a CLC-type exchanger," *J. Mol. Biol.*, vol. 362, no. 4, pp. 691–699, 2006.

[101] R. Estévez, M. Pusch, C. Ferrer-Costa, M. Orozco, and T. J. Jentsch, "Functional and structural conservation of CBS domains from CLC chloride channels," *J. Physiol. (Lond.)*, vol. 557, no. Pt 2, pp. 363–378, 2004.

[102] P. Fong, A. Rehfeldt, and T. J. Jentsch, "Determinants of slow gating in ClC-0, the voltage-gated chloride channel of Torpedo marmorata," *Am. J. Physiol.*, vol. 274, no. 4 Pt 1, pp. C966–973, 1998.

[103] B. Bennetts, "Cytoplasmic ATP-sensing Domains Regulate Gating of Skeletal Muscle ClC-1 Chloride Channels," *J. Biol. Chem.*, vol. 280, no. 37, pp. 32452–32458, 2005.

[104] P.-Y. Tseng, W.-P. Yu, H.-Y. Liu, X.-D. Zhang, X. Zou, and T.-Y. Chen, "Binding of ATP to the CBS domains in the C-terminal region of CLC-1," *J. Gen. Physiol.*, vol. 137, no. 4, pp. 357–368, 2011.

[105] S. Meyer, S. Savaresi, I. C. Forster, and R. Dutzler, "Nucleotide recognition by the cytoplasmic domain of the human chloride transporter ClC-5," *Nat. Struct. Mol. Biol.*, vol. 14, no. 1, pp. 60–67, 2007.

[106] G. Zifarelli and M. Pusch, "Intracellular regulation of human ClC-5 by adenine nucleotides," *EMBO Rep.*, vol. 10, no. 10, pp. 1111–1116, 2009.

[107] J. W. Scott, S. A. Hawley, K. A. Green, M. Anis, G. Stewart, G. A. Scullion, D. G. Norman, D. G. Hardie, and others, "CBS domains form energy-sensing modules whose binding of adenosine ligands is disrupted by disease mutations," *J. Clin. Invest.*, vol. 113, no. 2, pp. 274–284, 2004.

[108] M. I. Niemeyer, Y. R. Yusef, I. Cornejo, C. A. Flores, F. V. Sepúlveda, and L. P. Cid, "Functional evaluation of human ClC-2 chloride channel mutations associated with idiopathic generalized epilepsies," *Physiol. Genomics*, vol. 19, no. 1, pp. 74–83, 2004.

[109] T. J. Jentsch, K. Steinmeyer, and G. Schwarz, "Primary structure of Torpedo marmorata chloride channel isolated by expression cloning in Xenopus oocytes," *Nature*, vol. 348, no. 6301, pp. 510–514, 1990.

[110] N. Yang, A. L. George Jr, and R. Horn, "Molecular basis of charge movement in voltage-gated sodium channels," *Neuron*, vol. 16, no. 1, pp. 113–122, 1996.

[111] E. A. Richard and C. Miller, "Steady-state coupling of ion-channel conformations to a transmembrane ion gradient," *Science*, vol. 247, no. 4947, pp. 1208–1210, 1990.

[112] M. Pusch, U. Ludewig, A. Rehfeldt, and T. J. Jentsch, "Gating of the voltage-dependent chloride channel CIC-0 by the permeant anion," *Nature*, vol. 373, no. 6514, pp. 527–531, 1995.

[113] T. Y. Chen and C. Miller, "Nonequilibrium gating and voltage dependence of the ClC-0 Cl- channel," *J. Gen. Physiol.*, vol. 108, no. 4, pp. 237–250, 1996.

[114] M. Boshart, F. Weber, G. Jahn, K. Dorsch-Häsler, B. Fleckenstein, and W. Schaffner, "A very strong enhancer is located upstream of an immediate early gene of human cytomegalovirus," *Cell*, vol. 41, no. 2, pp. 521–530, 1985.

[115] E. Beck, G. Ludwig, E. A. Auerswald, B. Reiss, and H. Schaller, "Nucleotide sequence and exact localization of the neomycin phosphotransferase gene from transposon Tn5," *Gene*, vol. 19, no. 3, pp. 327–336, 1982.

[116] N. C. Shaner, R. E. Campbell, P. A. Steinbach, B. N. G. Giepmans, A. E. Palmer, and R. Y. Tsien, "Improved monomeric red, orange and yellow fluorescent proteins derived from Discosoma sp. red fluorescent protein," *Nature Biotechnol.*, vol. 22, no. 12, pp. 1567–1572, 2004.

[117] "PrimerX." [Online]. Available: http://www.bioinformatics.org/primerx/. [Accessed: 10-Jan-2013].

[118] R. F. Margolskee, B. McHendry-Rinde, and R. Horn, "Panning transfected cells for electrophysiological studies," *BioTechniques*, vol. 15, no. 5, pp. 906–911, 1993.

[119] F. L. Graham and A. J. van der Eb, "A new technique for the assay of infectivity of human adenovirus 5 DNA," *Virology*, vol. 52, no. 2, pp. 456–467, 1973.

[120] G. Miesenböck, D. A. De Angelis, and J. E. Rothman, "Visualizing secretion and synaptic transmission with pH-sensitive green fluorescent proteins," *Nature*, vol. 394, no. 6689, pp. 192–195, 1998.

[121] B. T. Archer, T. Ozcelik, R. Jahn, U. Francke, and T. C. Südhof, "Structures and chromosomal localizations of two human genes encoding synaptobrevins 1 and 2.," *J. Biol. Chem.*, vol. 265, no. 28, pp. 17267–17273, 1990.

[122] S. Schoch, "SNARE Function Analyzed in Synaptobrevin/VAMP Knockout Mice," *Science*, vol. 294, no. 5544, pp. 1117–1122, 2001.

[123] U. Testa, "Transferrin receptors: structure and function," *Curr. Top. Hematol.*, vol. 5, pp. 127–161, 1985.

[124] S. Bolte and F. P. Cordelieres, "A guided tour into subcellular colocalization analysis in light microscopy," *J. Microsc.-Oxford*, vol. 224, no. 3, pp. 213–232, 2006.

[125] K. S. Cole, "Some physical aspects of bioelectric phenomena," *Proc. Natl. Acad. Sci. U.S.A.*, vol. 35, no. 10, pp. 558–566, 1949.

[126] A. L. Hodgkin, A. F. Huxley, and B. Katz, "Measurement of current-voltage relations in the membrane of the giant axon of Loligo," *J. Physiol. (Lond.)*, vol. 116, no. 4, pp. 424–448, 1952.

[127] R. Miledi, I. Parker, and K. Sumikawa, "Properties of acetylcholine receptors translated by cat muscle mRNA in Xenopus oocytes.," *EMBO J.*, vol. 1, no. 11, pp. 1307–1312, 1982.

[128] E. Neher and B. Sakmann, "Single-channel currents recorded from membrane of denervated frog muscle fibres," , *Nature*, vol. 260, no. 5554, pp. 799–802, 1976.

[129] F. J. Sigworth and E. Neher, "Single Na+ channel currents observed in cultured rat muscle cells," , *Nature*, vol. 287, no. 5781, pp. 447–449, 1980.

[130] E. Neher, "Unit conductance studies in biological membranes," Elsevier North-Holland, 1981.

[131] M. H. Akabas, D. A. Stauffer, M. Xu, and A. Karlin, "Acetylcholine receptor channel structure probed in cysteine-substitution mutants," *Science*, vol. 258, no. 5080, pp. 307–310, 1992.

[132] D. A. Stauffer and A. Karlin, "Electrostatic potential of the acetylcholine binding sites in the nicotinic receptor probed by reactions of binding-site cysteines with charged methanethiosulfonates," *Biochemistry*, vol. 33, no. 22, pp. 6840–6849, 1994.

[133] E. Neher, "Correction for liquid junction potentials in patch clamp experiments," *Meth. Enzymol.*, vol. 207, pp. 123–131, 1992.

[134] S. H. Heinemann and F. Conti, "[7] Nonstationary noise analysis and application to patch clamp recordings," in *Method. Enzymol.*, vol. Volume 207, Bernardo Rudy, Ed. Academic Press, 1992, pp. 131–148.

[135] K. D. Gillis, "Admittance-based measurement of membrane capacitance using the EPC-9 patch-clamp amplifier," *Pflugers Arch.*, vol. 439, no. 5, pp. 655–664, 2000.

[136] J. Santos-Sacchi, "Reversible inhibition of voltage-dependent outer hair cell motility and capacitance," *J. Neurosci.*, vol. 11, no. 10, pp. 3096–3110, 1991.

[137] T. J. Rink, R. Y. Tsien, and T. Pozzan, "Cytoplasmic pH and free Mg2+ in lymphocytes.," *J. Cell. Biol.,* vol. 95, no. 1, pp. 189–196, 1982.

[138] A. J. Smith, A. A. C. Reed, N. Y. Loh, R. V. Thakker, and J. D. Lippiat, "Characterization of Dent's disease mutations of CLC-5 reveals a correlation between functional and cell biological consequences and protein structure," *Am. J. Physiol.-Renal*, vol. 296, no. 2, pp. F390–F397, 2009.

[139] A. J. Smith and J. D. Lippiat, "Direct endosomal acidification by the outwardly rectifying CLC-5 Cl−/H+ exchanger," *J. Physiol.*, vol. 588, no. 12, pp. 2033–2045, 2010.

[140] S. De Stefano, M. Pusch, and G. Zifarelli, "Extracellular Determinants of Anion Discrimination of the Cl−/H+ Antiporter Protein CLC-5," *Journal of Biological Chemistry*, vol. 286, no. 51, pp. 44134 –44144, Dec. 2011.

[141] F. Bezanilla, "The voltage sensor in voltage-dependent ion channels," *Physiol. Rev.*, vol. 80, no. 2, pp. 555–592, 2000.

[142] A. De Angeli, D. Monachello, G. Ephritikhine, J. M. Frachisse, S. Thomine, F. Gambale, and H. Barbier-Brygoo, "The nitrate/proton antiporter AtCLCa mediates

nitrate accumulation in plant vacuoles," *Nature*, vol. 442, no. 7105, pp. 939–942, 2006.

[143] G. Orhan, C. Fahlke, and A. K. Alekov, "Anion-and proton-dependent gating of ClC-4 anion/proton transporter under uncoupling conditions," *Biophys. J.*, vol. 100, no. 5, pp. 1233–1241, 2011.

[144] Y. Liu, M. Holmgren, M. E. Jurman, and G. Yellen, "Gated Access to the Pore of a Voltage-Dependent K+ Channel," *Neuron*, vol. 19, no. 1, pp. 175–184, 1997.

[145] J. Cui, D. H. Cox, and R. W. Aldrich, "Intrinsic voltage dependence and Ca2+ regulation of mslo large conductance Ca-activated K+ channels," *J. Gen. Physiol.*, vol. 109, no. 5, pp. 647–673, 1997.

[146] A. Accardi and M. Pusch, "Fast and slow gating relaxations in the muscle chloride channel CLC-1," *J. Gen. Physiol.*, vol. 116, no. 3, p. 433, 2000.

[147] N. Yang and R. Horn, "Evidence for voltage-dependent S4 movement in sodium channels," *Neuron*, vol. 15, no. 1, pp. 213–218, 1995.

[148] Z. Zhao, X. Li, J. Hao, J. H. Winston, and S. A. Weinman, "The ClC-3 chloride transport protein traffics through the plasma membrane via interaction of an N-terminal dileucine cluster with clathrin," *J. Biol. Chem.,* vol. 282, no. 39, pp. 29022–29031, 2007.

[149] H. H. Lim and C. Miller, "Intracellular proton-transfer mutants in a CLC Cl-/H+ exchanger," *J. Gen. Physiol.*, vol. 133, no. 2, p. 131, 2009.

[150] F. Bezanilla, E. Perozo, D. Papazian, and E. Stefani, "Molecular basis of gating charge immobilization in Shaker potassium channels," *Science*, vol. 254, no. 5032, pp. 679–683, 1991.

[151] L. Feng, E. B. Campbell, and R. Mackinnon, "Molecular mechanism of proton transport in CLC Cl-/H+ exchange transporters," *Proc. Natl. Acad. Sci. USA*, 2012.

[152] S. L. Rybak, F. Lanni, and R. F. Murphy, "Theoretical considerations on the role of membrane potential in the regulation of endosomal pH," *Biophys. J.*, vol. 73, no. 2, pp. 674–687, 1997.

8 Acknowledgements

I would like to thank Prof. Dr. Christoph Fahlke for the possibility to work in his group and to give me the chance to benefit from his scientific experience and his wisdom concerning the tackling of professional problems. He also made it possible for me to attend three scientific conventions in order to enrich my own experience.

I would like to thank in advance Prof. Dr. Kraft and Prof. Dr. Ngezahayo for being my co-referees, for taking the time and effort to read this thesis and take part in my defense.

Special thanks go to:

Prof. Dr. Alexi Kirilov Alekov, my present boss, whose creativity concerning science and jokes is matchless and was ever motivating, Dr. Jasmin Hotzy, my cell mate in the dark lab of fluorescence, who helped me a lot in stressful situations in work and life, Dr. David Ewers, for his refreshing ability to distract me from science, discussing about music and other important stuff and Nicole Schneider who was always a delightful conversation partner.

I must not forget to thank the people who keep the lab running: Christin Dähling our secretary and our technicians, Toni Becher, Birgit Begemann, Petra Kilian and Silke Schmidt and Bettina Wilhelm.

Furthermore, I would like to thank all the other colleagues of the Institute of Neurophysiology who were always very helpful when I had scientific question. Although I would like to, I could not name everybody personally because I have only 48 hours left to finish this thesis! I'm not sure if I will ever have colleagues as nice and fun as you.

Last but certainly not least I want to thank my parents for always supporting me.

9 Curriculum Vitae

Personal Information

Matthias Grieschat

born 20.07.1981 in Hildesheim, Germany

Educational and Professional Background

2008 – present	PhD studies at the Naturwissenschaftliche Fakultät, Gottfried Wilhelm Leibniz Universität Hannover, conducted at the Institut für Neurophysiologie, Medizinische Hochschule Hannover
01.10.2008 – present	Scientific employee at the Zentrum Physiologie, Institut für Neurophysiologie, Medizinische Hochschule Hannover
2003 – 2008	Biology studies at the Naturwissenschaftliche Fakultät, Gottfried Wilhelm Leibniz Universität Hannover degree: Dipl.-Biol.
2002 – 2003	Machine engineering studies at the Leibniz Universität Hannover abandoned
2001 – 2002	Alternative civilian service at Caritasverband Hannover e.V.
1998 – 2001	Gymnasium Sarstedt degree: Abitur
1994 – 1998	Gymnasim Sarstedt degree: mittlere Reife

10 List of publications

M. Grieschat and A. K. Alekov, "Glutamate 268 Regulates Transport Probability of the Anion/Proton Exchanger ClC-5," *J. Biol. Chem.*, vol. 287, no. 11, pp. 8101–8109, 2012.

R. E. Guzman, M. Grieschat, Ch. Fahlke, and A. K. Alekov, "ClC-3 is an intracellular chloride/proton exchanger with large voltage-dependent nonlinear capacitance," *ACS Chem. Neurosci.,* vol. 4, no. 6, pp. 994–1003, 2013